Stochastic Modeling of Deterioration in Nuclear Power Plant Components

by

Xianxun Yuan

A thesis
presented to the University of Waterloo
in fulfilment of the
thesis requirement for the degree of
Doctor of Philosophy
in
Civil Engineering

Waterloo, Ontario, Canada, 2007

© Xianxun Yuan 2007

I hereby declare that I am the sole author of this thesis. This is a true copy of the thesis, including any required final revisions, as accepted by my examiners.

I understand that my thesis may be made electronically available to the public.

Abstract

The risk-based life-cycle management of engineering systems in a nuclear power plant is intended to ensure safe and economically efficient operation of energy generation infrastructure over its entire service life. An important element of life-cycle management is to understand, model and forecast the effect of various degradation mechanisms affecting the performance of engineering systems, structures and components.

The modeling of degradation in nuclear plant components is confounded by large sampling and temporal uncertainties. The reason is that nuclear systems are not readily accessible for inspections due to high level of radiation and large costs associated with remote data collection methods. The models of degradation used by industry are largely derived from ordinary linear regression methods.

The main objective of this thesis is to develop more advanced techniques based on stochastic process theory to model deterioration in engineering components with the purpose of providing more scientific basis to life-cycle management of aging nuclear power plants. This thesis proposes a stochastic gamma process (GP) model for deterioration and develops a suite of statistical techniques for calibrating the model parameters. The gamma process is a versatile and mathematically tractable stochastic model for a wide variety of degradation phenomena, and another desirable property is its nonnegative, monotonically increasing sample paths. In the thesis, the GP model is extended by including additional covariates and also modeling for random effects. The optimization of age-based replacement and condition-based maintenance strategies is also presented.

The thesis also investigates improved regression techniques for modeling deterioration. A linear mixed-effects (LME) regression model is presented to resolve an inconsistency of the traditional regression models. The proposed LME model assumes that the randomness in deterioration is decomposed into two parts: the unobserved heterogeneity of individual units and additive measurement errors.

Another common way to model deterioration in civil engineering is to treat the rate of deterioration as a random variable. In the context of condition-based maintenance, the thesis shows that the random variable rate (RV) model is inadequate to incorporate temporal variability, because the deterioration along a specific sample path becomes deterministic. This distinction between the RV and GP models has profound implications to the optimization of maintenance strategies.

The thesis presents detailed practical applications of the proposed models to feeder pipe systems and fuel channels in CANDU nuclear reactors.

In summary, a careful consideration of the nature of uncertainties associated with deterioration is important for credible life-cycle management of engineering systems. If the deterioration process is affected by temporal uncertainty, it is important to model it as a stochastic process.

Acknowledgments

I would like to express my greatest gratitude to my supervisor, Professor Mahesh D. Pandey, for his enlightening discussions, refreshing encouragement and financial supports throughout the doctorate program. Without his help the thesis could not have completed.

My sincere thanks go to Professor S. T. Ariaratnam for sharing his life-long experience of teaching and research, for his parent-like love, and for his financial support to my wife and myself so that I can concentrate on the study at ease.

I would also like to thank two professors from the Delft University of Technology, the Netherland: Professor J. A. M. van der Weide taught me random measure and conditional expectation and Professor Jan M. van Noortwijk gave me the first concepts of gamma process and many first-hand research materials. From Professor van Weide I learned "less is more", meaning that we shall aim to simple probabilistic models, rather than complicated ones.

In several critical points of the study Professor J. F. Lawless helped me out from statistical side. Without him I would still have been struggling in some basic statistical notions such as likelihoods and score statistics.

The data used in the case studies of the thesis were provided by Dr Grant A. Bickel, Chalk River, Atomic Energy Canada Limited, to whom I am very grateful.

I am tremendously indebted to my first academic mentor, Professor Wei-Jian Yi, from Hunan University, China. For over ten years he has been encouraging me to explore a broader area of research in civil engineering.

The leisure time in Waterloo would be too boring if I had not known these fellows: Ying An, Wensheng Bu, Xiaoguang Chen, Suresh V. Datla, Qinghua Huang, Hongtao Liu, Yuxin Liu, Anup Sahoo, Jinyu Zhu, and lately, Tianjin Chen, Guru Prakash and Rizwan Younis. I thank them for sharing their wits and laughs during the coffee time.

My final and special thanks are due to my wife, parents, brothers and sisters, for their love, understanding, patience, support and sacrifice.

To My Parents

Contents

Contents **vi**

List of Figures **x**

List of Tables **xiv**

1 Introduction **1**

1.1 Background 1

1.2 Objectives 5

1.3 Model, Modeling and Proposed Methodology 6

1.3.1 Models and Modeling 6

1.3.2 Uncertainty Modeling and Model Uncertainties 9

1.3.3 Proposed Deterioration Modeling Strategy 11

1.4 Organization 12

2 Literature Review **14**

2.1 Advances in Engineering Reliability Theory 14

2.2 Stochastic Modeling of Deterioration 18

2.2.1 Random Variable Model 19

2.2.2 Marginal Distribution Model 21

2.2.3 Second-Order Process Model 22

2.2.4 Cumulative Damage/Shock Model 23

2.2.5 Pure Jump Process Model 26

2.2.6 Stochastic Differential Equation Model 29
2.3 Statistical Models and Methods for Deterioration Data 30
2.3.1 Nature of Deterioration Data 30
2.3.2 Mixed-Effects Regression Models 32
2.3.3 Statistical Inference for Stochastic Process Models 34
2.4 Concluding Remarks 36

3 Linear Mixed-Effects Model for Deterioration 38
3.1 Introduction 38
3.2 Linear Regression Models 39
3.2.1 Ordinary Least Squares Method 39
3.2.2 Weighted Least Squares Method 41
3.2.3 Limitation of Linear Regression Models in Lifetime Prediction . . 43
3.3 Linear Mixed-Effects Models 45
3.3.1 Parameter Estimation 47
3.4 Case Study — Creep Deformation of Pressure Tubes in Nuclear Reactors 49
3.4.1 Background 49
3.4.2 Exploratory Data Analysis 49
3.4.3 Linear Regression Models 51
3.4.4 Linear Mixed-Effect Model 52
3.5 Concluding Remarks 56

4 Gamma and Related Processes 60
4.1 Stationary Gamma Processes 60
4.1.1 Distribution and Sample Path Properties 61
4.1.2 Distribution of Lifetime 67
4.1.3 Distribution of Remaining Lifetime 69
4.1.4 Simulation 70
4.2 Nonstationary Gamma Processes 72
4.3 Local Gamma Processes 73

4.4 Mixed-Scale Gamma Processes 74
4.5 Hougaard Processes 77
4.5.1 Hougaard Distributions 77
4.5.2 Hougaard Processes 79
4.6 Summary 80

5 Statistical Inference for Gamma Process Models 81
5.1 Introduction 81
5.2 Estimating Parameters of Gamma Process Models 82
5.2.1 Methods of Moments 82
5.2.2 Maximum Likelihood Method 85
5.2.3 Effects of Sample Size 86
5.2.4 Comparison of Maximum Likelihood Method and Methods of Moments 89
5.3 Modeling Fixed-Effects of Covariates in Deterioration 91
5.3.1 Likelihood Ratio Test 92
5.4 Effects of Measurement Errors 93
5.5 Modeling Random Effects in Deterioration 95
5.5.1 Test of Random Effects 98
5.6 Case Study — Creep Deformation 102
5.7 Summary 104

6 Case Study — Flow Accelerated Corrosion in Feeder Pipes in CANDU Plants 106
6.1 Background 106
6.2 Wall Thickness Data and Exploratory Analysis 110
6.3 Gamma Process Model and Statistical Inference 115
6.3.1 Model Structures 115
6.3.2 Parameter Estimation 116
6.3.3 Model Checks 117
6.4 Prediction of the Lifetime and Remaining Lifetime 122
6.5 Probability Distribution of the Number of Substandard Feeders 129
6.6 Summary 133

7 Effects of Temporal Uncertainty in Planning Maintenance **135**

7.1 Introduction 135

7.2 Random Variable Model 136

7.3 Age-Based Replacement 137

7.3.1 Example: Age-Based Replacement of Pressure Tubes for Creep Deformation 138

7.4 Condition-Based Maintenance 139

7.4.1 The Strategies 140

7.4.2 Formulation for Random Variable Model 140

7.4.3 Formulation for Gamma Process Model 143

7.4.4 Example: Condition-Based Maintenance of Pressure Tubes for Creep Deformation 147

7.5 Sensitivity Analysis 149

7.5.1 Calibration of the Models 150

7.5.2 Age-Based Replacement 151

7.5.3 Condition-Based Maintenance 153

7.5.4 Comparison of Age-Based and Condition-Based Policies 153

7.6 Summary 157

8 Conclusions and Recommendations **159**

8.1 Conclusions 159

8.2 Recommendations for Future Research 162

A Abbreviations And Notations **163**

References **165**

List of Figures

1.1 Layout of a CANDU nuclear power plant 3

1.2 CANDU 6 reactor assembly (from http://canteach.candu.org) 4

1.3 Procedure of modeling uncertainties in deterioration 8

2.1 Typical cumulative damage models 24

2.2 Components of randomness in deterioration data: random effects, temporal uncertainty and measurement errors 32

3.1 Typical sample paths of diametral strain with average fluence 50

3.2 Standardized residuals from WLS 51

3.3 Standardized residuals from IWLS 52

3.4 Predicted versus observed diametral strains from IWLS. The circled crosses represent data from Tube C2 53

3.5 Normal quantile plot for within-unit residuals ε_{ij} 56

3.6 Normal quantile plot for the random slope Θ 57

3.7 Populational (dashed line) and individual (solid line) mean deterioration path of Tube C2. The circled crosses represent diametral strain measured from Tube C2 58

3.8 Probability density function of the lifetime of a typical pressure tube with flux 2.4×10^{17} n/(m^2·s) 59

4.1 Probability density functions of gamma random variables with unit scale parameter and different shape parameters 61

4.2 Time-scale effect of sample paths of a gamma process 63

4.3 A compound Poisson process goes to a gamma process when c goes to zero 66

4.4 Distribution of first passage time of a gamma process and its Poisson approximation 68

4.5 Distributions of the remaining lifetime of a gamma process based on different information 70

4.6 Comparison of a mixed-scale gamma distribution with its equivalent gamma distribution 76

5.1 Coefficient of variation of the estimated (a) shape and (b) scale parameters from different numbers of measurements. Dotted lines represent the analytical results, and solid lines the simulation results 88

5.2 Histograms of maximum likelihood estimates for stationary gamma process with or without consideration of measurement errors. Parameters are estimated based on 1000 sample paths of one record. True values of the parameters are $\alpha = 5$, $\beta = 2$, $\sigma_\varepsilon = 0.5$ 96

5.3 Histograms of maximum likelihood estimates for stationary gamma process with or without consideration of measurement errors. Parameters are estimated based on 50 sample paths of 5 record. True values of the parameters are $\alpha = 5$, $\beta = 2$, $\sigma_\varepsilon = 0.5$ 97

5.4 Histogram of the score statistic for 20 sample paths of 30 equally sampled records 101

5.5 Histogram of the score statistic for 500 sample paths of 30 equally sampled records 101

5.6 Predicted versus observed diametral strain increments from the stationary gamma process model 103

5.7 Comparison of probability density functions for the lifetime of a typical pressure tube with average flux 2.4×10^{17} n/(m^2·s) 104

6.1 Subsequent processes of flow-accelerated corrosion (Burrill and Cheluget 1998) 107

6.2 Illustration of end-fitting and outlet feeder pipe (Burrill and Cheluget 1999) 108

6.3 Ovality of the feeder cross section and initial wall thinning during fabrication (Kumar 2004) 109

6.4 Typical wall thinning paths. Left: 2” feeders; right: 2.5” feeders 113

6.5 Dependence of wall thinning rate on flow velocity. Left: 2” feeders; right: 2.5” feeders 114

6.6 Measured versus fitted values with 95% bounds: Group II 118

6.7 Measured versus fitted values with 95% bounds: Group III 118
6.8 Measured versus fitted values with 95% bounds: Group IV 119
6.9 Measured versus fitted values with 95% bounds: Group V 119
6.10 Measured versus fitted values with 95% bounds: Group VI 120
6.11 Measured versus fitted values with 95% bounds: Group VII 120
6.12 Probability density functions of feeder lifetime due to FAC 124
6.13 Mean lifetime of feeders against flow velocity 125
6.14 The latest measured wall thickness. Left: 2" feeders; right: 2.5" feeders . 126
6.15 Comparision of original (solid lines) and updated (dotted lines) lifetime distributions of the feeders with the least remaining thickness 127
6.16 Comparison of original (solid line) and updated (crosses) mean lifetimes of feeders 128
6.17 Histograms of probability of feeders reaching substandard state based on original (left panels) and on updated (right panels) lifetime distributions . 131
6.18 Probability distribution of the number of substandard feeders based on original (left panels) and on updated (right panels) lifetime distributions . 132
6.19 Survival functions of the time to the first appearance of a substandard feeder 133

7.1 Optimal age-based replacement policies for a pressure tube due to diametral expansion 139
7.2 CBM decision tree for the RV model 141
7.3 CBM decision tree for the GP model 144
7.4 Comparison of condition-based maintenance policy based on different deterioration models for a pressure tube due to diametral expansion 147
7.5 Decomposition of mean cost rate for the RV model 148
7.6 Decomposition of mean cost rate for the GP model 148
7.7 Probability of the pressure tube being substandard over time under the optimal CBM policy based on the GP model 149
7.8 Comparison of lifetime distributions of the equivalent RV and GP models for $\nu_T = 0.3$: (a) probability density function, and (b) survival function . 152
7.9 Comparison of age-based replacement policies in equivalent RV and GP mdoels: (a) optimal replacement age, and (b) minimal mean cost rate . . 153

7.10 Comparison of CBM results for equivalent RV and GP models: (a) optimal inspection interval, and (b) minimal mean cost rate 154

7.11 Comparison of the CBM policies with the ABR in the GP model 155

7.12 A two-dimensional CBM optimization for the GP model ($\nu_T = 0.3$) 156

7.13 Comparison of two-dimensional CBM policies with ABR policies 157

7.14 Maximum allowable inspection cost with COV of lifetime and PM to CM cost ratio 158

List of Tables

3.1 Number of repeated measurements of creep diametral strains in pressure tubes 50

5.1 Mean and standard errors of estimated parameters from different methods 90

6.1 Ratio of repeated measurements of Feeder wall thickness data 111

6.2 Geometry parameters of the 1st bends of outlet feeders in a CANDU 6 Plant 112

6.3 Maximum likelihood estimates and the score statistics for different groups 117

6.4 Likelihood ratio tests for the corrosion incubation period t_0 121

6.5 Likelihood ratio test of effects of bend direction 122

6.6 Maximum and minimum mean lifetimes and associated standard deviations for different groups 124

7.1 Parameters used in the model calibration 151

7.2 Example parameters in the RV and GP models 151

Chapter 1

Introduction

1.1 Background

The success and progress of human society depend on reliable physical infrastructure — roads, bridges, hospitals, fire stations, dams, sewage, gas pipelines, nuclear power plants, transmission lines, etc. — for distributing resources and essential services to the public. A common problem of the infrastructure is that, as service time progresses, the infrastructure ages, its performance deteriorates and its reliability declines. The deteriorating infrastructure can have an adverse impact on a utility's profit and sometimes even on a whole nation's economy (Choate and Walter 1983). Consider an example of the nuclear power generation industry. According to the International Atomic Energy Agency (IAEA), as of January 12, 2007, there were 114 out of 435, or 26% of operational nuclear reactors around the world that had been working over 30 years (International Atomic Energy Agency 2007). For a nuclear reactor with design life of 30-40 years, this implies that large investments are needed to maintain the generation infrastructure to meet the increasing energy needs in the next 10 to 20 years. In Canada particularly, nuclear utilities are planning several big refurbishment programs to replace or upgrade the aging systems, structures and components of the nuclear power plants. These programs involve billions

of dollars (Atomic Energy of Canada Limited 2007).

To ensure safety and reliability throughout the service life, including any extended life, aging in the infrastructure must be effectively managed. In nuclear generation industry, aging management programs that integrate equipment qualification, in-service inspection, deterioration modeling and preventive maintenance have been implemented (Pachner 2002). Aging management deals with problems such as when and where an inspection should be undertaken, what specific maintenance actions and when these actions should be taken. A characteristic feature of the aging management is that decisions often must be made under uncertainty. One of the most important uncertainties is the uncertainty in the deterioration rate and the time to failure, or the lifetime. Traditionally, the uncertainty in aging and deterioration is characterized by a lifetime distribution, in which aging is described by its failure rate function. But the lifetime distribution model is suitable only to time-based maintenance (e.g., age-based replacement) as it only quantifies whether a component is functioning or not. It cannot be used for condition-based maintenance optimization, which is at the core of an aging management program. The need for an advanced stochastic model of deterioration to support condition assessment, life prediction and efficient life-cycle management program of the aging infrastructure is compelling.

A nuclear power plant (NPP) is a complex technical system consisting of a vast number and variety of engineered subsystems, structures and components (SSCs) that experience uncertain aging and degradation. As sketched in Figure 1.1, a CANDU™[1] nuclear power plant consists of a reactor core, heat transport system (e.g. feeder pipes and steam generators), secondary side (e.g. turbine and generator), and safety systems. Among the many SSCs, fuel channels inside the reactor core, steam generators, and feeders connecting them are the three key, potentially life-limiting systems (Figure 1.2). Working in high-temperature and high-pressure environment, the zirconium alloy pressure tubes may

[1]CANDU, abbreviated for CANadian Duterium Uranium, is a trademark for Atomic Energy of Canada Limited.

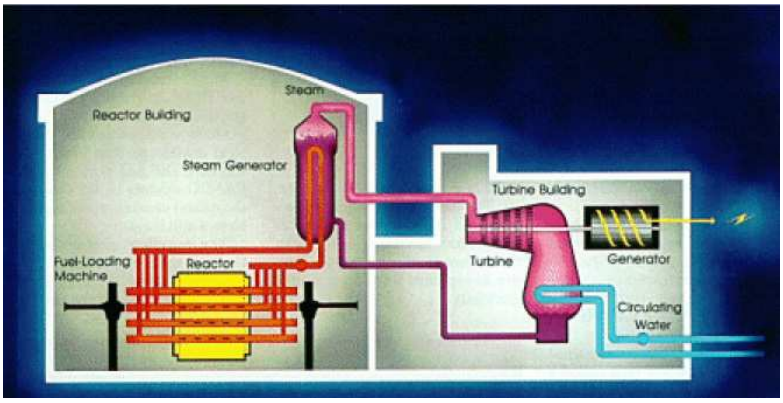

Figure 1.1: Layout of a CANDU nuclear power plant

experience different kinds of degradation phenomena such as delayed hydride cracking, sag, elongation, diametral expansion, and even a break before leak, due to irradiation enhanced deformation and embrittlement (IAEA 1998). Similarly, the heat exchanger tubes in the steam generators are susceptible to different types of degradation such as pitting, denting, fretting, stress corrosion cracking, high-cycle fatigue, and wastage (IAEA 1997). For the other CANDU reactor assemblies (e.g., calandria vessels, end shields, feeders), the following potential degradation mechanisms have been identified (IAEA 2001) : neutron irradiation embrittlement, stress corrosion cracking, corrosion (pitting, denting, flow-accelerated), erosion, fatigue, stress relaxation, creep, and mechanical wear.

In general, the deterioration data from field inspections during previous outages exhibits considerable variability. The data suffers from both sampling uncertainty and temporal uncertainty. The sampling uncertainty arises from the fact that the inspected components are generally a small portion of the overall population over a limited time horizon. Due to the small sample size, the determination of a representative distribution type becomes difficult, resulting in modeling error. Another consequence of the small sample size is that it hinders an accurate estimation of the distribution parameters. Inference of the population parameters from the finite samples therefore suffers from aforementioned uncertainties. The uncertainty inherent in the progression of deterioration

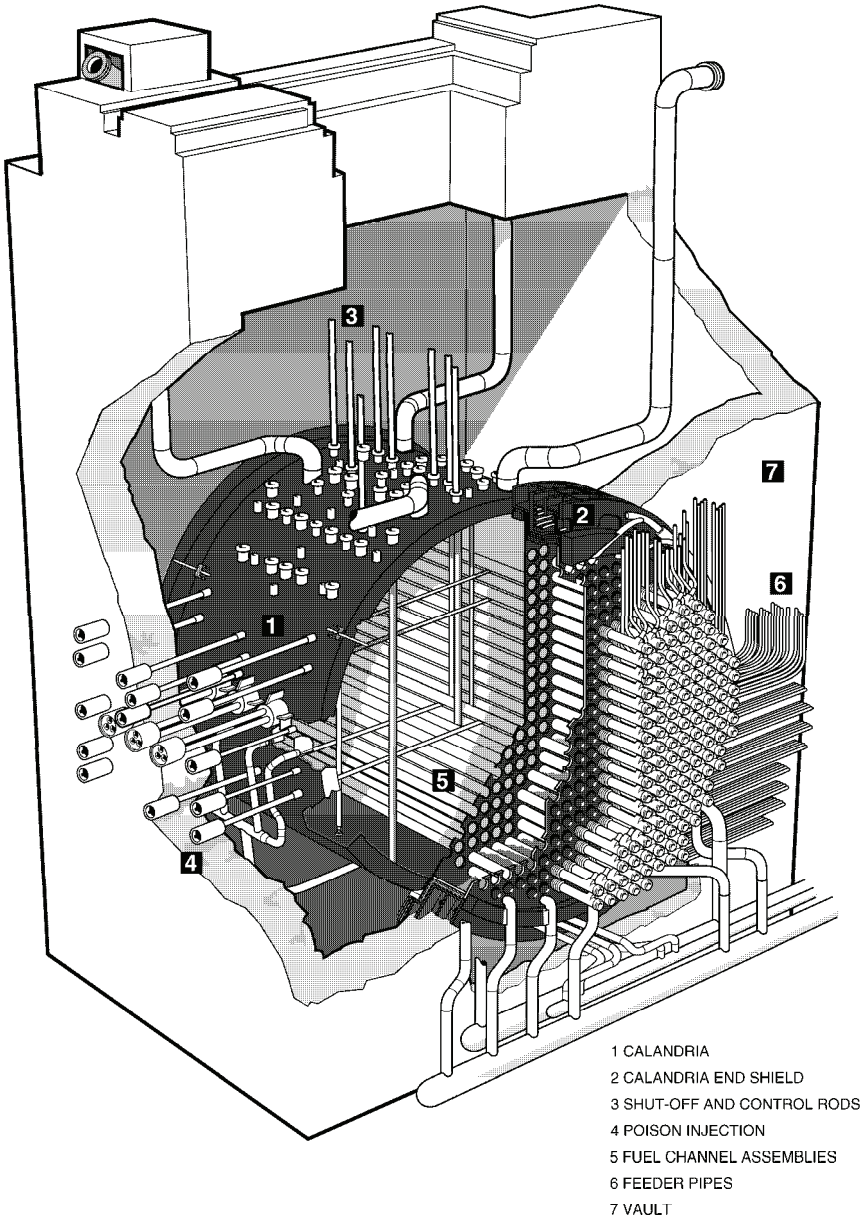

Figure 1.2: CANDU 6 reactor assembly (from http://canteach.candu.org)

over time is referred to as temporal uncertainty.

Traditional regression-based models assume a deterministic functional relationship between the response and the independent variables. The choice of the functional form is usually guided by certain empirical relationship from existing scientific investigations. The randomness of the response is characterized by adding an extra "error" term. The parameters of the model are usually estimated by the ordinary or generalized least square technique, depending on the assumption of the error structure (Rao 1973; Weisberg 2005).

Although the regression models are probably one of the most sophisticated statistical techniques known to engineers, its limitation in reliability prediction was reported recently (Pandey, Yuan, and van Noortwijk 2006). In addition to some common modeling difficulties such as error diagnostics and normality check, an important limitation is that the repeated measurements, although from the same component and therefore dependent, are treated as independent observations in the linear or nonlinear regression models. Mixed-effects models (Crowder and Hand 1990) can be used to model the covariance structure for the repeated measurements, but the random-variable nature of the regression models prevent a proper consideration of the effects of temporal uncertainties in prediction of the remaining lifetime. This motivates the exploration of stochastic process based models to take into account the temporal uncertainty in aging management of nuclear power plant systems.

1.2 Objectives

The thesis aims to develop a stochastic process model for generic deterioration phenomena in nuclear power plant components. In particular, the thesis attempts to answer the following questions:

- What is the need for a stochastic process based model of deterioration? A common practice in deterioration modeling is to use random variable models via regression

techniques. The stochastic process model differs from the random variable model in that the former takes into account time-varying uncertainty inherent in the deterioration. To answer this question, we examine the significance of the temporal uncertainty on preventive maintenance decision-making by comparing the results from the random variable model with those from the stochastic process model.

- Which stochastic process model shall be used? There are a large inventory of stochastic process models, for example, discrete-state Markov chain models, Wiener processes, compound Poisson processes, renewal processes, etc. In the thesis, a gamma process model is investigated. We examine the mathematical characteristics of the gamma process and their implications in modeling physical degradation mechanisms.

- How does one estimate model parameters from available deterioration data? As the main body of the modeling procedure, the question includes model verification (i.e., parameter estimation) and model validation.

- Applications. An important objective of the thesis is to show that stochastic models are useful in practical life-cycle management of NPPs. For illustration purposes, two case studies are presented, one for the creep deformation of pressure tubes in the CANDU reactor core and the other at more details for the wall thinning of feeder pipes due to flow-accelerated corrosion.

1.3 Model, Modeling and Proposed Methodology

1.3.1 Models and Modeling

What do we mean by a model and a stochastic model in particular of a system or a phenomenon? Simply speaking, a model is a physical, mathematical, or computational

representation of a system that can be used to predict the system's behavior. A small-scaled beam in a structural laboratory can be treated as a physical model of some highway bridge. An artificial neural network is an example of computer models for some complex system of which the input and output have complex nonlinear relationship. Here we focus on stochastic model of deterioration that are used to predict the deterioration in the future and the time at which the deterioration reaches a critical level.

A mathematical model consists of a set of structural assumptions and embedded parameters and it can be expressed conceptually as $M = (S, \theta)$, in which S denotes the model structure and θ the model parameters (Draper 1995). Depending on the model structure S, mathematical models can be categorized as deterministic models and stochastic models. A stochastic model includes certain random or chance elements in its structural assumptions whereas a deterministic model assumes the system behavior is predictable with certainty. Deterioration usually evolves randomly with time. Failing to include inherent uncertainties in the deterioration model would make the understanding of the systems unrealistic. Therefore, a stochastic deterioration model is necessary.

By modeling we mean an iteratively refining process of identifying important parameters, making reasonable assumptions, specifying model structure, estimating model parameters, assessing model performance, and modifying assumptions and model structure. In the case of deterioration modeling, the deterioration process $X(t)$, or X for brevity, is the important parameter that we want to know its value in the future time for the purpose of maintenance decision. Sometimes other variables may also be helpful for the prediction of X. They are called explanatory variables or covariates and labeled as Y in general although they may be random processes as well. For modeling deterioration that exhibits obvious variability, assumptions are made as the first step about the mean deterioration curve (e.g., linear or quadratic with time) and about the dependence structure of the deterioration process (e.g., Markov assumptions, or more strongly, independent increments). Then the model parameters are estimated from observations of both X and Y that are possibly contaminated by measurement errors. So far the induc-

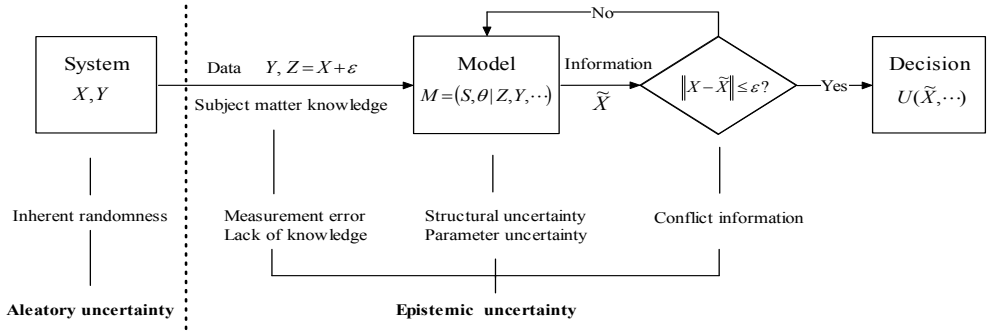

Figure 1.3: Procedure of modeling uncertainties in deterioration

tion stage of the modeling is completed. Next, we compare the deduction results $\tilde{X}$ from the constructed models with (usually new) observations. According to certain prescribed acceptance criterion, say $\left\|X - \tilde{X}\right\| \le \varepsilon$, the model is either accepted or rejected for its inadequacy. If accepted, it can then be used for supporting our decision-making (e.g. risk-informed in-service inspection), which may be based on some utility criteria U that is a function of $\tilde{X}$. If the model is rejected, we shall then modify the model assumptions, re-estimate the parameters, and so on, until it is accepted. The whole modeling procedure is shown in Figure 1.3.

Since no model is correct in the sense that there is no model that can consistently represent all aspects of the system under study, we should be alert to distinguish important errors in the model. Keeping this in mind can help build a model that is no more refined than necessary for the application. That said, however, it does not mean that we do not need to consider the uncertainty the model has brought to the information, represented by $\tilde{X}$, upon which the decision making is based. As a matter of fact, how to deal with the model uncertainty has become an important topic in modeling (Ferson et al. 2004; Oberkampf et al. 2004), and in particular, in stochastic deterioration modeling (Ang and De Leon 2005) in which the situation is compounded by the inherent uncertainty of

deterioration. We elaborate this matter in detail in the next.

1.3.2 Uncertainty Modeling and Model Uncertainties

Uncertainties are generally categorized as aleatory uncertainty and epistemic uncertainty (Bedford and Cooke 2001; Aven 2003). Also known as irreducible uncertainty, the aleatory uncertainty refers to the inherent indeterminacy or unpredictability of a system or a phenomenon. The epistemic uncertainty relates to the phenomenon that the decision maker does not have the information which is quantitatively and qualitatively appropriate to describe or predict the system's behavior. While aleatory uncertainty is a property of the system, the epistemic uncertainty is a situational property of the interactions among the system, the modeler and the decision maker (Zimmermann 2000). As shown in Figure 1.3, causes of epistemic uncertainty in deterioration include measurement error of data, lack of knowledge of the deterioration mechanism, inappropriateness of the model structure, parameter uncertainty due to scarce data, and conflict information of the system from different models.

Aleatory uncertainties in deterioration can be further classified into unit-varying uncertainty and time-varying uncertainty. Although both uncertainties can be characterized by probability, the specific probabilistic models for these two uncertainties are different. For the unit-varying uncertainty, or random effect across units, a random variable model may be adequate. But for the time-varying uncertainty, or temporal uncertainty, a model considering the stochastic time dependence is essential.

Many researchers have studied the epistemic uncertainty in different applications (e.g., statistical inference (Box 1976; Draper 1995; Laskey 1996), probabilistic risk analysis (Hora 1996; Parry 1996; Bedford and Cooke 2001; Aven 2003), expert systems (Zimmermann 2000), system identification (Moon and Aktan 2006), etc.). According to the cause of the epistemic uncertainty and the form of data (e.g., numerical, interval or linguistic), different theories may be applied, for example, probability theory, possibility theory,

fuzzy logic, evidence theory, expert judgement, interval arithmetic, and convex modeling. For details of those theories, refer to Zimmermann (2000) and the references therein.

Most of existing research, however, focused on parameter uncertainty in the Bayesian framework. Draper (1995) attempted to attack the uncertainty in the model structure using the so-called standard Bayesian solution. The entire model $M = (S, \theta)$ was treated as a nuisance parameter and the conditional predictive distributions $p\,(\tilde{x}\,|y, z\,)$ is expressed as

$$\begin{aligned} p\,(\tilde{x}\,|y, z\,) &= \int_{\mathcal{M}} p\,(\tilde{x}\,|y, z, M\,)\, p\,(M\,|y, z\,)\, dM \\ &= \int\int p\,(\tilde{x}\,|y, z, \theta, S\,)\, p\,(\theta\,|y, z, S\,)\, p\,(S\,|y, z\,)\, d\theta dS, \end{aligned} \tag{1.1}$$

in which $p\,(M\,|y, z\,)$ is written as $p\,(\theta, S\,|y, z\,) = p\,(\theta\,|y, z, S\,)\, p\,(S\,|y, z\,)$ and denotes the posterior distribution of the model M, and x, y, z denotes the deterioration, covariates, and noise-contaminated measurements, respectively, as in Figure 1.3. When $p\,(S\,|y, z\,)$ is concentrated on S^*, a specifically chosen model, (1.1) is reduced to

$$p\,(\tilde{x}\,|y, z\,) = \int p\,(\tilde{x}\,|y, z, \theta\,)\, p\,(\theta\,|y, z\,)\, d\theta, \tag{1.2}$$

which assesses the parameter uncertainty only, as done in Ang and De Leon (2005). Working backwards from $p\,(\theta, S\,|y, z\,)$ to the prior distribution upon which the posterior model probabilities are based gives

$$p\,(\theta, S\,|y, z\,) = cp\,(S)\, p\,(\theta\,|S\,)\, p\,(y, z\,|\theta, S\,)\,, \tag{1.3}$$

where c denotes a normalization constant, $p\,(S)$ the prior distribution of the model structure, $p\,(\theta|S)$ the prior conditional distribution of the model parameter given a model structure, and $p\,(y, z\,|\theta, S\,)$ the likelihood function. The standard Bayesian solution hopes an automatic updating process from $p\,(S)$ to $p\,(S\,|y, z\,)$ via Bayesian formula. But the

difficult part of the Bayesian updating is the specification of $p(S)$, because, as Draper argued, the space of all possible models is either "too big to support a diffuse $p(S)$" or "too small to be well calibrated". This difficulty makes the standard Bayesian solution inapplicable in practice.

A less-ambitious but very pragmatic solution is the model expansion approach. This approach starts with a single structural choice S^* and then it is expanded in directions suggested by context, by model calibrations, or by other considerations. One special case of this approach is the conventional sensitivity analysis in which the assumptions in S^* are challenged by qualitatively exploring how much the conclusions would change if an alternative set of plausible assumptions were made. This thesis adopts the model expansion approach for modeling updating. This is detailed in the next subsection.

1.3.3 Proposed Deterioration Modeling Strategy

It would be extremely satisfying if a theory could be formulated in such a way that all of the physical and chemical processes can be dealt with on a microscopic scale and the observed characteristics of the deterioration process can be portrayed. Such theory, also known as mechanistic model — truly rooted in the physics of the deterioration — does not seem to be available at present. While existing physical theories (e.g., thermodynamics, statistical physics) are helpful in providing important insights into and qualitative explanation for the deterioration process, they cannot yet give a basis for the micro-macro modeling of the deterioration and for obtaining results of interest in engineering. In light of these difficulties, it is rational and important to construct a phenomenological or empirical model in order to provide a reasonable basis for prediction of deterioration.

Thus, the thesis adopts an empirical, data-driven methodology for deterioration modeling. A model that has a simple structure and captures important uncertainties and other sample path characteristics of the deterioration is preferable. If the model is meant to be applicable in practice, its parameters should also be easily estimated, especially

when data is relatively scarce. This thesis proposes a gamma process model. We will show that this model is mathematically simple but it is also easy to expand to more advanced models if necessary.

As far as validating the model assumptions is concerned, we use the above mentioned model expansion approach. We start with a simple gamma process model, its stationarity and relationship with covariates depending on context and subject matter knowledge of deterioration. The model parameters are estimated by using maximum likelihood method. After that, we expand the gamma process model into a mixed-scale gamma process of which the scale parameter is a random variable. This new model considers the random effects across the units. Likelihood-based procedures are used to test whether the gamma process is a good model.

1.4 Organization

The thesis is divided into eight chapters, including this first introductory chapter. Chapter 2 provides a literature review of the deterioration modeling from both probabilistic and statistical points of view. Chapter 3 starts with traditional linear regression models, followed by a linear mixed-effects model that is proposed to solve a logical inconsistency of the traditional regression model in lifetime prediction. Chapter 4 focuses on theoretical aspects of gamma processes and other related processes. In particular, the definition, distribution and sample path properties, first passage time, simulation, and generalizations of gamma processes are discussed in details. Chapter 5 deals with statistical aspects of gamma processes. Methods of parameter estimation in cases of single sample path records, covariates, measurement errors and random effects, are developed in this chapter. Likelihood ratio test and score test are also discussed for model validation. Creep deformation of pressure tubes in fuel channels of CANDU reactor is modeled by both a linear mixed-effects model and a stationary gamma process model. This case study is reported in Chapter 3 and 5, respectively. Another case study of feeder piping system in

which the wall thickness gets thinning due to flow-accelerated corrosion is performed in Chapter 6. This particular degradation is modeled by a gamma process model. Chapter 7 examines the significance of temporal uncertainty on deterioration modeling and preventive maintenance decision-making. Finally Chapter 8 describes conclusions of the thesis and highlights other interesting topics for the future research.

Commonly used abbreviations and notations are listed in Appendix A and References are documented at the end of the thesis.

Chapter 2

Literature Review

2.1 Advances in Engineering Reliability Theory

Reliability, to simply put, is the ability of a physical object (e.g., an electronic device, a bridge, a product line, etc.) to perform its required function under stated conditions for a specified period of time. Opposite to reliability is failure, referring to the event of failing to perform the required function or failing to conform to performance standards. Probabilistic reliability theory define reliability as the probability that the object performs its required function throughout its service life under specified conditions. Clearly, reliability and probability of failure sum up to 1.

Since any physical object deteriorates over time and the environment in which the object works always changes, reliability is also a time-related concept. The time at which the object fails to perform the required function is called the failure time, or lifetime. The probability distribution of lifetime characterizes the object's reliability over time and can be expressed by probability density function (pdf), cumulative distribution function (CDF), survival function (SF), or failure rate function (also known as hazard rate function). The relationship among these functions can be found in many textbooks of reliability theory, for example, in Gertsbakh (2000). The SF denotes the reliability at

any given time and is thus also called reliability function.

Reliability theory evolved apart from the mainstream of probability and statistics. It was originally a tool to help nineteenth-century maritime insurance and life insurance companies compute profitable rates to charge their customers. The reliability theory did not join engineering until the end of the second world war. But once engineers found out the utility of reliability theory, they advanced the theory in two different approaches at an almost isolated manner. Safety being their major concern in design, civil and structural engineers defined the reliability as the probability of the structural strength being greater than the stress applied from loads on the structure (Freudenthal 1947). They expressed the reliability as the following mathematical form:

$$p_r = \int_{R \geq L} f(r, l)\, \mathrm{d}r\mathrm{d}l, \tag{2.1}$$

in which p_r denotes the reliability, R and L denotes the random strength and stress, respectively; $f(r, l)$ denotes their joint probability distribution. The lower case of R and L represents a realization of the corresponding random variable. To calculate the reliability, one first establishes probabilistic models for the strength and the stress separately. Depending on the nature of randomness, the strength and the stress may be modeled by either a random variable or a stochastic process. For time-variant variables such as wind load and deteriorating strength, extreme value analysis is usually employed to find the statistical distributions of their maximum or minimum values during the nominal design life, assuming that the stochastic processes are stationary. The strength and stress may be further modeled if necessary as functions of some basic random variables. The reliability is then calculated using first-order or second-order reliability methods, or simulation techniques. This is called the *Stress-Strength Interference (SSI) approach.* Details on the methods for reliability analysis based on the SSI approach can be found in, e.g., Ang and Tang (1975), Thoft-Christensen and Baker (1982), Madsen, Krenk, and Lind (1986), Ditlevsen and Madsen (1996), and Melchers (1999). A recent thorough investigation of

this approach in a statistical inference fashion can be found in Kotz, Lumelskii, and Pensky (2003). Although the SSI approach is traditionally used in structural engineering, strength and stress should be better understood as the capacity and demands accordingly. Knowing this one would not be puzzled that nowadays many other engineering disciplines and even social sciences such as psychology also employ the SSI approach to reliability analysis.

Engineers in other disciplines such as electrical and electronic engineering and plant engineering concerns mainly the system availability and maintainability. To ensure system availability, the component lifetimes are essential information. Life testing and statistical inference from the lifetime data are their approach. This is called the *Lifetime approach.* How to deal with incomplete information such as censored or missed failure time data is one of the main themes in the research of lifetime data analysis. For more details on these topics, refer to, for example, Barlow and Proschan (1981), Gertsbakh (1989), Nelson (1990), Crowder et al. (1991), Meeker and Escobar (1998), Kalbfleisch and Prentice (2002), and Lawless (2003).

Although both approaches give a probabilistic measure of reliability, they have their own advantages and disadvantages. One of the advantages of the SSI approach is that it provides the sensitivity information during the reliability analysis. This is important because from the sensitivity information engineers would know the direction of optimizing their designs in order to achieve the reliability and cost target. Its drawback is that it usually gives only the reliability at one point of time and fails to provide an explicit interpretation of the reliability profile along time. Although many research efforts have been made in the last two decades to accommodate the stochastic process into the SSI approach via outcrossing theory, the present time-dependent reliability analysis still needs many unrealistic assumptions and simplifications.

The advantage of the Lifetime approach is that one can easily see from the failure rate function the deterioration of the system performance as the time elapses, which enables

one to specify the maintenance policies as early as the design stage. But this approach does not directly consider the physical mechanism of failures. As a result, condition-based maintenance decisions can hardly be made from this approach.

The last two decades have witnessed the trend of merging the two isolatedly developed approaches into a stochastic process approach. As systems become more and more reliable, collecting enough data for confident statistical inferences is more and more difficult because of prohibitive cost and tight time constraint in the competitive market environment. Even if enough data can be collected from accelerated life tests, the validation of underlying failure mechanisms is difficult. Furthermore, a lifetime distribution is argued to be static in the sense that it is not suitable for describing the lifetime of items that operate in dynamic environments and hence not applicable for condition-based maintenance decision making. From the viewpoint of modern civil engineers, on the other hand, their major concern has been shifted from designing and building new structures and facilities to maintaining the existing but aging ones with safety and satisfying performance. The traditional time-dependent reliability theory using the SSI approach is clearly not adequate as the Poisson assumption underlying in the outcrossing technique implies a *no-action-until-failure* paradigm (Mori and Ellingwood 1993, 1994a, 1994b). One way to overcome the above difficulties is by examining the underlying failure mechanisms using appropriate stochastic processes and thus updating the lifetime distribution in a dynamic fashion with the aids of inspection data (Singpurwalla 1995). It is in this context that van Noortwijk and his co-workers advocate the use of stochastic process based models in bridge maintenance decision making (van Noortwijk and Frangopol 2004; Frangopol, Kallen, and van Noortwijk 2004; van Noortwijk and Klatter 2004). It is believed that the merge in the framework of the *stochastic process approach* be the new direction of reliability theory.

2.2 Stochastic Modeling of Deterioration

Deterioration modeling is closely related to failure modeling in the context of risk and reliability analysis. Deterioration-related failures can be classified into shock failures and first passage failures. A shock failure, also called a traumatic or 'hard' failure in literature, occurs when a traumatic event (e.g., severe earthquakes, tornadoes, tsunami, lightning, etc.) happens , no matter how healthy the system was before the event happens. In contrast, a first passage failure relates directly to the continuous deterioration process and is thus also classified as a 'soft' failure. It occurs when the deterioration process reaches to some threshold over which that the system no longer works. This literature review places emphasis on the first passage type of failures except explicitly mentioned otherwise. For a review of general stochastic failure models, see, for example, Singpurwalla (1995).

There are many different degradation mechanisms, brittle fracture, creep, fatigue, wear and corrosion, just to name a few. We are not going to discuss physical modeling of a specific deterioration phenomenon; rather we treat deterioration as a stochastic process and review the inherent probabilistic structures in different models. For a general overview of the physical and mechanical mechanisms of various deterioration phenomena, readers may refer to the special tutorial series in IEEE Transactions on Reliability starting with Dasgupta and Pecht (1991).

The literature review of stochastic deterioration models in the next is to be proceeded in the order of model complexity. Starting from the simplest random variable models, the discussion is followed by marginal distribution models, second-order process models, and finally full distribution models. The full distribution models are further divided into cumulative damage models, pure jump process models, and stochastic differential models.

2.2.1 Random Variable Model

A random variable model describes the randomness of the deterioration process by a finite-dimension random vector Θ as

$$X(t) = g(t; \Theta) \tag{2.2}$$

where g is a deterministic function with $g(0, \Theta) \equiv 0$. Once the probability distribution of Θ is determined, the distribution of $X(t)$ is also known using, for example, transformation techniques for functions of random variables (Soong 2004). The distribution of the first passage time, defined as

$$\Pr\{T \leq t\} = \Pr\{X(t) \geq \zeta, X(s) < \zeta, \text{ for } 0 \leq s < t\}, \tag{2.3}$$

where ζ is the predetermined failure threshold, can be computed in a straightforward manner as well.

Usually the functional form of g in (2.2) is suggested from empirical studies. For example, the well-known Paris-Erdogan law expresses the fatigue crack size at time t, $A(t)$, by the following nonlinear function (Sobczyk and Spencer 1992):

$$A(t) = \frac{A_0}{\left[1 - C\beta A_0^{\beta} t\right]^{1/\beta}}, \tag{2.4}$$

in which A_0 denotes the initial crack size at $t = 0$; C and β are empirical material constants that are functions of stress intensity factor. A simple stochastic Paris-Erdogan law replaces the parameters (A_0, C, β) with random variables in order to capture the scatter in stress intensity, material properties and environmental factors.

Two special forms of random variable models were extensively used in time-dependent structural reliability analysis. The first one relates to the deterioration modeling of structural resistance $R(t)$ that assumes a random initial resistance R_0 and a deterministic

and possibly nonlinear deterioration curve $g(t)$ (Kameda and Koike 1975; Oswald and Schueller 1984; Ellingwood and Mori 1993; Mori and Ellingwood 1993a; Mori and Ellingwood 1993b; Lewis and Chen 1994; Enright and Frangopol 1998; Melchers 1999; Huang and Askin 2004), i.e.,

$$R(t) = R_0 [1 - g(t)]. \tag{2.5}$$

The other special random variable model is the so-called random rate model, in which the deterioration is assumed a linear function of time with a random deterioration rate, i.e.,

$$X(t) = Bt, \tag{2.6}$$

in which B denotes the deterioration rate. If there is another constant A added in the linear model above and both the intercept A and the rate B are normally distributed, then the distribution of the first passage time is called Bernstein's distribution, a three-parameter normal distribution with variance a function of time as (Gertsbakh and Kordonskiy 1969)

$$F_T(t) = \Pr\{A + Bt \geq \zeta\} = 1 - \Phi\left[\frac{\zeta - \mu_A - \mu_B t}{\sqrt{\sigma_A^2 + \sigma_B^2 t^2}}\right] = 1 - \Phi\left[\frac{t - \alpha_0}{\sqrt{\alpha_1 + \alpha_2 t^2}}\right] \tag{2.7}$$

where $\Phi(\cdot)$ denotes the cumulative distribution function of standard normal distribution, μ_A, μ_B, σ_A^2 and σ_B^2 are mean and variance of A and B, respectively, and $\alpha_0 = (\zeta - \mu_A)/\mu_B$, $\alpha_1 = \sigma_A^2/\mu_B^2$ and $\alpha_2 = \sigma_B^2/\mu_B^2$.

Motivations of using random variable models are two-fold. First, the random variable models are simple. Second, they are directly related to statistical analysis of deterioration data. Given a set of deterioration data, an analyst's first response may be using regression techniques — fit the data with some kind of curves! That idea is exactly what appears in (2.2) if some or all of the model parameters are randomized to model the random effects across samples. In this context, the random variable models are also called *general degradation path* models. Typical example of such is Lu and Meeker (1993). More detailed

discussions on statistical methods and models for deterioration data are to be made in Section 2.2.7.

2.2.2 Marginal Distribution Model

Instead of randomizing the parameters of general deterioration curves, a marginal distribution model specifies directly a probability distribution for the deterioration at any time t as

$$X(t) \sim D[\theta_1(t), \cdots, \theta_n(t)], \tag{2.8}$$

in which D denotes symbolically the distribution, and $\theta_1, \cdots, \theta_n$ are the associated parameters of D, which are usually assumed to be functions of time to reflect the change with time of moments of deterioration. The parameters can be estimated by moment methods or by the least squares technique as proposed by Zuo, Jiang, and Yam (1999) for Weibull distribution.

Extreme cautions should be exercised, however, when the distribution of first-passage time is to be derived when using the marginal distribution models. Since the marginal distribution model does not specify the correlation between values of deterioration at two different times, the sample path behavior of $X(t)$ is not specified. Therefore, Simply applying the following equation

$$\Pr\{T \leq t\} = \Pr\{X(t) \geq \zeta\} = 1 - F_X(\zeta; \theta_1(t), \cdots, \theta_n(t)), \tag{2.9}$$

in which F_X is the CDF of $X(t)$, to find the first passage time distribution is not correct. But this type of calculations has been observed not rarely in the literature (Li 1995; Yang and Xue 1996; Xue and Yang 1997; Zuo, Jiang, and Yam 1999). In order to solve the problem, additional assumptions are necessary for the dependence structure of the deterioration path. One of the simplest assumptions for this is through auto-covariance functions, which leads to second-order process models as discussed next.

2.2.3 Second-Order Process Model

A second-order process model, as indicated by the name, specifies the first two moments of deterioration, i.e., the mean and auto-covariance function. Since the deterioration must be non-negative and nonstationary, direct specification of its auto-variance functions is inconvenient. To bypass this difficulty, an auxiliary non-negative stationary process $Y(t)$ is multiplied, for example, with the mean deterioration curve $g(t)$ as

$$X(t) = Y(t)\, g(t)\,. \tag{2.10}$$

To further reflect the non-Gaussian property of $X(t)$, $Y(t)$ is assumed a translation process that is generated from a stationary zero-mean Gaussian process $G(t)$ with specific correlation structure by the memoryless transformation (Grigoriu 1984; Zheng and Ellingwood 1998):

$$Y(t) = F^{-1}\left[\Phi\left\{G(t)\right\}\right], \tag{2.11}$$

where F is the cumulative distribution function of $Y(t)$.

An example of this kind is the log-normal process proposed by Yang and Manning (1996) for fatigue crack growth as the following. Instead of a random variable model such as (2.4), the authors introduced a stationary log-normal process to capture the fluctuations in fatigue crack growth as

$$\frac{dA}{dt} = X(t)\, g(t, \Theta)\,, \tag{2.12}$$

in which $X(t)$ is the log-normal process with a unit median and a covariance function as follows

$$\operatorname{cov}\left[X(t_1), X(t_2)\right] = \sigma_X^2 e^{-|t_2 - t_1|/\tau}, \tag{2.13}$$

in which τ is the so-called correlation length. In order to get a simple closed-form expression for the crack exceedance probability and thus the distribution of service time to

reach any crack size, they further proposed a second-order approximation for the quantity $\int_0^t X(s)\,ds$. With the correlation being considered, the analysis method was proved to be flexible enough to cover a wide range of dispersion characteristics in predicting the stochastic crack growth (McAllister and Ellingwood 2001; Wu and Ni 2003).

Note, however, it is not easy in the real world to collect sufficient data for an accurate estimation of the correlation or covariance functions. Therefore, strong assumptions (e.g., a constant coefficient of correlation along time) may have to be made (Li and Melchers 2005a, b) , which jeopardizes the applications of the model in more general deterioration modeling practices.

2.2.4 Cumulative Damage/Shock Model

In a cumulative damage (CD) model, deterioration is deemed to be caused by shocks and accumulates additively. CD models are also called shock models in the literature. Let us denote by D_i the damage size caused by the ith shock and by $N(t)$ the number of shocks up to time t. Then the deterioration, $X(t)$, is expressed by

$$X(t) = \sum_{i=1}^{N(t)} D_i. \tag{2.14}$$

Suppose the times between two successive shocks are modeled by W_1, W_2, ... We have

$$N(t) = \min\left\{ n = 0, 1, 2, \cdots \middle| \sum_{i=1}^{n+1} W_i > t \right\}. \tag{2.15}$$

That is, $N(t)$ is a counting process that counts the number of shocks up to time t. Therefore, the CD model specifies two probability laws: one for the counting process $N(t)$, or equivalently for the inter-occurrence time W_i, and the other for the damage size D_i each shock causes. The simplest example of the CD model is the compound Poisson process in which $N(t)$ follows a Poisson process, or W_i follows an exponential

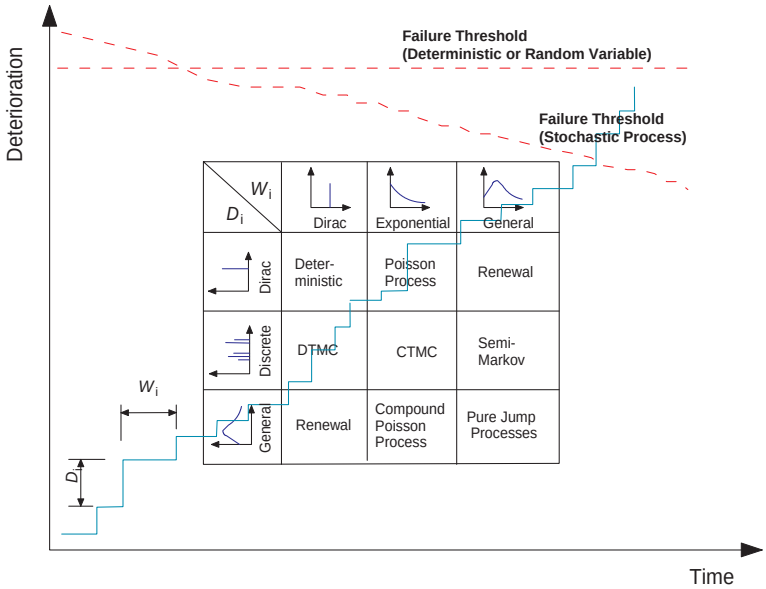

Figure 2.1: Typical cumulative damage models

distribution, whereas D_i is a non-negative random variable. When the damage size D_i is fixed or follows a Dirac distribution, the compound Poisson process reduces to a simple Poisson process scaled by the value of D_i.

Figure 2.1 shows several typical cumulative damage models according to different assumptions on W_i and D_i. If W_i is fixed, say $W_i = 1$, and D_i is discretely distributed, $X(t)$ is a discrete-time Markov chain model, as the discrete distribution of D_i stipulates a transition probability as

$$\Pr\{X_{t+1} = j \,|X_t = i\} = \Pr\{D_i = j - i\}. \tag{2.16}$$

If W_i is not fixed but follows an exponential distribution, then the deterioration becomes a continuous-time Markov chain model. Yet if W_i follows a general distribution, a semi-Markov chain characterizes the deterioration. These correspond to the three models in the middle row of the table in Figure 2.1. If both W_i and D_i follow some general

distributions, the deterioration is said, in the terminology of Morey (1966), to follow a compound renewal model.

The survival function, $S(t)$, or probability that a component will survive t units of time in a CD model has the following general mathematical form:

$$S(t) = \sum_{k=0}^{\infty} \Pr\{M > k\} \Pr\{N(t) = k\}, \tag{2.17}$$

in which M denotes the random number of shocks survived. For the first passage type of failures, $\Pr\{M > k\}$ equals the kth convolution of distribution function of D_i, i.e., $\Pr\{M > k\} = F_1(\zeta) * F_2(\zeta) * \cdots * F_k(\zeta)$, in which $F_i(\cdot)$ is the CDF of D_i and ζ is the failure threshold. For a shock-type failure, i.e., shocks either make the component fail if $D_i \geq \zeta$ or have no influence otherwise, $\Pr\{M > k\} = \prod_{i=1}^{k} [1 - F_i(\zeta)]$. This model is also called an *extreme shock model* (Gut and Hüsler 1999).

Fatigue of metals and composite materials has provided the first stimulus from engineering for the development of mathematical models of cumulative damage. The first deterministic CD model was proposed, according to Saunders (1982), by Palmgren in 1924, who sought to calculate the lifetime of ball bearings due to high-cycle fatigue. This result, now known as Palmgren-Miner rule (Miner 1945), was reinterpreted by Birnbaum and Saunders (1958) in a renewal process framework. Later they proposed a new lifetime distribution for fatigue, now bearing their names, based also on renewal theory (Birnbaum and Saunders 1969). More recently, the Markov chain models were successfully applied to model fatigue crack growth (Bogdanoff and Kozin 1985; Ganesan 2000a; Ganesan 2000b).

Largely owing to its nice "*no after-effect*" property and the ease of statistical inference, the Markov chain models have also been widely used for bridge deck deterioration (Madanat and Ibrahim 1995a; Madanat and Ibrahim 1995b; DeStefano and Grivas 1998), storm water pipe deterioration (Micevski, Kuczero, and Coombes 2002) and many other deterioration phenomena.

Compound Poisson processes were first proposed by Mercer and Smith (1959) for modeling the wear of a conveyor belt. Later Morey (1966) generalized it to a compound renewal process model. Gertsbakh and Kordonskiy (1969) used the Poisson process model to explain when an exponential distribution or a gamma distribution is appropriate for the lifetime.

Since semi-Markov process was presented by Lévy and Smith independently in 1954, the semi-Markov chain model has been applied to various fields. Its applications before 1984 can be found in Janssen (1984). More recent applications on reliability are summarized by Limnios and Oprişan (2001). The applications of SMC on deterioration modeling for maintenance optimization can be found in, for example, Feldman (1976), Gottlieb (1982), Posner and Zuckerman (1986),Osaki (1985), and Abdel-Hameed (1995).

Esary, Marshall, and Proschan (1973) first proposed the shock models in the general form of (2.17) and assumed shocks are governed by a homogeneous Poisson process. These shock models were later extended into the cases of nonhomogeneous Poisson processes and pure birth processes by Abdel-Hameed and Proschan (1973, 1975).

There are three common assumptions underlying in the CD models: (1) $W_1, W_2, \cdots$ are independent and identically distributed (i.i.d.); (2) $D_1, D_2, \cdots$ are also i.i.d.; and (3) W_i's and D_i's are independent of each other. Relaxation of these assumptions leads to a pure jump process model in general, which is to be discussed in the next subsection.

2.2.5 Pure Jump Process Model

A stochastic process $X(t)$ is said to be an increasing pure jump process if $X(0) = 0$ and for each $t \geq 0$ we have (Abdel-Hameed 1984a; Drosen 1986)

$$X(t) = \int_{(0,t]\times(0,\infty)} c(X(s-), z)N(ds, dz), \tag{2.18}$$

in which $X(s-)$ is the left limit of $X(t)$ at time s; and $N(ds, dz)$ is called *random measure* or jump measure that is an integer-valued random variable characterizing the number of shocks occurring in the time interval $[s, s + ds)$ with magnitudes in $[z, z + dz)$. A simple example of the random measure is a Poisson random measure that is independent and Poisson distributed for any disjoint subsets $(s_k, t_k] \times (u_k, v_k]$, $(k = 1, 2, \ldots)$. The non-negative, deterministic function $c(x, z)$ represents the damage caused by a shock of magnitude z when the deterioration state is x. We often assume $c(x, z)$ a non-decreasing function of z in order to reflect the fact that greater shocks usually induce bigger damages.

This construction has several advantages. First of all, it describes explicitly the dependence of damage size on both the shock magnitude and the present deterioration level through function $c\,(x, z)$. Moreover, unlike in the compound Poisson process, the occurrence intensity of shocks in the pure jump process can be related to the magnitude of shock, z, as well. Furthermore, the pure jump process $X(t)$ can have an infinite number of shocks or jumps in a finite time interval. For example, suppose $N(ds, dz) = dsdz/z^2$, then $N([s, t] \times (0, \epsilon)) = \int_s^t ds \int_0^\varepsilon dz/z^2 = +\infty$ for any $\epsilon > 0$ and $0 \leq s < t$. The infiniteness of the number of jumps/shocks, when some conditions for boundedness of $X\,(t)$ are satisfied, allows one to model, in a unified way, different shocks that may be very big but rare, or very small but frequent. For details on this discussion, see Drosen (1986).

Examples of pure jump processes include compound Poisson processes, pure-birth processes, gamma processes, and Lévy processes, just name a few. When $N\,(ds, dz)$ is a Poisson random measure and $c\,(x, z)$ is a function only of z, the pure jump process becomes a Lévy process, of which the gamma process is a special case. When the function $c(x, z)$ is an arbitrary Borel function, $X\,(t)$ is called a marked point process. More details about random measure, Lévy processes and marked point processes can be found in Daley and Vere-Jones (1988), Sato (1999), Sato (2001), and Cont and Tankov (2005).

Abdel-Hameed (1984a) gave a concise non-measure introduction of pure jump Markov processes. He may be the first person who used the pure jump process to model the dete-

rioration Abdel-Hammed (1984b, 1984c). Drosen (1986) also investigated the pure jump shock models in reliability. Shaked and Shanthikumar (1988) gave a weaker condition than that in Drosen (1986) on the parameters of the pure jump process under which the first passage time has certain lifetime distribution properties such as increasing failure rate. Abdel-Hameed (1987) studied the inspection and maintenance policies of devices subject to pure jump shock damage.

As a special pure jump process, a gamma processes is a continuous-time stochastic process with stationary and independent increments that are gamma distributed with common scale parameter. Due to its mathematical tractability, gamma processes have been used during the last three decades to model a vast variety of degradation phenomena such as concrete creep (Çinlar, Bazănt, and Osman 1977), rock transport in berm breakwaters (van Noortwijk and van Gelder 1996), rock rubble displacement (van Noortwijk, Cooke, and Kok 1995), current-induced scour erosion in block mats of the Eastern-Scheldt barrier in the Netherlands (van Noortwijk and Klatter 1999), sand erosion in Dutch coastline (van Noortwijk and Peerbolte 2000), fatigue crack growth (Lawless and Crowder 2004), steel corrosion of pressure vessel (Kallen and van Noortwijk 2005), feeder wall thinning due to flow accelerated corrosion (Yuan, Pandey, and Bickel 2006), and diametral expansion of fuel channels in nuclear power plants under neutron irradiation and thermal stresses.

Relevant to the pure jump process models are Markov additive processes (MAP). The MAP model, introduced by Çinlar (1972), provides a more flexible tool to model the additive deterioration under a dynamic environment that is further modeled by a Markov model. An important result of interest is that when the additive process is a gamma process with its shape parameter varying as a function of a Brownian motion, the first passage lifetime distribution is Weibull (Çinlar 1977). The optimal replacement policy for systems governed by a MAP has been discussed by Feldman (1977).

2.2.6 Stochastic Differential Equation Model

Both the CD models and the pure jump process models take a macroscopic approach to modeling deterioration. Emphases have been placed on the probabilistic mechanisms of deterioration growth with no explicit consideration of the effects of the external and internal driving forces on the growth of deterioration. A stochastic differential model, however, provides a microscopic description of the deterioration development.

Suppose a differential equation of the following form has been derived from empirical investigations

$$\frac{dX(t)}{dt} = m(X(t), t), \tag{2.19}$$

in which $m(\cdot)$ is a deterministic function and represents the mean curve in the differential relationship. To describe the variability over the mean trend, it is reasonable to add a noise term in the right hand side as

$$\frac{dX(t)}{dt} = m(X(t), t) + \sigma(X(t), t)\varepsilon(t), \tag{2.20}$$

in which $\varepsilon(t)$ denotes the noise term and $\sigma(\cdot)$ is another deterministic function to represent the interaction between the noise and the present deterioration state. The noise $\varepsilon\,(t)$ is usually assumed to be a Gaussian white noise, namely, for any two different times the noises are independent and identically distributed normal variables. Under this assumption, (2.20) can be rewritten as

$$dX(t) = m(X(t), t)dt + \sigma(X(t), t)dB(t) \tag{2.21}$$

in the Itô's sense, where $B(t)$ represents the standard Wiener process.

The process $X(t)$ satisfying (2.21) is known as a diffusion process. Its conditional probability density function, $p(x, t|x_0, t_0)$, at any time t given $X\,(t_0) = x_0$ satisfies the

Fokker-Planck (FP) equation as

$$\frac{\partial}{\partial t}p(x,t|x_0,t_0) + \frac{\partial}{\partial x}\left[m(x,t)p(x,t|x_0,t_0)\right] - \frac{1}{2}\frac{\partial^2}{\partial x^2}\left[\sigma^2(x,t)p(x,t|x_0,t_0)\right] = 0, \qquad (2.22)$$

with certain initial and boundary conditions (Karlin and Taylor 1981). Theoretically, the first passage time distribution can be found by solving the FP equation. However, very few exact solutions exist in practice, and approximations and numerical methods are usually used. For more details, see, for example, Lin and Cai (1995), and Soong and Grigoriu (1993).

Stochastic differential models have been applied to random fatigue crack growth (Sobczyk and Spencer 1992). Lemoine and Wenocur (1985) and Wenocur (1988) discussed the stochastic differential models with extra Poisson killing due to traumatic failures and they expressed the survival probability as a Feymann-Kac functional.

The assumption of Gaussian white noises may be too strong in some cases. Some efforts have been made to relax this assumption into, say non-Gaussian white noise. Grigoriu (2002) discussed in details stochastic calculus with Lévy and Poisson white noises using advanced analysis tools such as martingale theory. Ciampoli (1998) presented a reliability assessment methodology for deteriorating structural systems using stochastic differential equations driven by Poisson noises. A case study of deteriorating shear walls in a nuclear power plant due to expansive alkine-aggregate reactions of concrete was reported by Ciampoli (1999).

2.3 Statistical Models and Methods for Deterioration Data

2.3.1 Nature of Deterioration Data

Deterioration data often show some sort of randomness. The randomness underlying in the deterioration data can be decomposed into three parts: random effects, temporal un-

certainty or serial correlation, and measurement errors (Verbeke and Molenberghs 2000). Figure 2.2 illustrates the three stochastic components in deterioration data. Suppose the units of the population under consideration work in the same environment; that is, the fixed effects due to known covariates are assumed to have been considered. The thick solid line represents the population average path. The two thick dot-dash lines represent the individual average paths for unit i and j. The difference between the population and individual average path is referred to as random effects, effects due to unit heterogeneity that is not explained by observed covariates. The thin solid sinuous lines represent the actual deterioration path of the units. The haphazard curves demonstrate the temporal uncertainty meaning that knowing the present deterioration state does not necessarily ensure a certain prediction in the future. Since the deterioration usually does not change too abruptly, there exists some correlation between two neighboring time points. Therefore the temporal uncertainty is sometimes referred to as serial correlation. The dotted lines in the figure represent the actual observations of the deterioration of the units. The difference between the solid and dotted lines is due to the measurement error. An adequate statistical model for deterioration data should be able to consider all these three parts of randomness.

Deterioration data are often highly unbalanced in the sense that not an equal number of measurements is available for all units and/or that measurements are not taken at fixed instants of time. Due to their unbalanced nature, many deterioration data sets cannot be analyzed by using multivariate regression techniques Therefore, new statistical models and methods are needed.

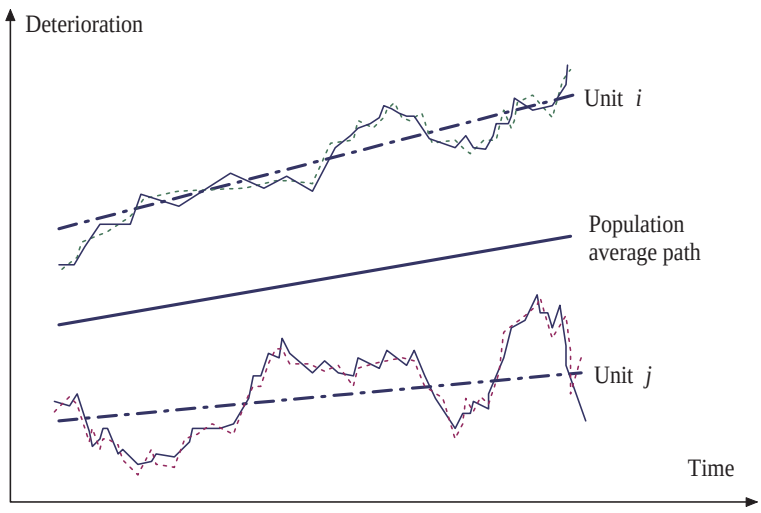

Figure 2.2: Components of randomness in deterioration data: random effects, temporal uncertainty and measurement errors

2.3.2 Mixed-Effects Regression Models

A general nonlinear mixed-effects (NLME) regression model for the ith unit with n_i measurements is expressed as (Pinheiro and Bates 2000)

$$\left.\begin{array}{c} y_{ij} = \eta\left(\beta, \Theta_i, x_{ij}, z_{ij}\right) + \varepsilon_{ij}, \quad i = 1, \ldots, n, \;\; j = 1, \ldots, m_i \\ \Theta_i \sim N\left(0, D\right), \, \varepsilon_i = \left(\varepsilon_{i1}, \ldots, \varepsilon_{im_i}\right)^T \sim N\left(0, \sigma^2 \Lambda_i\right) \end{array}\right\} \tag{2.23}$$

where $\eta(\cdot)$ is a nonlinear function denoting the average deterioration path, β is a p-dimensional vector of fixed effects; Θ_i is a q-dimensional random effects vector associated with the ith unit and it is assumed Gaussian distributed with mean zero and covariance matrix D; x_{ij} and z_{ij} are covariate vectors associated with fixed-effects parameters β and random-effects vector Θ_i, respectively; and ε_{ij} is a normally distributed within-unit error term. For deterioration models, the time, t_{ij}, at which the jth measurement of the ith unit is taken, is usually a natural covariate. In order to describe the temporal dependence structure of deterioration within one unit, the error terms ε_{ij} are assumed

to be correlated with covariance matrix $\sigma^2\Lambda_i$. The random-effects variable Θ_i are often assumed independent of each other and also independent of ε_i's. To correspond to the randomness decomposition as shown in Figure 2.2, the error terms can be factorized into two parts, one representing the stationary and independent measure error and the other representing the inherent serial correlation and/or heteroscedasticity (i.e., the changing variance). Accordingly, the covariance matrix Λ_i is expressed as

$$\Lambda_i = I_n + \tilde{\Lambda}_i, \tag{2.24}$$

where I_n is a unit matrix and $\tilde{\Lambda}_i = \Lambda_i - I_n$. When $\eta(\cdot)$ is a linear function of β and Θ_i,

$$y_{ij} = x_{ij}\beta + z_{ij}\Theta_i + \varepsilon_{ij}, \tag{2.25}$$

the NLME model becomes a linear mixed-effects (LME) regression model. When Θ_i's are identically zero, i.e., $D = 0$, the LME and NLME model degerate into the conventional linear and nonlinear models, respectively.

Parameter estimation for both LME and NLME models can be performed by the method of maximum likelihood in general. For LME models, the estimation is relatively simple due to the Gaussian and linearity assumptions. Computational efforts are mild and can be further reduced if the least squares (LS) technique, or the generalized LS technique when serial correlation or changing variance is considered, is incorporated with the profile likelihood maximization. In order to obtain unbiased estimate for σ^2, the restricted maximum likelihood method is usually used. In contrast, NLME models have no closed-form likelihood function for most cases, as the likelihood functions include a complicated high-dimensional integration. Numerical integration techniques are usually used but the numerical integration introduces numerical stability problems during the maximization procedure. More discussions on computing likelihood functions for NLME models can be found in Pinheiro and Bates (2000).

A computationally simple and intuitively appealing alternative to the maximum likelihood method is the so-called two-stage method (Lu and Meeker 1993). The two-stage method is carried out as the following: First of all, the deterioration model is fitted to each sample path separately and the Stage 1 estimates of the model parameters, say β, θ_i and σ^2, are obtained. Then, in the second stage, the Stage 1 estimates of the random-effects variables θ_i are treated as realizations of random variable Θ so that its mean and variance can be estimated accordingly. The Stage 1 estimates of fixed-effects parameter β and error term parameter σ^2 are usually pooled to obtain the population means. This method has also been adopted by some other researchers, for example, Caregy and Koenig (1991), and Crk (2000).

Statistical inferences for the mixed-effects models are traditionally made using large-sample theory (Lehmann 1999; Pinheiro and Bates 2000). Lu and Meeker (1993) proposed a parametric bootstrap simulation to find the confidence intervals for the estimated quantities. Liski and Nummi (1996) suggested an interative Expectation-Maximization (EM) algorithm for predicting future measurements for a unit with repeated measurements. In a Bayesian framework, Robinson and Crowder (2000) presented a Markov chain Monte Carlo (MCMC) simulation technique for estimating model parameters and constructing confidence bands of associated lifetime distributions. A similar MCMC technique was used by Hamada (2005) for a set of laser degradation data.

Applications of the mixed-effects models to designs of accelerated degradation tests or reliability improvement programs can be found at Meeker and Escobar (1998) and Chiao and Hamada (2001).

2.3.3 Statistical Inference for Stochastic Process Models

Two basic stochastic processes have been used extensively to model deterioration for lifetime and reliability prediction. They are Wiener process (or Brownian motion) models and gamma process models. Since the two processes have the common property of inde-

pendent increments, likelihood functions can be easily constructed and thus the maximum likelihood method is frequently used for parameter estimation and inferences. Recently a geometric Brownian motion was proposed for deterioration modeling in order to reflect the fact that deterioration is usually positive (Park and Padgett 2006). But estimating its parameters would not be more difficult than for the Wiener process, as a logarithm transform makes the former back to a Wiener process.

It has long been recognized that the first passage time of a Wiener process is an inverse Gaussian distribution. But the applications of Wiener processes on modeling degradation for lifetime in engineering may be traced back to Doksum and Hoyland (1992). Whitmore (1995) discussed the effect of measurement errors in degradation data when using a Wiener process model. Whitmore and Schenkelberg (1997) proposed a time-scale transformation of Wiener processes for accelerated degradation data. More acceleration models were considered by Padgett and Tomlinson (2004).

A breakthrough of using Wiener process models is Whitmore, Crowder, and Lawless (1998), in which they proposed a bivariate Wiener process model, one for the latent, unobservable deterioration process and the other for the observable marker that is somehow correlated with the deterioration. The term *marker* here is another name for a covariate that is usually time-varying and it is used widely in biomedical applications. An example of such a marker is the measurement of the deterioration contaminated by measure errors. Extensions of their work include Lee, DeGruttola, and Schoenfeld (2000) in which they considered static covariates and uncertain baseline information, and Hashemi, Jacqmin-Gadda, and Commenges (2003) in which they further considered random effects in the model.

Although the Wiener process has independent and Gaussian distributed increments, the likelihood function for a set of sample path records of a failed or surviving unit is not straightforward because of the diffusion property. Lu (1995) realized this fact and chose to use the terminology of *truncated Wiener process* to indicate the version of Wiener

process restricted by the predefined failure threshold ζ. Using four different methods, he derived the joint probability density function of $X(t)$ and the event $A = \{X(s) < \zeta \text{ for } 0 \leq s \leq t\}$ as the following

$$f(x, A) = \left\{ \frac{1}{\sqrt{2\pi\nu t}} \exp\left(-\frac{(x - \delta t)^2}{2\nu t} \right) \right\} \left[1 - \exp\left(\frac{2\zeta(x - \zeta)}{\nu t} \right) \right] \tag{2.26}$$

where δ and ν are the drift and diffusion coefficient, respectively. Note the term in the brace bracket is the density function for a conventional Wiener process. This expression can then be used for establishing the likelihood function (Lu 1995).

In contrast to Wiener processes, a gamma process has monotone increasing sample paths. This property makes the likelihood construction simple and straightforward. We are going to discuss the parameter estimation of gamma processes in detail in Chapter 5.

2.4 Concluding Remarks

Early studies on deterioration modeling adopted simple probabilistic models such as random variable models or marginal distribution models that focused more on the statistics of cross-sectional deterioration data. These methods provide ad hoc analyses and they do not consider an important issue of temporal dependence in a clear cut manner. Later on, more sophisticated stochastic models such as Markov pure jump models and stochastic differential models emerged. However, the focus of these studies was to derive probabilistic characteristics of lifetime and conditions for maintenance optimization. Statistical model fitting and validation through practical data were rarely investigated in the early literature. Some stochastic models are so complicated that the parameter estimation becomes unpractical.

In recent years, stochastic models with a rich probabilistic structure and simple methods for statistical inference (e.g. gamma process models) are emerging due to modern developments in computational technology and theory of stochastic processes. It is be-

lieved that use of such advanced models will become more common in the analysis of deterioration data.

Chapter 3

Linear Mixed-Effects Model for Deterioration

3.1 Introduction

Before discussing gamma process models, we would like to examine regression models at first. The regression model has a simple mathematical structure and has been extensively used for deterioration modeling in the engineering community. In this chapter we would like to discuss the underlying assumptions about the randomness of deterioration in this model and its limitation in predicting lifetime. To overcome the limitation, we propose a mixed-effects model in which the heterogeneity of individual units is described by a Gaussian random variable. A case study of creep deformation of pressure tubes in a CANDU reactor is performed, in which both regression and mixed-effects models are used.

3.2 Linear Regression Models

3.2.1 Ordinary Least Squares Method

Consider n units that have been inspected for deterioration. Suppose for now that each unit was inspected only once in a time interval $[0, t]$. Given the deterioration data (y_i, t_i), $i = 1, \ldots, n$, where y_i is the measured deterioration for the ith unit at time t_i, a linear regression (LR) model is expressed for each unit as

$$y_i = \beta_0 + \beta_1 t_i + \varepsilon_i \tag{3.1}$$

where ε_i is random noise, which is added to account for the deviation of the observed deterioration from the expected linear relationship. Depending on the context, the random noise can be interpreted as the measurement error or any other effect that cannot be explained by the explanatory variables (here, the time only). The noises $\varepsilon_1, \ldots, \varepsilon_n$ are usually assumed to be independent and identically distributed (i.i.d.) Gaussian random variables with mean zero and constant variance σ^2. In matrix form, we have

$$\mathbf{y} = \mathbf{X}\beta + \varepsilon, \qquad \varepsilon \sim N\left(\mathbf{0}, \sigma^2 \mathbf{I}\right), \tag{3.2}$$

in which

$$\mathbf{y} = \begin{pmatrix} y_1 \\ \vdots \\ y_n \end{pmatrix}, \mathbf{X} = \begin{pmatrix} 1 & t_1 \\ \vdots & \vdots \\ 1 & t_n \end{pmatrix}, \beta = \begin{pmatrix} \beta_0 \\ \beta_1 \end{pmatrix}, \varepsilon = \begin{pmatrix} \varepsilon_1 \\ \vdots \\ \varepsilon_n \end{pmatrix}. \tag{3.3}$$

and $\mathbf{I}_n$ denotes the n-dimensional unit diagonal matrix. Without loss of generality, we assume that the time is the only explanatory variable of deterioration. But this assumption can be easily relaxed by augmenting the matrix $\mathbf{X}$. Clearly, $\mathrm{E}\left[y\left(t\right)\right] = \beta_0 + \beta_1 t$ and $\mathrm{Var}\left[y\left(t\right)\right] = \mathrm{Var}\left(\varepsilon\right) = \sigma^2$.

The ordinary least squares (OLS) solution of the LR model minimizes the residual

sum of squares (RSS) defined by

$$RSS = (\mathbf{y} - \mathbf{X}\beta)^T (\mathbf{y} - \mathbf{X}\beta) \tag{3.4}$$

where the superscript T denotes the tranpose of a vector or a matrix. Simple algebraic operations lead to the OLS estimates

$$\hat{\beta} = \left(\mathbf{X}^T\mathbf{X}\right)^{-1} \mathbf{X}^T\mathbf{y} \tag{3.5}$$

and the unbiased estimate for the variance σ^2

$$\hat{\sigma}^2 = \frac{\left(\mathbf{y} - \mathbf{X}\hat{\beta}\right)^T \left(\mathbf{y} - \mathbf{X}\hat{\beta}\right)}{n-2}, \tag{3.6}$$

where the denominator $n-2$ is the degree of freedom of the LR model which in general case equals the number of observations minus the dimension of β.

It is well known that under the Gauss-Markov assumptions (i.e., $\mathrm{E}(\varepsilon) = \mathbf{0}$, and $\mathrm{Var}(\varepsilon) = \sigma^2\mathbf{I}$) the OLS estimator $\hat{\beta}$ is the best linear unbiased estimator (BLUE) for β, i.e., among all estimates that are linear combinations of the y's and unbiased, the OLS estimator has the smallest variance (Rao 1973; Rawlings, Pantula, and Dickey 2001). Under the extra assumption of Gaussian distribution for ε, the estimator $\hat{\beta}$ follows a multivariate Gaussian distribution and $\hat{\sigma}^2$ chi-square distribution. In particular, we have

$$\hat{\beta} \sim N\left(\beta, \sigma^2\mathbf{V}\right) \tag{3.7}$$

where $\mathbf{V} = \left(\mathbf{X}^T\mathbf{X}\right)^{-1}$, and

$$\frac{(n-2)\ \hat{\sigma}^2}{\sigma^2} \sim \chi^2_{(n-2)}. \tag{3.8}$$

It has been proved that the estimators $\hat{\beta}$ and $\hat{\sigma}^2$ are independent of each other (Rao 1973). So if the estimated value is used for σ^2 in (3.7), $\hat{\beta}$ becomes a multivariate Student's t

distribution. Based on this fact, we can construct confidence intervals (or region) for β. Note that equations (3.7) and (3.8) represent the probability measures for the sampling uncertainty of the estimates. When the number of data points n approaches infinity, the variance matrix $\mathbf{V}$ will go to zero and $\chi^2/(n-2)$ will concentrate on 1, and therefore the distribution of the estimators will degenerate to the true values, β and σ^2, respectively.

The unbiased estimate for the mean deterioration $\mu_y = \mathrm{E}[y]$ at a specified value of time, say τ, is

$$\hat{\mu}_y(\tau) = \mathbf{x}(\tau)\hat{\beta} = \hat{\beta}_0 + \hat{\beta}_1\tau, \tag{3.9}$$

where $\mathbf{x}(\tau) = (1 \quad \tau)$. As a linear combination of $\hat{\beta}$, the estimator of the mean deterioration, $\hat{y}(\tau)$, is also normally distributed with mean $\mathbf{x}(\tau)\beta$ and variance $\mathbf{x}(\tau)\mathbf{V}\mathbf{x}^T(\tau)\sigma^2$. Hence

$$\frac{\hat{\mu}_y(\tau) - \mu_y(\tau)}{\hat{\sigma}\sqrt{\mathbf{x}(\tau)\mathbf{V}\mathbf{x}^T(\tau)}} \sim t_{(n-2)} \tag{3.10}$$

the Student's t distribution with $n-2$ degrees of freedom. (3.9) is also an unbiased estimate for the future random observation of deterioration at time τ, $y(\tau)$. But the variance of the estimator includes an additional term for variance of the random noise ε, i.e. $\mathrm{Var}[\hat{y}(\tau)] = \mathrm{Var}\left(\mathbf{x}(\tau)\hat{\beta}\right) + \mathrm{Var}(\varepsilon) = \left(\mathbf{x}(\tau)\mathbf{V}\mathbf{x}^T(\tau) + 1\right)\sigma^2$. Similarly, we have

$$\frac{\hat{y}(\tau) - y(\tau)}{\hat{\sigma}\sqrt{1 + \mathbf{x}(\tau)\mathbf{V}\mathbf{x}^T(\tau)}} \sim t_{(n-2)}. \tag{3.11}$$

(3.10) and (3.11) can be used for constructing the confidence intervals for the mean deterioration and for the future observations of deterioration. The confidence interval about the future observation is also called a prediction interval.

3.2.2 Weighted Least Squares Method

The basic assumption for OLS to validate is that the random noises ε_i's are independent and have the same variance. When this assumption does not hold true, the model (3.2)

should be modified and the weighted least squares (WLS) method may be used to estimate the model parameters. This situation happens when the deterioration in one unit is measured several times in the inspection history or the variance of deterioration varying with time t.

When the units were inspected several times and we have m_i (> 1) repeated measurements of deterioration for the ith unit, the measured deterioration y_{i1}, y_{i2}, $\ldots$, y_{im_i} should be reasonably assumed dependent, i.e., $\varepsilon_i = (\varepsilon_{i1}, \ldots, \varepsilon_{im_i})^T \sim N\left(0, \sigma^2 \mathbf{\Sigma}\right)$ where $\mathbf{\Sigma}$ is a positive definite matrix. When Σ is given, the estimates for β and σ^2, using the weighted least squares, are

$$\hat{\beta} = \left(\mathbf{X}'\mathbf{\Sigma}^{-1}\mathbf{X}\right)^{-1} \mathbf{X}'\mathbf{\Sigma}^{-1}\mathbf{y} \tag{3.12}$$

and

$$\hat{\sigma}^2 = \frac{\left(\mathbf{y} - \mathbf{X}\hat{\beta}\right)^T \mathbf{\Sigma}^{-1} \left(\mathbf{y} - \mathbf{X}\hat{\beta}\right)}{n-2}. \tag{3.13}$$

But when Σ is not known, parametric models for the correlation may be helpful although validation of the correlation structure is difficult (Verbeke and Molenberghs 2000). An *ad hoc* way is to ignore the dependence and to assume $\mathbf{\Sigma}$ is a diagonal matrix with m_i on the diagonal so that each unit has the same contribution to the RSS.

Quite often the variance of deterioration may not be constant, but be a function of the mean value of deterioration, i.e., for the ith unit,

$$\sigma_i^2 = f\left(\mu_{yi}\right), \tag{3.14}$$

in which $\mu_{yi} = \beta_0 + \beta_1 t_i$. The function f is called variance function. In this case, the traditional approach to fitting is to use an iteratively weighted least squares (IWLS) technique (Sen 1990; Weisberg 2005). For each iteration, we use the WLS to estimate β, and then evaluate the residuals from which the variance function is estimated. This iteration procedure continues until convergence.

The modern approach to fitting the variance function is to use a generalized linear model (GLM) in which the distribution of the response (i.e., deterioration in our case) belongs to the exponential dispersion family with the form (Dobson 2002; Lindsey 1997; McCullagh and Nelder 1983)

$$f\left(y;\theta,\phi\right)=\exp\left\{\left(y\theta-b\left(\theta\right)\right)/a\left(\phi\right)+c\left(y;\phi\right)\right\},$$

for some specific functions $a\left(\phi\right), b\left(\theta\right)$ and $c\left(y;\phi\right)$. Since $\mu = E\left[Y\right] = b'\left(\theta\right)$ and $Var\left[Y\right] = b''\left(\theta\right)a\left(\phi\right) = V\left(\mu\right)a\left(\phi\right)$, the GLM has greater flexibility than the traditional LR model in modeling the relationship between the mean and variance. But the dependence of deterioration is more difficult to model in GLM than in the traditional LR model, because dependence in Gaussian distributions amounts to correlation whereas in other distributions this relationship breaks down. Since the dependence structure is vital in lifetime prediction, the limitation of LR in lifetime prediction to be discussed next may also apply to the GLM. Therefore we are not going to discuss the GLM any further.

3.2.3 Limitation of Linear Regression Models in Lifetime Prediction

In the linear regression model in which the random noises are assumed i.i.d. Gaussian random variables, the deterioration level $y\left(\tau\right)$ at a future time τ can be predicted from the Student's t distribution with $n-2$ degrees of freedom, as shown in (3.11). One may want to use this result to predict the lifetime of a unit, which is defined as the first time that the deterioration $y\left(\tau\right)$ exceeds a prescribed failure threshold, ζ. This immediately leads to

$$F_T\left(\tau\right)=\Pr\left\{y(\tau)\geq\zeta\right\}=1-tcdf\left(\frac{\zeta-\mathbf{x}\left(\tau\right)\hat{\beta}}{\hat{\sigma}\sqrt{1+\mathbf{x}\left(\tau\right)\mathbf{V}\mathbf{x}^T\left(\tau\right)}};n-2\right), \tag{3.15}$$

where $tcdf\left(u;\nu\right)$ denotes the cumulative distribution function of a Student's t distribution with ν degrees of freedom evaluated at u. However, this estimation of lifetime distribution

is not correct. Recall that the lifetime is defined as the first time when the deterioration path exceeds a threshold ζ, or symbolically,

$$T \equiv \inf\{y(t) \geq \zeta\} = \{t \,|\, y(t) \geq \zeta, Y(s) < \zeta \text{ for } 0 \leq s < t\}. \tag{3.16}$$

Equation (3.15) used the fact of $Y(t) \geq \zeta$ but missed the condition "$Y(s) < \zeta$ for $0 \leq s < t$". In order for the condition to be included, the sample path behavior of the LR model has to be considered carefully. But the assumption that random noises are i.i.d. Gaussian in the LR models implies that the deterioration should be a Gaussian white noise adding to the deterministic, mean curve $\mu_y(t) = \beta_0 + \beta_1 t$. Since the Gaussian white noise is so erratic, no meaning can be attached to its first-passage time. Therefore, the probability estimated by (3.15) should not be understood as the lifetime distribution in the first passage sense.

When the random noises are assumed correlated Gaussian for repeated measurements, the deterioration becomes a Gaussian process with linear mean function and some specified covariance function. In this case, the distribution of predicted deterioration in (3.11) is only an approximation because $\hat{\beta}$ and $\hat{\sigma}^2$ are no longer independent in this case. Even worse, an exact expression for the distribution of the first passage time of second-order Gaussian processes is still lacking to the author's knowledge. Intensive research efforts have been made to find the distribution of the first passage time in the last four to five decades, but most of the results were based either on upcrossing theory with Poisson assumptions for differentiable processes or on the Fokker-Planck equation for diffusion processes (Lin and Cai 1995).

One way to solve the problem could be by interpreting the error term ε_i as an measurement error. This interpretation implies a deterministic deterioration model because the actual deterioration becomes a linear function, i.e., $\bar{y}(\tau) = \beta_0 + \beta_1 \tau$. The randomness in the observed deterioration comes from the measurement error. Since it is the actual

but not the observed deterioration that defines the failure time, the lifetime is

$$T = \frac{\zeta - \beta_0}{\beta_1}, \tag{3.17}$$

in which no inherent randomness exists unless a Bayesian view is taken for β's. When the sampling uncertainty of β_0 and β_1 is considered, the probability distribution of the lifetime can be derived. Recall that the joint distribution of β_0 and β_1 is a multivariate t distribution, as indicated by (3.7), the lifetime distribution is similar to the Bernstein's distribution (Gertsbakh and Kordonskiy 1969) except that in the latter both the intercept and slope are independent and normally distributed, c.f. (2.7). But keep in mind that the lifetime distribution here is a measure of sampling uncertainty propagated to the lifetime.

Since the interpretation of the error term as measurement errors does not always make sense, especially when a varying variance as (3.14) is seen from the regression. A linear mixed-effects model discussed in the next may provide a logically consistent way to deal with varying variance, correlation in deterioration and lifetime prediction.

3.3 Linear Mixed-Effects Models

It would be more adequate to interpret the random noise ε as a term that includes both random effects and measurement errors. This is equivalent to assuming the regression coefficients as random variables instead of fixed, though unknown, parameters. This assumption leads to a linear mixed-effects (LME) model. Symbolically, we have, for unit i $(i = 1, \ldots, n)$,

$$y_i = \Theta_{0i} + \Theta_{1i} t_i + \varepsilon_i = \mathbf{x}\boldsymbol{\Theta}_i + \varepsilon_i \tag{3.18}$$

where $\mathbf{x} = (1 \quad t_i)$; $\mathbf{\Theta}_i = (\Theta_{0i} \quad \Theta_{1i})^T$ are assumed to be a bivariate Gaussian distribution with mean vector β and covariance matrix $\mathbf{D}$ as

$$\mathbf{D} = \begin{bmatrix} d_{11} & d_{12} \\ d_{21} & d_{22} \end{bmatrix}. \tag{3.19}$$

Assume $\mathbf{\Theta}_1, \ldots, \mathbf{\Theta}_n$ are i.i.d. Also assumed is that $\varepsilon_1, \ldots, \varepsilon_n$ are i.i.d. Gaussian $N\left(0, \sigma^2\right)$. Then the deterioration y_i is a linear function of three Gaussian random variables Θ_{0i}, Θ_{1i} and ε_i. Hence, y_i follows also a Gaussian distribution with mean $\mathrm{E}\left(\Theta_{0i} + \Theta_{1i} t_i + \varepsilon_i\right) = \beta_0 + \beta_1 t_i$ and variance $\mathbf{x}\mathbf{D}\mathbf{x}^T + \mathrm{Var}\left(\varepsilon\right) = d_{11} + \left(d_{12} + d_{21}\right) t_i + d_{22} t_i^2 + \sigma^2$. Hence, by introducing random effects into the linear model, the varying variance is explained and the awkward iteratively weighted least squares procedure discussed earlier is avoided.

The LME model also fits well the cases of repeated measurements. Indeed, for unit i that has m_i repeated measurements, the LME model has the following general form:

$$\mathbf{y}_i = \mathbf{X}_i \beta + \mathbf{Z}_i \mathbf{\Theta}_i + \varepsilon_i, \;\; \mathbf{\Theta}_i \sim N\left(\mathbf{0}, \mathbf{D}\right), \quad \varepsilon_i \sim N\left(0, \sigma^2 \mathbf{I}_{m_i}\right), \tag{3.20}$$

where

$$\mathbf{y}_i = \begin{pmatrix} y_{i1} \\ \vdots \\ y_{im_i} \end{pmatrix}, \mathbf{X}_i = \begin{pmatrix} \mathbf{x}_{i1} \\ \vdots \\ \mathbf{x}_{im_i} \end{pmatrix} = \begin{pmatrix} 1 & t_{i1} \\ \vdots & \vdots \\ 1 & t_{im_i} \end{pmatrix}, \beta = \begin{pmatrix} \beta_0 \\ \beta_1 \end{pmatrix}, \varepsilon_i = \begin{pmatrix} \varepsilon_{i1} \\ \vdots \\ \varepsilon_{im_i} \end{pmatrix} \tag{3.21}$$

and $\mathbf{\Theta}_i$ is a q-dimensional random vector and $\mathbf{Z}_i$ is a covariate associated with $\mathbf{\Theta}_i$. The dimension q can be 1 or 2, depending on whether the randomness of the intercept and slope is significant or not. Although the measurement errors $\varepsilon_{i1}, \ldots, \varepsilon_{i,m_i}$ are still assumed independent of each other, the observed values of deterioration at different times are no longer independent, as the covariance of y_{ij} and y_{ik} equals $\mathbf{z}_{ij}\mathbf{D}\mathbf{z}_{ik}^T > 0$ for $j \neq k$. Hence, the correlation between the repeated measurements of the same unit is considered while different sample paths are kept independent of each other.

In the LME model, the estimation of lifetime distribution is much straightforward. Since ε_i's are measurement errors, the lifetime distribution can be easily derived based on the actual deterioration $\bar{y}(\tau) = \mathbf{x}(\tau)\beta + \mathbf{z}(\tau)\boldsymbol{\Theta}$ in which $\boldsymbol{\Theta}$ is a bivariate Gaussian vector. Unlike in (3.17) where the uncertainty of lifetime comes only from the sampling uncertainty, this estimation includes the inherent randomness of the deterioration through the random coefficient $\boldsymbol{\Theta}$.

3.3.1 Parameter Estimation

Several methods of parameter estimation have been developed for linear mixed models. Among them, maximum likelihood (ML) and restricted maximum likelihood (REML) are the two most frequently used methods. For the model of (3.20), the likelihood function of the parameters in $\beta, \mathbf{D}$ and σ^2 is ready from the marginal distribution of $\mathbf{y}_i$, the deterioration for unit i. It is clear that the marginal distribution of $\mathbf{y}_i$ is $N(\mathbf{X}_i\beta, \mathbf{V}_i)$, where

$$\mathbf{V}_i = \mathbf{Z}_i\mathbf{D}\mathbf{Z}_i^T + \sigma^2\mathbf{I}_{m_i}. \tag{3.22}$$

Hence the log likelihood for unit i is

$$l_i = -\frac{1}{2}(\mathbf{y}_i - \mathbf{X}_i\beta)^T \mathbf{V}_i^{-1}(\mathbf{y}_i - \mathbf{X}_i\beta) - \frac{1}{2}\log|\mathbf{V}_i| \tag{3.23}$$

where $|\mathbf{V}_i|$ denotes the determinant of $\mathbf{V}_i$. In fact, given the variance $\mathbf{D}$ and σ^2, the regression coefficients β can be found from the generalized least squares as

$$\hat{\beta} = \left(\sum_{i=1}^{n}(\mathbf{X}_i^T\mathbf{V}_i^{-1}\mathbf{X}_i)\right)^{-1}\left(\sum_{i=1}^{n}(\mathbf{X}_i^T\mathbf{V}_i^{-1}\mathbf{y}_i)\right). \tag{3.24}$$

Substituting this estimate into the log likelihood function gives the profile log likelihood function of variance components $\mathbf{D}$ and σ^2. The variance components can then be obtained by maximizing the profile log likelihood. Since ML estimates tend to underestimate

the variance components, the REML method is usually adopted. But when the number of parameters is not very big, the estimates from both methods shall not differ too much. More technical details about ML and REML can be found in several contemporary textbooks about linear mixed models, for example, Pinheiro and Bates (2000).

Many numerical optimization routines can be used for the maximization purpose. Quite a few of them (e.g. MATLAB optimization toolbox) implement optimizations without the need of feeding explicitly gradient information. One further advantage of these routines is that they also provide useful outputs such as the maximized log likelihood and the Hessian matrix. The latter is used to derive the observed information matrix and standard errors of the maximum likelihood estimates (*m.l.e.*).

Estimation of the random coefficient $\mathbf{\Theta}$ for a specific unit is required when one wants to predict the future deterioration of the unit. Using the fact that $(\mathbf{y}_i \,|\, \mathbf{\Theta} = \theta_i) \sim N\left(\mathbf{X}_i\beta + \mathbf{Z}_i\theta_i, \sigma^2 I\right)$ and $\mathbf{\Theta}_i \sim N\left(\mathbf{0}, \mathbf{D}\right)$, the estimate for θ_i is

$$\hat{\theta}_i = \mathbf{D}\mathbf{Z}_i^T \left(\mathbf{Z}_i\mathbf{D}\mathbf{Z}_i^T + \sigma^2\mathbf{I}_{m_i}\right)^{-1} \left(\mathbf{y}_i - \mathbf{X}_i\beta\right). \tag{3.25}$$

This estimator is an empirical Bayes estimator as it can be regarded as the posterior mean of $\mathbf{\Theta}_i$ given observation $\mathbf{y}_i$. By 'empirical Bayes' we mean the fact that the (hyper)parameters in the prior distribution β and $\mathbf{D}$ are estimated from data but not from *a prior* assumption (Carlin and Louis 2000). More discussion on the relationship of mixed models and Bayesian analysis can be found in Demidenko (2004).

3.4 Case Study — Creep Deformation of Pressure Tubes in Nuclear Reactors

3.4.1 Background

Creep deformation of pressure tubes in fuel channels of a nuclear reactor due to irradiation damage induced by fast neutrons is an important degradation phenomenon, which must be considered for management of an aging reactor. The creep-induced diametral expansion of the pressure tubes causes flow by-pass of primary heat transport coolant around the fuel bundles and this may result in lower critical heat flux values. Safety margins to prevent fuel from overheating during operation must be maintained. The current design limit for pressure tube diametral strain, defined by the relative increase in the inner tube diameter at a chosen operating time from its original value, varies from station to station but the safety margins up to 5.1% have been validated. A challenging problem for plant engineers is to predict the end-of-life, the time when the pressure tubes exceeds the 5.1% diametral strain, based on the diametral expansion data collected from the inspection and surveillance program.

The objective of the case study is to estimate the creep strain rate and the lifetime of a pressure tube, with lifetime defined as the time when the diametral creep strain reaches the substandard threshold 5.1%. We also hope that the ideas introduced in the previous sections can be illustrated in the case study.

3.4.2 Exploratory Data Analysis

In this study, diametral expansion data from 61 out of the total 380 pressure tubes in a CANDU 6 reactor are analyzed. The 61 tubes were inspected at five different points in time, giving in total 76 measurements of the creep strain. The associated average flux and cumulative irradiation fluence are also recorded for every tube in the reactor. The measurements are highly unbalanced in the sense that most of the tubes were measured

Table 3.1: Number of repeated measurements of creep diametral strains in pressure tubes

Number of repeated measurements	1	2	3	4	5	Total
Number of tubes	51	7	2	0	1	61

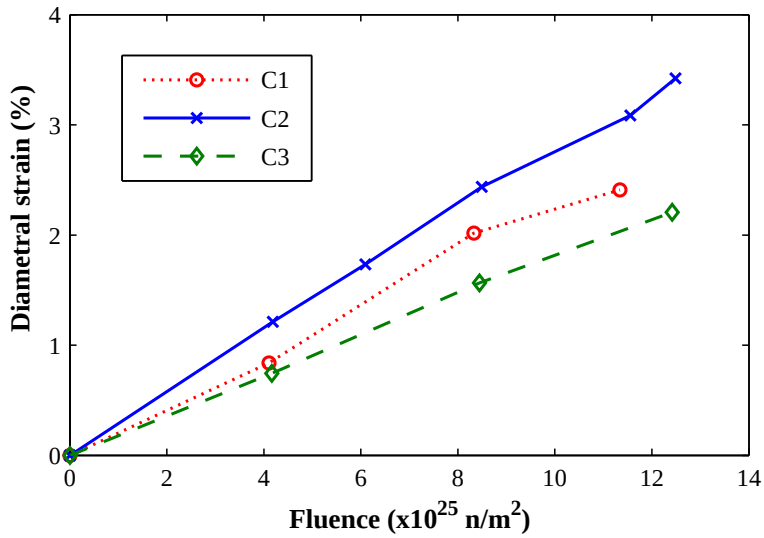

Figure 3.1: Typical sample paths of diametral strain with average fluence

only once and one tube five times (Table 3.1). To get some idea of the growth trend of the creep deformation, we plot in Figure 3.1 the sample paths of three tubes that were measured 3 or more times. They all show a fairly linear trend, which implies that a linear model can be used.

Note in this study we use as the time index the average fluence which is the product of average flux with operating time (measured by effective full power year or EFPY). Since different tubes have different average flux, the average fluences are different for the tubes even though they might be inspected at the same time.

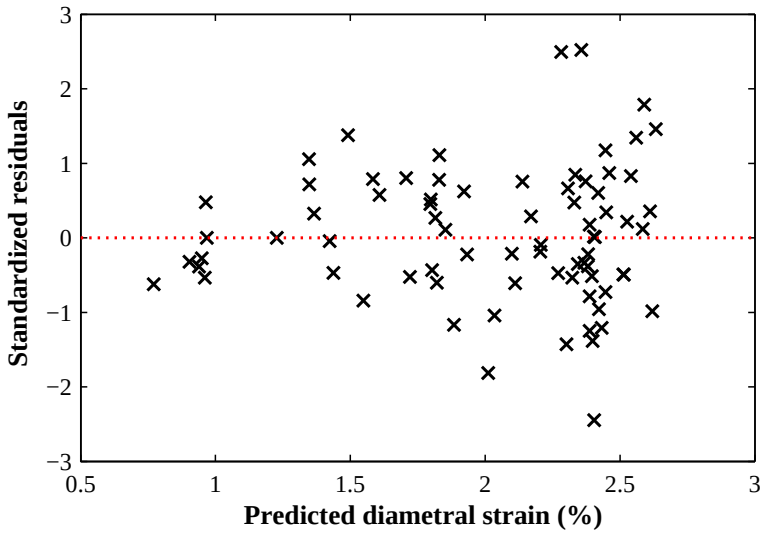

Figure 3.2: Standardized residuals from WLS

3.4.3 Linear Regression Models

Denote by y the creep strain in percentage and by Ψ the tube's average fluence at time t. As mentioned above, $\Psi = \phi t$, where ϕ is the average flux in unit of $\mathrm{n}/(\mathrm{m}^2 \cdot \mathrm{s})$. As a simple attempt, we first assume a linear regression model

$$y_i = a_0 + a_1 \Psi + \varepsilon_i, \tag{3.26}$$

for $i = 1, 2, \ldots, 76$, in which ε_i's are assumed to be independent of each other and $\varepsilon_i \sim N\left(0, m_i \sigma^2\right)$ where m_i is the number of repeated measurements. Using the WLS technique, the estimates are $\hat{a}_0 = 0.1234$ and $\hat{a}_1 = 0.2010$. But the residuals plot in Figure (3.2) shows that the residuals increases with the predicted diametral strain μ_y, indicating a varying variance of y. This is against the underlying assumptions of the WLS that σ^2 is a constant.

A quadratic variance function, $\sigma_i^2 = c\mu_{yi}^2$ where $\mu_{yi} = a_0 + a_1 \Psi_i$, is chosen to stabilize the variance. The corresponding IWLS estimates are $\hat{a}_0 = 0.0564$, $\hat{a}_1 = 0.2083$ and

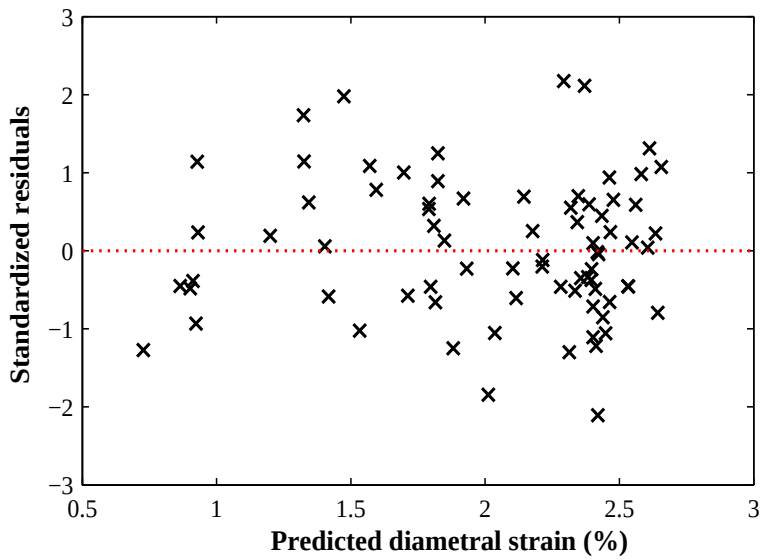

Figure 3.3: Standardized residuals from IWLS

$\hat{c} = 0.0127$. Now the standardized residuals shown in Figure (3.3) look more or less homogeneous. The fitted versus measured diametral strain is plotted in Figure 3.4. It is found that most of the observed data are within the 95% confidence bounds except tube C2 which are systematically outside of the bounds.

3.4.4 Linear Mixed-Effect Model

Although the variance function $\sigma_i^2 = c\bar{y}_i^2$ succeeded to stabilize the variance of error, the linear regression model is not appropriate for lifetime prediction, as we discussed earlier. This variance function, however, suggests a linear mixed-effects model as

$$\text{Model I:} \qquad y_{ij} = \beta_0 + \beta_1 \Psi_{ij} + \Theta_{0i} + \Theta_{1i}\Psi_{ij} + \varepsilon_{ij}, \tag{3.27}$$

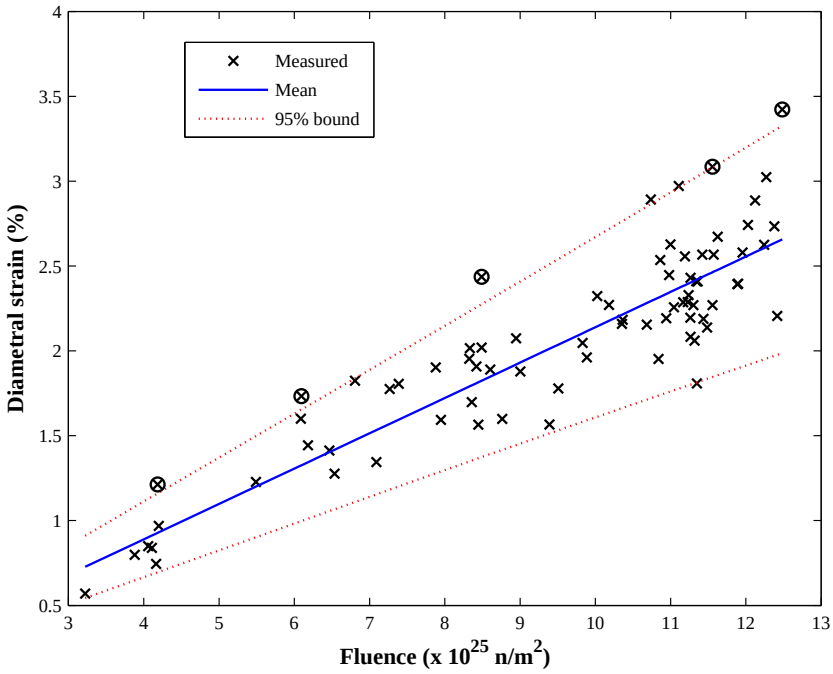

Figure 3.4: Predicted versus observed diametral strains from IWLS. The circled crosses represent data from Tube C2

for $i = 1, \ldots, n = 61$ and $j = 1, \ldots, m_i$ where most of m_i equals 1 as shown in Table 3.1. In the form of (3.20), we have $\mathbf{X}_i = \mathbf{Z}_i$ and

$$\mathbf{X}_i = \begin{pmatrix} \mathbf{x}_{i1} \\ \vdots \\ \mathbf{x}_{i,m_i} \end{pmatrix} = \begin{bmatrix} 1 & \Psi_{i1} \\ \vdots & \vdots \\ 1 & \Psi_{i,m_i} \end{bmatrix} \tag{3.28}$$

There are 6 parameters in total to be estimated: β_0, β_1, d_{11}, $d_{12} = d_{21}$, d_{22} and σ^2. Since the covariance matrix of $\mathbf{b}$, $\mathbf{D}$, should be nonnegative definite, this gives an implicit constraint for the parameter space of all the d's. To avoid the nuisance, we reparameterize $\mathbf{D}$ by using the Cholesky factorization, i.e.,

$$\mathbf{D} = \mathbf{U}^T\mathbf{U} \tag{3.29}$$

where $\mathbf{U}$ is an upper triangle matrix including entities u_{11}, u_{12} and u_{22} which can be any real number in theory. If the noise variance is also reparameterized as $\sigma^2 = \exp(s)$, then the log likelihood function can be maximized with respect to $\theta = (\beta_0,\, \beta_1,\, u_{11},\, u_{12},\, u_{12},\, s)^T$ in an unconstrained fashion.

The maximum likelihood estimates for the parameters are $\hat{\beta}_0 = 0.0503$, $\hat{\beta}_1 = 0.2090$, $\hat{\sigma}_\varepsilon = 0.0831$, $\hat{\sigma}_{\Theta_0} = 0.0353$, $\hat{\sigma}_{\Theta_1} = 0.0197$ and $\hat{\rho}(\Theta_0, \Theta_1) = 0.9999$ where $\hat{\rho}(\Theta_0, \Theta_1)$ represents the coefficient of correlation of the intercept Θ_0 and slope Θ_1. The corresponding maximized log likelihood is -82.53.

Since the coefficient of correlation of Θ_0 and Θ_1 (both have been assumed to be random variables) is very close to 1, we can thus assume only Θ_1 is random and $\Theta_0 = \alpha\Theta_1$ where α is a constant. Therefore we have $Z_i = (\alpha + \Psi_{i1}, \ldots, \alpha + \Psi_{im_i})^T$, or

$$\text{Model II:} \qquad y_{ij} = \beta_0 + \beta_1\Psi_{ij} + (\alpha + \Psi_{ij})\,\Theta_{1i} + \varepsilon_{ij}. \tag{3.30}$$

Under this new assumption, we have $\hat{\beta}_0 = 0.0503$, $\hat{\beta}_1 = 0.2090$, $\hat{\sigma}_\varepsilon = 0.0831$, $\hat{\sigma}_{\Theta_1} = 0.0197$

which are the same as before and $\hat{\alpha} = 1.7916$ which equals $\hat{\sigma}_{\Theta_0}/\hat{\sigma}_{\Theta_1} = 0.0353/0.0197$.

Alternatively, we choose the slope, denoted as Θ for brevity, as the only random coefficient and let the intercept fixed for all units. This amounts to assuming $\mathbf{Z}_i = (\Psi_{i1}, \ldots, \Psi_{i,m_i})^T$ or

$$\text{Model III:} \qquad y_{ij} = \beta_0 + \beta_1 \Psi_{ij} + \Psi_{ij}\Theta_i + \varepsilon_{ij} \tag{3.31}$$

Under this assumption, we obtain $\hat{\beta}_0 = 0.0637$, $\hat{\beta}_1 = 0.2077$, $\hat{\sigma}_\varepsilon = 0.0864$, $\hat{\sigma}_\Theta = 0.0232$ with maximized log likelihood of -83.08. It is clear from the likelihood ratio test that it is plausible to assume a fixed intercept. We adopt Model III for the next discussion.

In order to validate the assumptions of (1) normal within-unit measurement errors and (2) normal random slope in the model, the normal quantile plots for the within-unit residuals ε_{ij} $(i = 1, \ldots, n = 61;\ j = 1, \ldots, m_i)$ and for the random slope Θ are shown in Figure 3.5 and 3.6, respectively. Both plots are close to a straight line and symmetrical about zero except one data point from Tube C1 in Figure 3.5 which may be considered as an outlier. Hence no obvious evidence is shown against the assumptions.

Figure 3.7 plots the fitted versus observed diametral strain in both populational and individual levels. Comparing to Figure 3.4, the populational mean path is very close to that from IWLS. Recall that in the LR model, measurements of Tube C2 are out of the predictive bound. In the LME model, however, we can estimate the random slope Θ for the tube. For Tube C2, we have $\mathbf{X}_i = (1 \quad \Psi_{i1}; \ldots; 1 \quad \Psi_{i5})$, $\mathbf{Z}_i = (\Psi_{i1}, \ldots, \Psi_{i5})^T$and $D = \sigma^2_\Theta$. So from (3.25) we get $\hat{\theta}_i = 0.0594$. That is, the total deterioration rate for Tube C2 equals $\beta_1 + \hat{\theta}_i = 0.2671$. The individual mean path for Tube C2 is shown as a thick solid line in Figure 3.7 A conservative (without considering the uncertainty in β's) prediction bound for the diametral strain of Tube C2 is plotted as well. In the LME model, the five measurements all lie within the 95% bound.

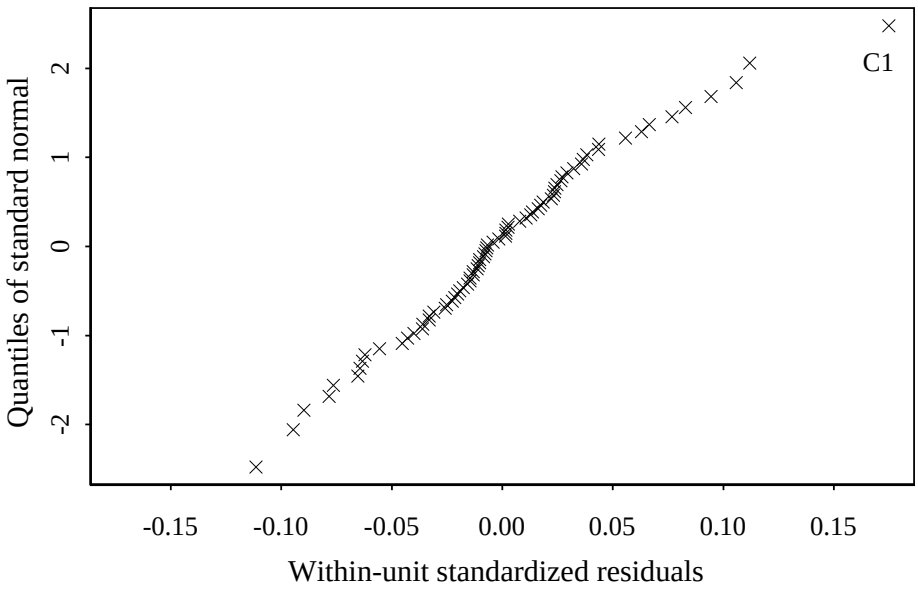

Figure 3.5: Normal quantile plot for within-unit residuals ε_{ij}

The lifetime distribution can then be calculated from the following expression:

$$F_T(\tau) = \Pr(\beta_0 + \beta_1\tau + \Theta\tau \geq \zeta) = \Pr\left(\Theta \geq \frac{\zeta - \beta_0}{\tau} - \beta_1\right) = 1 - \Phi\left(\frac{\zeta - \beta_0}{\tau\sigma_\Theta} - \frac{\beta_1}{\sigma_\Theta}\right). \tag{3.32}$$

Figure 3.8 shows the lifetime distribution of a typical pressure tube with failure threshold $\zeta = 5.1\%$. For an illustration, the lifetime density function for a typical tube with average flux 2.4×10^{17} n/(m^2·s) is plotted in Figure 3.8.

3.5 Concluding Remarks

Traditional regression models consist of a parameterized mean function and an error term that quantifies the deviation of the observations from the mean function. The errors are usually assumed independent of each other. While the data analysis becomes

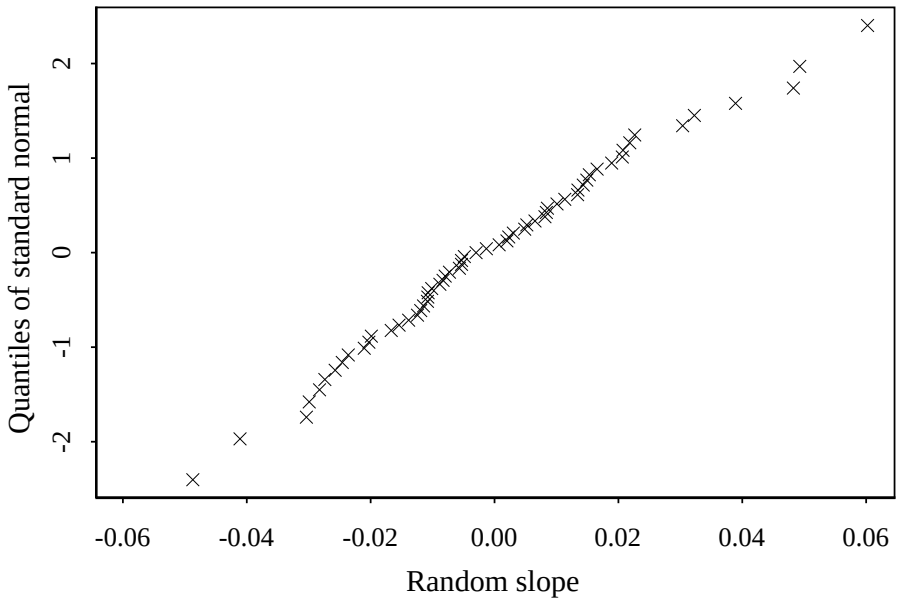

Figure 3.6: Normal quantile plot for the random slope Θ

straightforward under this assumption, it compromises the lifetime prediction. Although the independence assumption can be relaxed and replaced with some correlation structure, exact solutions for the lifetime under such assumptions are not yet available, unless further unrealistic approximations or assumptions are introduced.

This chapter presents a linear mixed-effects model to solve the problem. The feature of an LME model is that the inherent randomness of deterioration is decomposed into unobserved heterogeneity of individual units, or random effects, and additive measurement errors. By introducing the random effects into the model, the varying variance of deterioration and correlation in deterioration are characterized, which leads to a logical method for lifetime estimation.

The case study of creep deformation of pressure tubes starts with a simple linear regression model with variance of error weighted by the number of repeated measurements. The LR model is improved by an iteratively weighted least squares technique to stabilize

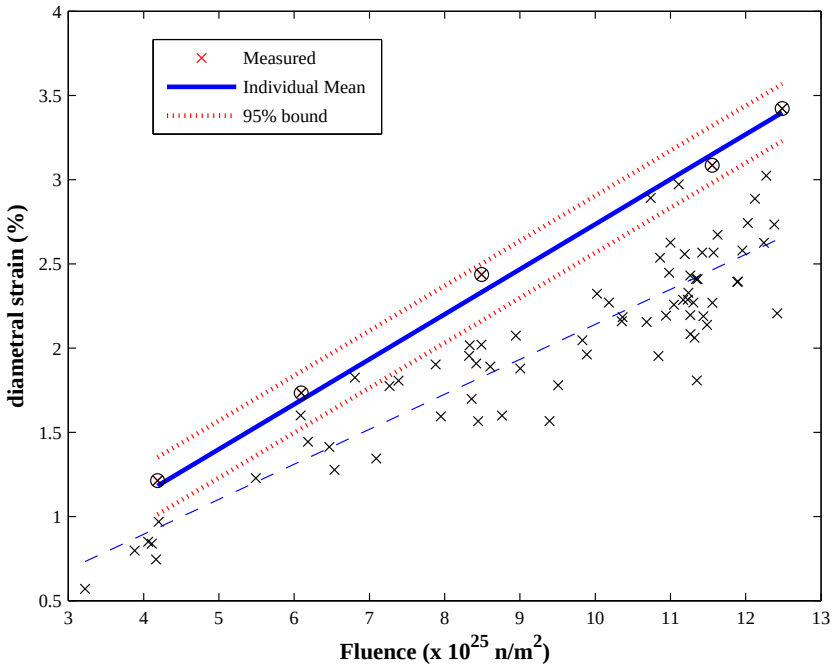

Figure 3.7: Populational (dashed line) and individual (solid line) mean deterioration path of Tube C2. The circled crosses represent diametral strain measured from Tube C2

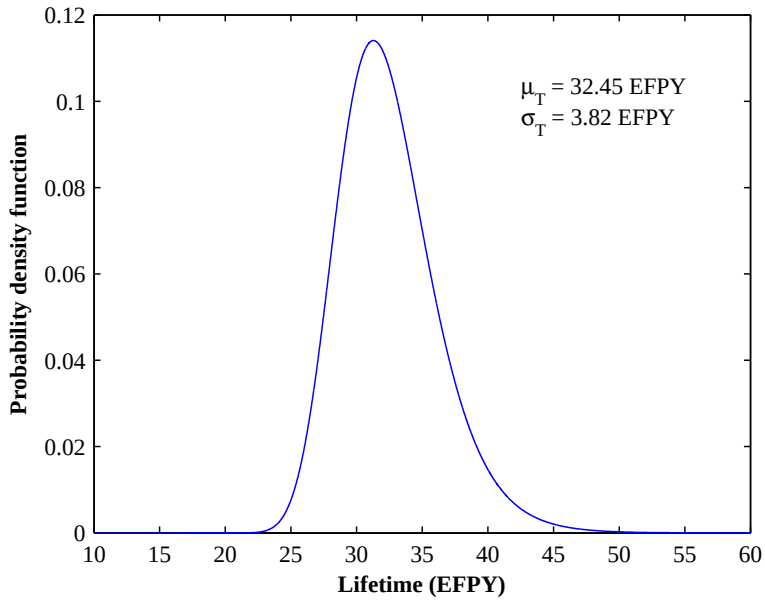

Figure 3.8: Probability density function of the lifetime of a typical pressure tube with flux 2.4×10^{17} n/(m^2·s)

the variance of residuals. The LME model is a better alternative with a random slope. As a result the tubes with high deterioration rate, which were classified as outliers in the LR model, are now fitted quite well in the LME model.

Despite a success in fitting the data in pressure tube example, the LME model is essentially a random variable model. For this reason, LME or LR models are inadequate to quantify the temporal variability and not well suited for condition-based maintenance optimization, as discussed in Chapter 7.

Chapter 4

Gamma and Related Processes

This chapter discusses basic concepts and properties of gamma and other related processes. We start with a stationary gamma process. Its characteristics are discussed from distribution, sample paths, lifetime and simulation perspectives. The discussion is then extended to nonstationary gamma processes, local gamma processes, mixed-scale gamma processes and finally Hougaard processes. The relationship among these stochastic processes is investigated.

4.1 Stationary Gamma Processes

A gamma distributed random variable X with shape parameter $a > 0$ and scale parameter $b > 0$ has probability density function

$$f_Z(z) = \frac{(z/b)^{a-1}}{b\Gamma(a)} \exp(-z/b) \tag{4.1}$$

for $z \geq 0$, where $\Gamma(u) = \int_0^\infty s^{u-1}e^{-s}\mathrm{d}s$ is the gamma function. We write $Z \sim Ga(a, b)$ to mean a random variable Z follows gamma distribution with shape a and scale b. Depending on the value of shape parameter a, the probability density function of Z can

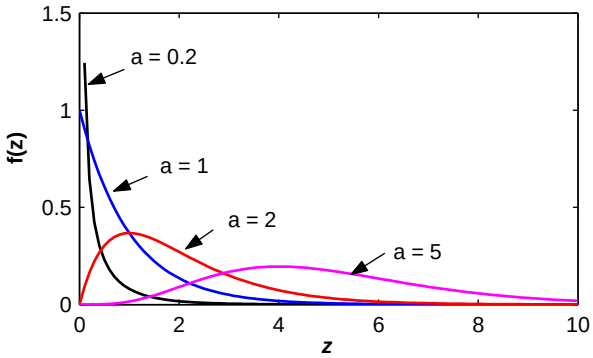

Figure 4.1: Probability density functions of gamma random variables with unit scale parameter and different shape parameters

be monotonically decreasing or nearly of a bell shape (Figure 4.1). The mean and variance of Z are ab and ab^2, respectively.

A continuous-time stochastic process $\{X(t), t \geq 0\}$ is called a stationary gamma process with shape parameter $\alpha > 0$ and scale parameter $\beta > 0$ if it has the following properties (Singpurwalla 1997):

(i) $X(0) = 0$ with probability one;

(ii) $\Delta X(t) = X(t + \Delta t) - X(t) \sim Ga(\alpha \Delta t, \beta)$ for any $t \geq 0$ and $\Delta t > 0$; and

(iii) For any choices of $n \geq 1$ and $0 \leq t_0 < t_1 < \cdots < t_n < \infty$, the random variables $X(t_0), X(t_1) - X(t_0), \ldots, X(t_n) - X(t_{n-1})$ are independent.

In short, a stationary gamma processes is a continuous-time stochastic processes with stationary, independent and gamma distributed increments.

4.1.1 Distribution and Sample Path Properties

The gamma distribution is infinitely divisible in the sense that if Z is a gamma r.v., then for every positive integer n there exist n i.i.d. r.v. $Z_1, Z_2, \ldots, Z_n$ that sum to

Z (Sato 1999). In the other direction we have that the sum of n independent gamma random variables, each having shape a_i $(i = 1, \ldots, n)$ and the same scale b, is still gamma distributed with shape $\sum a_i$ and scale b. Therefore, at any time $t > 0$, $X(t)$ is a gamma random variable, i.e., $X(t) \sim Ga(\alpha t, \beta)$. As t gets large, the probability density function of $X(t)$ changes from a monotonically decreasing function to a bell shape as shown in Figure 4.1.

Another important characteristic of gamma distribution is the so-called "gamma-bridge" property. That is, for two independent gamma r.v. $U \sim Ga(\alpha_1, \beta)$ and $V \sim Ga(\alpha_2, \beta)$ the ratio $U/(U+V)$ is beta distributed and independent of U (Johnson, Kotz, and Balakrishnan 1994). This implies that the ratio of $X(u)$ to $X(t)$ for $0 < u < t < \infty$ follows a beta distribution with parameter αu and $\alpha(t-u)$. This property can be used for simulating gamma processes. We will discuss this in detail later on.

As far as the sample path properties of gamma process are concerned, we first note that gamma process is Markovian because of its independent increments and that its sample path is non-negative and monotonically increasing. Note also that the mean and variance of $X(t)$ are

$$\mathrm{E}[X(t)] = \alpha\beta t \text{ and } \mathrm{Var}[X(t)] = \alpha\beta^2 t, \tag{4.2}$$

both linear functions of time. The coefficient of variation (COV), defined by the ratio of the standard deviation to the mean, is thus

$$\mathrm{COV}[X(t)] = 1/\sqrt{\alpha t}. \tag{4.3}$$

The decreasing COV suggests that the sample paths get closer and closer to the mean path over time in the relative sense. Figure 4.2 plots two sample paths of the same gamma process with $\alpha = 3$ and $\beta = 2$ at two different time scale. The solid line represents the path at a small scale with time t_1 ranging from 0 to 2 and the dashed line corresponds to time frame t_2 from 0 to 20. The dashed line looks very close to a straight line — the

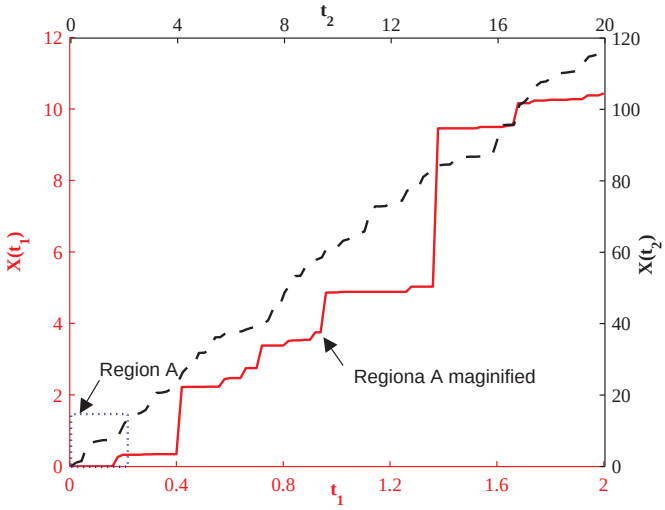

Figure 4.2: Time-scale effect of sample paths of a gamma process

mean path, whereas the solid line has a more haphazard behavior. As a matter of fact the solid line can also be thought of as a magnification of the dashed line in the dotted area. Therefore, concluding by visual inspection of one sample path of deterioration that the deterioration has very little temporal uncertainty may be incorrect. We must be careful for this time-scale effect when modeling deterioration in practice.

Another important feature of gamma process is that it is a pure jump process. That is, the sample path is not continuous as one may perceive. This needs a little elaboration. Although this can be shown by the Lévy-Khintchine decomposition theorem (Sato 1999), we want to show this in a way that is not so technical but more intuitive to engineers.

The basic idea is to relate the gamma process directly with a compound Poisson process (CPP). Recall from Section 2.2.4 that a compound Poisson process is a continuous-time stochastic process $\{Y(t), t \geq 0\}$ given by

$$Y(t) = \sum_{i=1}^{N(t)} D_i \tag{4.4}$$

where $\{N(t), t \geq 0\}$ is a homogeneous Poisson process with rate λ, and D_i $(i = 1, 2, \ldots)$ are i.i.d. random variables with CDF G, which are also independent of $\{N(t), t \geq 0\}$. Suppose D_i are positive random variables, i.e., $G(0) = 0$. Suppose also the CDF G is differentiable and has pdf g. Then the Laplace transform of $Y(t)$ is

$$\mathrm{E}\left[e^{-sY(t)}\right] = \exp\left\{\lambda t \int_0^\infty \left(e^{-su} - 1\right) G(\mathrm{d}u)\right\} = \exp\left\{t \int_0^\infty \left(e^{-su} - 1\right) \nu_P(\mathrm{d}u)\right\}, \quad (4.5)$$

in which

$$\nu_P(\mathrm{d}u) = \lambda G(\mathrm{d}u) = \lambda g(u)\mathrm{d}u \quad (4.6)$$

is called the Lévy measure of $Y(t)$.

Consider now a gamma process $\{X(t), t \geq 0\}$ with shape α and scale β. The Laplace transform of $X(t)$ is

$$\mathrm{E}\left\{e^{-sX(t)}\right\} = \left(\frac{1}{1+\beta s}\right)^{\alpha t} = \exp\{-\alpha t \log(1+\beta s)\} = \exp\left\{t \int_0^\infty \left(e^{-su} - 1\right) \nu_\Gamma(\mathrm{d}u)\right\}, \quad (4.7)$$

in which

$$\nu_\Gamma(\mathrm{d}u) = (\alpha/u)\, e^{-u/\beta}\mathrm{d}u. \quad (4.8)$$

Comparing (4.7) to (4.5) we can find that the gamma process is closely related to a CPP if λ and G in the CPP is appropriately chosen the limit of a compound Poisson process. Indeed, according to Dufresne, Gerber, and Shiu (1991), we may assume the Poisson rate $\lambda = \alpha\beta^c\Gamma(c)$ and G as a gamma distribution, i.e., $D_i \sim Ga(c, \beta)$. Then

$$\nu_P(\mathrm{d}u) = \lambda g(u)\mathrm{d}u = \alpha\beta^c\Gamma(c)\frac{u^{c-1}}{\beta^c\Gamma(c)}e^{-u/\beta}\mathrm{d}u = \frac{\alpha}{u^{1-c}}e^{-u/\beta}\mathrm{d}u. \quad (4.9)$$

As c tends to zero from above, the Poisson rate λ goes to infinity, the random jumps D_i gets more and more concentrated at zero (Figure 4.1), and the Lévy measure ν_P of the CPP tends to ν_Γ of the gamma process.

The Lévy measure $\nu(y) \equiv \nu([y,\infty))$ represents the mean number of jumps of sizes greater than y in a unit interval of time. In particular, $\nu(0)$ is the mean number of all jumps. For a CPP, $\nu_P(0) = \lambda \int_0^\infty G(\mathrm{d}u) = \lambda$ is finite. For a gamma process, however, $\nu_\Gamma(0) = \alpha \int_0^\infty u^{-1} e^{-u/\beta} \mathrm{d}u = \infty$. But it is easily checked that the mean number of jumps of sizes larger than any positive number ε is finite, or $\nu_\Gamma(\varepsilon) = \alpha \int_\varepsilon^\infty u^{-1} e^{-u/\beta} \mathrm{d}u < \infty$ for any $\varepsilon > 0$. Therefore, within any finite time interval there are infinitely many small jumps of size less than ε for any $\varepsilon > 0$ but only a finite number of big jumps. However, the cumulative sum of all these jumps in a finite time interval $[t, t+\Delta t)$ is always finite, no matter how infinitely many jumps there are. That is

$$\mathrm{E}\left[X(t, t+\Delta t)\right] = \sum_{i=1}^{N(t,t+\Delta t)} D_i = \int_t^{t+\Delta t} \int_0^\infty u\, \nu_\Gamma(du)\, \mathrm{d}s = \alpha\beta\Delta t. \tag{4.10}$$

Adding these facts altogether explains why the gamma process is a pure jump process while its sample path looks continuous.

The sample paths and associated jump sizes of two CPPs and one gamma process are plotted in Figure 4.3. The gamma process has a shape parameter $\alpha = 1$ and scale parameter $\beta = 1/\sqrt{2}$. Its sample path is shown in Figure 4.3(e). The two CPPs have a intensity rate $\lambda = \alpha\beta^c\Gamma(c)$ and a gamma distribution $Ga(c, \beta)$ for the jumps. Figure 4.3(a) shows a sample path of the CPP with $c = 2$. Only 8 jumps occur. The jump sizes and associated occurrence times are shown in Figure 4.3(b). In contrast, Figure 4.3(c) shows a sample path of the CPP with $c = 0.01$, which is very similar to the sample path of the gamma process, the limiting case when $c = 0$. The jumps shown in Figure 4.3(d) have a skewer distribution, for most of them are small jumps. Figure 4.3(f) shows the magnified plot of (d) for the jumps with size less than 0.03. It is not difficult to imagine that, when c is sufficiently close to zero, a similar plot to (f) can be obtained even a smaller truncation than 0.03 is chosen.

To summarize, the sample path of a gamma process embraces both minute invisible jumps and big traumatic jumps. This feature makes the gamma process a very good

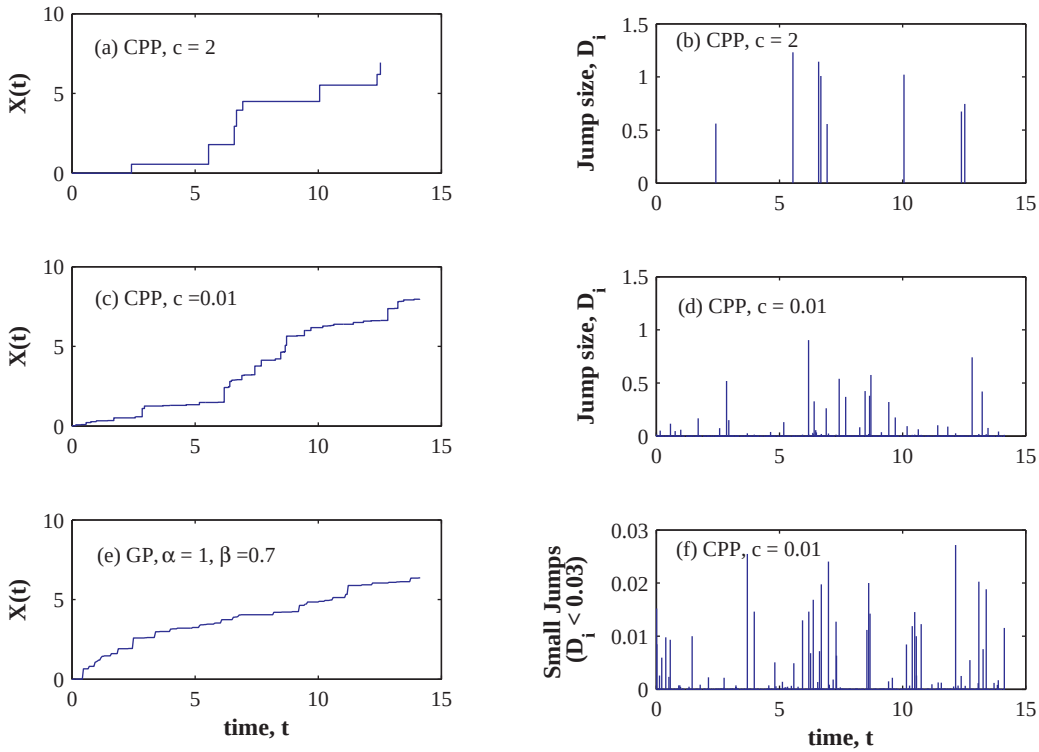

Figure 4.3: A compound Poisson process goes to a gamma process when c goes to zero

candidate for deterioration models, as the deterioration may develop in a very slow, invisible fashion due to daily usage and in some points of time it may grow very quickly when some traumatic events (e.g., earthquakes, forced outages) happen. The gamma process fits both types of damage modes.

4.1.2 Distribution of Lifetime

Many physical failures and performance failures (that is the system performance no longer conforms to a standard) are of first passage type. That is, once the deterioration process $X(t)$ of an item reaches a certain critical level ζ, the item fails. The failure time T is then defined as the first time when the sample path of $X(t)$ exceeds ζ. Symbolically, we have

$$T \equiv \inf\{X(t) \geq \zeta\} = \{t \,|\, X(t) \geq \zeta, X(s) < \zeta \text{ for } 0 \leq s < t\}. \tag{4.11}$$

When $X(t)$ is a stationary gamma process, the distribution of the first passage time is, according to the monotonicity of its sample paths,

$$F_T(t) = \Pr(T \leq t) = \Pr(X(t) \geq \zeta) = \frac{\Gamma(\zeta/\beta, \alpha t)}{\Gamma(\alpha t)} \tag{4.12}$$

where $\Gamma(w, z)$ denotes the incomplete gamma function, defined as

$$\Gamma(w, z) = \int_w^\infty u^{z-1} e^{-u} \mathrm{d}u. \tag{4.13}$$

The first two moments of the lifetime are expressed as

$$\mathrm{E}[T] = \int_0^\infty (1 - F_T(t))\, dt, \quad \text{and} \tag{4.14a}$$

$$\mathrm{E}\left[T^2\right] = 2\int_0^\infty t\,(1 - F_T(t))\, dt, \tag{4.14b}$$

which should be evaluated numerically.

A discrete-time approximation of (4.12) can be made by choosing $t_n = n/\alpha, n =$

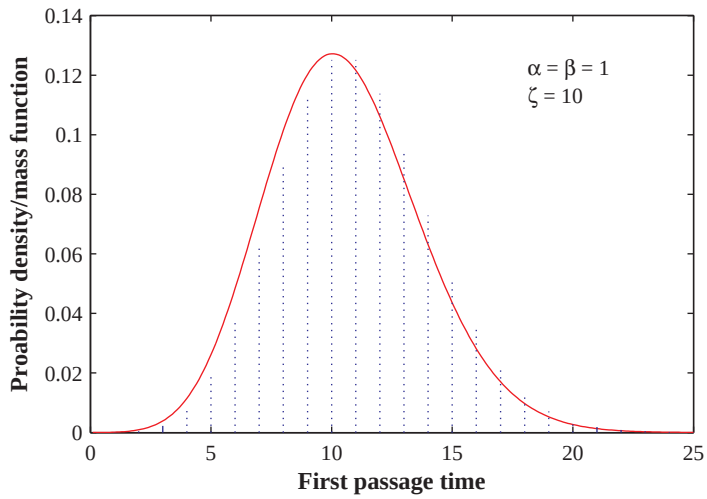

Figure 4.4: Distribution of first passage time of a gamma process and its Poisson approximation

$0, 1, \ldots$. Let $q_n = \Pr\{t_n < T_\xi \leq t_{n+1}\}$. Then one has

$$q_n = \frac{\Gamma(\zeta/\beta, n+1)}{\Gamma(n+1)} - \frac{\Gamma(\zeta/\beta, n)}{\Gamma(n)} = \frac{(\zeta/\beta)^n}{n!} e^{-\zeta/\beta}, \tag{4.15}$$

which is a Poisson distribution. That is, the probability of first passage time being the time interval $(n/\alpha, (n+1)/\alpha]$ follows a Poisson distribution with parameter ζ/β. This result was first observed by van Noortwijk et al. (1995). From the property of Poisson distribution, the mean and variance of the lifetime equals $\zeta/(\beta\alpha)$ and $\zeta/\left(\beta\alpha^2\right)$, which is remarkable as if they were derived directly from (4.2).

Figure 4.4 shows an example for the pdf of the first passage time and its Poisson approximation for the gamma process with unit shape and scale and failure threshold of 10. The exact values of the mean and variance are 10.495 and 10.022, respectively while the Poisson approximation gives both of 10.

4.1.3 Distribution of Remaining Lifetime

The distribution of remaining lifetime, the remaining time to the first passage level ζ, of the stationary gamma process, given its value at time s, $X(s) = x_s < \zeta$, is readily established using the independent increments property as

$$\begin{aligned} F_T(t \mid s) &= \Pr(T \leq t \mid X(s) = x_s) \\ &= \Pr(X(t) - X(s) \geq \zeta - x_s) \\ &= \frac{\Gamma\left[(\zeta - x_s)/\beta, \alpha(t-s)\right]}{\Gamma\left[\alpha(t-s)\right]} \end{aligned} \tag{4.16}$$

for $t \geq s$, which is the same as (4.12) with ζ and t replaced by $\zeta - x_s$ and $t - s$, respectively. If more recent values of the gamma process is known, the remaining lifetime distribution can be updated in the same way.

This update scheme of remaining lifetime is different from the way based on known surviving time. In the traditional lifetime approach to reliability modeling, the remaining lifetime distribution, given the item has survived up to the present time s, is given as

$$F_T(t \mid s) = \Pr(T \leq t \mid T > s) = \frac{F_T(t) - F_T(s)}{1 - F_T(s)} \tag{4.17}$$

for $t > s$.

Figure 4.5 shows three different distributions of the remaining lifetime after the item has survived 8 units of time for the gamma process in Figure 4.4. The distribution of the time-based remaining lifetime (with the only information of $s = 8$) is the truncated version of the original distribution at $s = 8$. But the real remaining lifetime can differ a lot from this truncated lifetime, depending on the actual level of state $x(s)$ at time $s = 8$.

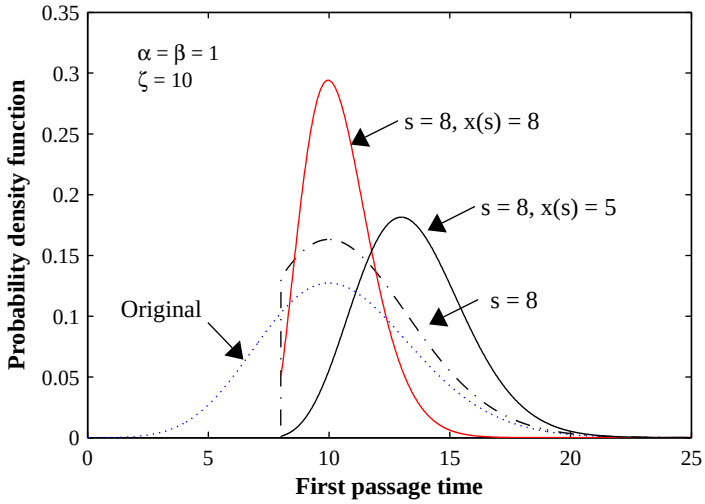

Figure 4.5: Distributions of the remaining lifetime of a gamma process based on different information

4.1.4 Simulation

A natural approach to simulating the gamma process makes use of the property of the independent increments. To generate a sample path from time 0 to t, we partition the time into n small subintervals: $0 = t_0 < t_1 < t_2 < \cdots < t_n = t$. Then, we draw random independent increments one by one directly from the gamma density $Ga\left(\alpha\Delta t_i, \beta\right)$ where $\Delta t_i = t_i - t_{i-1}$. A sample path of the gamma process is then formed by taking the successive summation of the increments up to time t. When n is large enough, we can approximate very well the sample paths of gamma processes.

The second approach uses the gamma-bridge property mentioned in subsection 4.1.1. Particularly, the conditional distribution of the ratio $X\left(t/2\right)/X\left(t\right)$, given $X\left(t\right)$, is symmetric beta with parameter $\alpha t/2$. Thus, we first simulate a value for $X\left(t\right)$ from gamma density $Ga\left(\alpha t, \beta\right)$. Then we obtain $X\left(t/2\right)$ by simulating a value for the ratio $X\left(t/2\right)/X\left(t\right)$, which has a symmetric beta distribution with parameters $\alpha t/2$. Given the value of $X\left(t/2\right)$ and $X\left(t\right)$, we obtain further $X\left(t/4\right)$ and $X\left(3t/4\right)$, respectively. Similarly, we can sample

$X(t/8)$, $X(3t/8)$, $X(5t/8)$, $X(7t/8)$, and so on (Dufresne, Gerber, and Shiu 1991).

The approach to simulation applies the functional representation theory of stochastic processes. Sometimes it is possible to represent a stochastic process as a countable sum of some deterministic functions with random variable coefficients. If so, then we can generate a finite number of random coefficients and approximate the sample path by the finite summation. The well-known Karhunen-Loeve expansion is an example of this application to stationary second-order Gaussian processes (Ghanem and Spanos 2003). Another example is the Wiener process, for which we have

$$W(t) = Y_0 t + \sqrt{2} \sum_{m=1}^{\infty} Y_m \frac{\sin(mt)}{m}, \tag{4.18}$$

where $W(t)$ denotes the Wiener process and Y_0, $Y_1, \ldots$ are independent normal random variables with zero means and unit variance. We wish a similar representation for gamma processes.

Indeed, it has been found (Ferguson and Klass 1972) that an independent increment process without Gaussian components can be represented as a countable sum of step functions each with a random point of discontinuity at a random height. For a stationary gamma process $\{X(t), 0 \leq t \leq 1\}$ with shape α and scale β in specific, it can be expanded as a compound Poisson process with the ordered random heights $J_1 \geq J_2 \geq \cdots$ having the following distributions:

$$\Pr(J_1 \leq x_1) = \exp\{-\nu_\Gamma(x_1, \infty)\} = \exp\left\{-\alpha \int_{x_1}^{\infty} y^{-1} e^{-y/\beta} dy\right\} \tag{4.19}$$

and

$$\Pr(J_j \leq x_j \mid J_{j-1} = x_{j-1}, \ldots, J_1 = x_1) = \exp\{-\nu_\Gamma(x_j, x_{j-1})\}. \tag{4.20}$$

Under this representation, the gamma process is expressed as

$$X(t) = \sum_{j=1}^{\infty} J_j I_{[0,t]}(U_j), \tag{4.21}$$

where $U_1, U_2, \ldots$ are independent and identically uniformly distributed on $[0,1]$ and independent of $J_1, J_2, \ldots$; and $I_{[0,t]}(\cdot)$ is indicator function. One advantage of this simulation is that the fineness of the sample path can be controlled by the number of jumps, n. The disadvantage is also obvious: more computational efforts are needed to generate the sequence of random jump heights.

4.2 Nonstationary Gamma Processes

A nonstationary gamma process $\{X(t), t \geq 0\}$ is a continuous-time stochastic process with increments $\Delta X(t)$ that are independent and have gamma distribution $Ga(\Delta\alpha(t), \beta)$, in which $\alpha(t) \geq 0$, is a nondecreasing continuous function with $\alpha(0) = 0$ and $\Delta\alpha(t) = \alpha(t + \Delta t) - \alpha(t)$. $\alpha(t)$ is called the shape function and $\beta > 0$ is again the scale parameter. Clearly, when the shape function is linear of time, i.e., $\alpha(t) = \alpha t$, the process becomes a stationary gamma process with shape parameter α and scale parameter β.

Since the nonstationary gamma process can be obtained by a deterministic nonlinear time transformation from the stationary gamma process, many results for stationary gamma processes are readily extended to the nonstationary case. For example, for any fixed t, $X(t)$ is still gamma distributed; its mean and variance are $\mathrm{E}[X(t)] = \alpha(t)\beta$ and $\mathrm{Var}[X(t)] = \alpha(t)\beta^2$; and $X(t)$ is also a pure jump process. We are not going to give further details for the nonstationary gamma process.

4.3 Local Gamma Processes

A local gamma process is a continuous-time stochastic process $X(t)$ with shape function $\alpha(t)$ and scale function $\beta(t)$, satisfying the following properties (Çinlar 1980):

(i) Almost surely, the sample path is right-continuous and increasing and starts from 0.

(ii) The shape function $\alpha(t)$ is increasing and right-continuous, and scale function $\beta(t)$ is strictly positive and finite.

(iii) For every $0 < t < \infty$, $\int_0^t d\alpha(u)/\beta(u) < \infty$.

(iv) For every $t \geq 0$, $\Delta t > 0$ and $s \geq 0$, the Laplace transform of the increments, $\Delta X(t) = X(t + \Delta t) - X(t)$, is

$$\begin{aligned} \mathrm{E}\left\{e^{-s\Delta X(t)}\right\} &= \exp\left\{\int_t^{t+\Delta t} d\alpha(u) \int_0^\infty x^{-1}\left(e^{-sx} - 1\right) e^{-x/\beta(u)} dx\right\} \\ &= \exp\left\{-\int_t^{t+\Delta t} \log(1 + s\beta(u)) d\alpha(u)\right\}. \end{aligned} \tag{4.22}$$

In essence, the local gamma process has the property that increments within *infinitesimal* time interval are gamma distributed, i.e.,

$$\Delta X(t) = X(t + \Delta t) - X(t) \dot{\sim} Ga(\alpha(t + \Delta t) - a(t), \beta(t^*)), \quad \text{for } \Delta t \to 0 \tag{4.23}$$

where $\dot{\sim}$ denotes "approximately distributed as" and t^* is anytime between t and $t + \Delta t$. Note that for any fixed t, $X(t)$ does not necessarily follow a gamma distribution unless the scale function $\beta(t)$ is constant.

A simple example of the local gamma process is the case where $\beta(t) = bt$ and $\alpha(t) = at$, both linear function of time t. Then

$$\begin{aligned} -\log \mathrm{E}\left\{e^{-sX_t)}\right\} &= \int_0^t a \log(1 + sbu) du \\ &= a\left[(1/sb + t)\log(1 + sbt) - t\right], \end{aligned} \tag{4.24}$$

Or

$$\mathrm{E}\left\{e^{-sX_t)}\right\} = e^{at}(1 + sbt)^{-\frac{a(1+sbt)}{sb}}. \tag{4.25}$$

However, no simple analytical form exists for the distribution of which the characteristic function is as such. Saddlepoint approximation (Daniels 1954; Goutis and Casella 1999) may be helpful for evaluating the probability density function.

Çinlar (1980) has shown that any local gamma process can be transformed into stationary gamma process by a change of scale using $\beta(t)$ and a change of time using α, or formally we write

$$X(t) = \int_0^{\alpha(t)} \frac{1}{\beta(s)} dY(s), \tag{4.26}$$

where the integration is with respect to the sample paths of $Y(t)$, a stationary gamma process with unit shape and scale parameter. With this construction, the local gamma process is also known as *extended gamma process* (Dykstra and Laud 1981), or *weighted gamma process* (Ishwaran and James 2004).

4.4 Mixed-Scale Gamma Processes

A mixed-scale gamma process $X(t)$ is a nonstationary gamma process with a shape function $\alpha(t) \geq 0$ and a random scale parameter B that follows an inverse gamma distribution, i.e. $W = B^{-1} \sim Ga\left(\delta, \gamma^{-1}\right)$. It is first proposed by Lawless and Crowder (2004) to model the random effects in degradation growth data. The scaled $X(t)$ follows

an F distribution. In particular,

$$\frac{\delta X(t)}{\gamma\alpha(t)} \sim F(2\alpha(t), 2\delta), \tag{4.27}$$

which follows from

$$\begin{aligned} f_{X(t)}(x) &= \int_0^\infty ga\left(x; \alpha(t), w^{-1}\right) ga\left(w; \delta, \gamma^{-1}\right) dw \\ &= \int_0^\infty \frac{w^{\alpha(t)} x^{\alpha(t)-1}}{\Gamma(\alpha(t))} e^{-xw} \frac{\gamma^\eta w^{\delta-1}}{\Gamma(\delta)} e^{-\gamma w} dw \\ &= \frac{\Gamma(\delta+\alpha(t))}{\Gamma(\alpha(t))\Gamma(\delta)} \frac{\gamma^\delta x^{\alpha(t)-1}}{(\gamma+x)^{\delta+\alpha(t)}}. \end{aligned} \tag{4.28}$$

Figure 4.6 shows the probability density function of a mixed-scale gamma random variable with $\alpha(t) = 2$, $\gamma = 10$ and $\delta = 10$ in comparison with an equivalent gamma density function with shape parameter 2 and scale parameter 1. It is found that the mixed-scale gamma density has a heavier tail.

It is clear that the increments are only conditionally independent. The joint probability density function of $\Delta X_i = X(t_i) - X(t_{i-1})$ for $i = 1, \ldots, n$ and $0 = t_0 < t_1 < \cdots < t_n$ is

$$\begin{aligned} f(\Delta x_1, \cdots, \Delta x_n) &= \int_0^\infty ga\left(w; \delta, \gamma^{-1}\right) \prod_{i=1}^n ga\left(\Delta x_i; \Delta\alpha_i, w^{-1}\right) dw \\ &= \frac{\Gamma(\delta+\alpha_n)}{\Gamma(\delta)\prod_{i=1}^n \Gamma(\Delta\alpha_i)} \frac{\gamma^\delta \prod_{i=1}^n (\Delta x_i)^{\Delta\alpha_i - 1}}{(\gamma+x_n)^{\delta+\alpha_n}}, \end{aligned} \tag{4.29}$$

where $x_n = x(t_n)$, $\alpha_n = \alpha(t_n)$, $\Delta\alpha_i = \alpha(t_i) - \alpha(t_{i-1})$ and $\Delta t_i = t_i - t_{i-1}$. The coefficient of correlation between two increments at two disjoint time intervals is

$$\rho(\Delta X_i, \Delta X_j) = \sqrt{\frac{\Delta\alpha_i \Delta\alpha_j}{(\Delta\alpha_i + \delta - 1)(\Delta\alpha_j + \delta - 1)}} \tag{4.30}$$

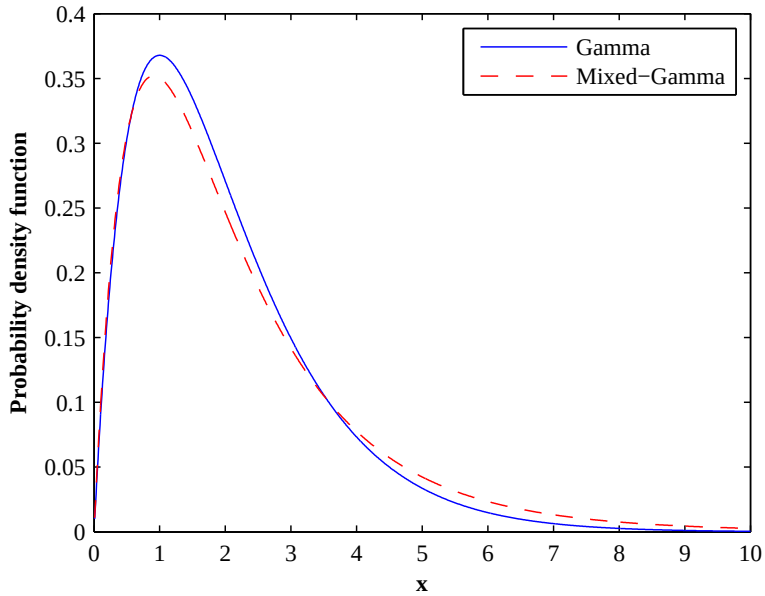

Figure 4.6: Comparison of a mixed-scale gamma distribution with its equivalent gamma distribution

for $\delta > 1$. From (4.29) we can also derive the conditional distribution of $\Delta X(t) = X(t+s) - X(s)$ conditional on $X(s) = x_s$ as

$$f(\Delta x \,|\, x_s) = \frac{\Gamma(\delta + \alpha_{t+s})}{\Gamma(\alpha_s)\,\Gamma(\delta + \Delta\alpha)} \frac{(\gamma + x_s)^{\delta+\alpha_s}\,\Delta x^{\Delta\alpha - 1}}{(\gamma + x_s + \Delta x)^{\delta+\alpha_{s+t}}}, \tag{4.31}$$

or

$$\frac{\delta + \alpha_s}{\gamma + x_s} \frac{\Delta X(t)}{\Delta\alpha} \sim F(2\Delta\alpha, 2\delta + 2\alpha_s) \tag{4.32}$$

where $\Delta\alpha = \alpha(t+s) - \alpha(s)$ and $\alpha_s = \alpha(s)$.

Similar to (4.12), the first passage time of the mixed-scale gamma process has a distribution function as

$$\Pr(T_\zeta \le t) = \Pr(X(t) \ge \zeta) = 1 - F\left(\frac{\delta\zeta}{\gamma\alpha(t)}; 2\alpha(t), 2\delta\right). \tag{4.33}$$

The remaining lifetime distribution given $X(s) = x_s$ is, following from (4.32),

$$\Pr(T_\zeta \leq t \,|\, X(s) = x_s) = 1 - F\left(\frac{\delta + \alpha_s}{\gamma + x_s}\frac{(\zeta - x_s)}{\Delta\alpha}; 2\Delta\alpha, 2\delta + 2\alpha_s\right). \tag{4.34}$$

4.5 Hougaard Processes

Hougaard processes include compound Poisson processes, gamma processes, inverse Gaussian processes, positive stable processes, and deterministic paths as special cases, and hence are very flexible for deterioration modeling. This section discusses basic properties of Hougaard processes. But before doing so, let us first introduce a three-parameter family of distribution, named Hougaard distribution.

4.5.1 Hougaard Distributions

A non-negative random variable X is said to follow a Hougaard distribution if its Laplace transform, $\varphi(s) = \mathrm{E}\left[e^{-sX}\right]$, has the following differential form:

$$\frac{d\log\varphi(s)}{ds} = -\delta(\theta + s)^{\alpha-1}, \tag{4.35}$$

with $\log\varphi(0) = 0$, where $\alpha \leq 1$, $\delta > 0$, $\theta \geq 0$. For $\alpha \neq 0$,

$$\varphi(s) = \exp\left\{-(\delta/\alpha)\left[(\theta + s)^\alpha - \theta^\alpha\right]\right\}. \tag{4.36}$$

For $\alpha = 0$, $\varphi(s) = [\theta/(\theta + s)]^{-\delta}$ is the Laplace transform of gamma distribution with shape parameter δ and scale parameter $1/\theta$. We denote the Hougaard distribution by $X \sim H(\alpha, \delta, \theta)$ where α, δ, θ are called index, shape and scale parameter, respectively. Clearly, the family of Hougaard distributions includes gamma distribution as a special case. Some other special cases are

- Dirac distribution. For $\alpha = 1$, X is concentrated on δ.

- Inverse Gaussian distribution when $\alpha = 1/2$.
- Positive stable distribution. For $\theta = 0$ and $0 < \alpha < 1$, $\varphi(s) = \exp\{-(\delta/\alpha)\, s^{\alpha}\}$, which is the Laplace transform of positive stable distribution with characteristic exponent α.
- Poisson-Gamma distribution. For $\alpha < 0$, $\varphi(s) = \exp\{-(\delta/\alpha)\,[(\theta+s)^{\alpha} - \theta^{\alpha}]\}$, which is the Laplace transform of $Y = X_1 + \cdots + X_N$ where N is a Poisson distribution with mean $-\delta\theta^{\alpha}/\alpha$ and X_i $(i = 1, 2, \ldots)$ are independent gamma random variable with as shape $-\alpha$ and scale parameter $1/\theta$, respectively.

Although Hougaard distribution has a very simple expression for its Laplace transform, it does not have explicit expression for its density function. It is known that the Hougaard density function, denoted by $h(x;\alpha,\delta,\theta)$, has an infinite series representation based on positive stable distribution. For $0 < \alpha < 1$, $\delta > 0$, $\theta \geq 0$ is

$$h(x;\alpha,\delta,\theta) = \exp\left(\delta\theta^{\alpha}/\alpha - \theta x\right) g(x;\alpha,\delta), \tag{4.37}$$

where

$$g(x;\alpha,\delta) = -\frac{1}{\pi x}\sum_{k=1}^{\infty}\frac{\Gamma(k\alpha+1)}{k!}\left(-\delta x^{-\alpha}/\alpha\right)^{k}\sin(\alpha k\pi) \tag{4.38}$$

is the probability density of positive stable distribution with index α and parameter δ. This series may converge very slowly especially near the origin in which the terms $x^{-\alpha k}$ become unmanageable for large k and α. For that reason, Hougaard (1986) gave a saddlepoint approximation for the Hougaard density function

$$f^{*}(x) = \sqrt{\frac{q\,(\delta/x)^{q}}{2\pi x}}\exp\left[\delta\theta^{\alpha}/\alpha - \theta x - \frac{x\,(\delta/x)^{q}}{q-1}\right], \tag{4.39}$$

where $q = 1/(1-\alpha)$. The approximation is exact only for $\alpha = 1/2$, which corresponds to the inverse Gaussian distribution. It can be shown that the mode of the pdf is located at $x = \delta^{1/\alpha}\left[\frac{2(1-\alpha)}{2-\alpha}\right]^{(1-\alpha)/\alpha}$.

Hougaard (1986) is the first person who introduced the new three-parameter family of distributions and applied it as a frailty distribution in survival models for heterogeneous populations. He derived the new distribution by using a technique called "exponential tilting" from the positive stable distribution. Later, he named it *power variance function* (PVF) distribution to reflect the fact that the variance of the distribution is a power function of its mean (Hougaard 2000). Fook Chong (1992) documented basic properties and methods of parameter estimation of Hougaard distributions and Hougaard processes.

4.5.2 Hougaard Processes

A Hougaard process $\{H(t), \geq 0\}$ is a continuous-time stochastic process that has stationary independent increments and its Laplace transform, $\varphi(s) = E\left[e^{-sH(t)}\right]$, has the following differential form

$$\frac{d \log \varphi(s)}{ds} = -\delta t (\theta + s)^{\alpha - 1}, \tag{4.40}$$

with $\log \varphi(0) = 0$, where $\alpha \leq 1$, $\delta > 0$, $\theta \geq 0$. The Lévy measure of the Hougaard process is

$$\nu_H(\mathrm{d}u) = \frac{\delta}{\Gamma(1-\alpha) u^{\alpha+1}} e^{-\theta u} \mathrm{d}u. \tag{4.41}$$

When $\alpha = 0$, $\nu_H(\mathrm{d}u) = \nu_\Gamma(\mathrm{d}u)$ as shown in (4.8). When $\alpha < 0$, $\nu_H(\mathrm{d}u)$ is the Lévy measure for a compound Poisson process, as shown in (4.9). Therefore, the Hougaard processes include as special cases gamma processes ($\alpha = 0$, $\delta > 0$, $\theta > 0$), inverse Gaussian processes ($\alpha = 1/2$, $\delta > 0$, $\theta > 0$), positive stable processes ($0 < \alpha < 1$, $\delta > 0$, $\theta = 0$), compound Poisson processes with gamma increments($\alpha < 0$, $\delta > 0$, $\theta > 0$) and deterministic paths ($\alpha = 1$).

4.6 Summary

This chapter discusses basic properties of gamma processes and several other closely related processes. A stationary gamma process has stationary, independent and gamma distributed increments. It has linear mean and variance functions. It is Markovian and its sample paths are non-negative and monotonically increasing. The relation of the gamma process with a compound Poisson process is illustrated. It has been shown that the gamma process can be easily adapted to both minute damages and traumatic ones, which is an important property for deterioration modeling.

Nonstationary gamma process, local gamma process, mixed-scaled gamma process and Hougaard process are also discussed in this chapter. A common feature among them is that they all have positive and independent (or conditionally independent) increments and are pure jump processes. Nonstationary gamma process can be regarded as a deterministic time transform of the stationary process. The mixed-scale gamma process has a random scale parameter but for a given sample path, it is a deterministic constant. In contrast, the local gamma process has a time-varying scale parameter. Hougaard process includes many known stochastic processes as its special cases. However, it does not have an explicit expression for the probability density function, which makes it less amenable to practical applications.

Chapter 5

Statistical Inference for Gamma Process Models

5.1 Introduction

Consider the general case in which n units are inspected for deterioration. Suppose each unit is inspected at different instants of time and for the ith unit we have $m_i\,(\geq 1)$ measurements of the deterioration at different points of time. Suppose also each unit is associated with a vector of covariate variables $\mathbf{z}_i$. Then the observed data of each unit have the following form: $(x_{ij},\, t_{ij},\, z_i)$ in which x_{ij} denotes the deterioration at time t_{ij} where $i = 1, \ldots, n$ and $j = 1, \ldots, m_i$. The numbers of repeated measurements m_i's are not necessarily the same for different units.

This chapter discusses techniques for parameter estimation and hypothesis tests of gamma process models of deterioration. Section 5.2 discusses the simplest cases in which there exists no covariate in the deterioration data and the n units are modeled by a stationary gamma process with the same shape and scale parameters. Two schemes of method of moments and the maximum likelihood method are developed. The three

methods are then compared in a simulation study. To study the effects of sample size on estimation accuracy, asymptotic variances of the maximum likelihood estimates are also derived. Section 5.3 presents likelihood-based techniques for modeling the fixed-effects of covariates. Section 5.4 discusses parameter estimation when the deterioration data are contaminated with measurement errors. The effects of measurement errors are studied through Monte Carlo simulations. Statistical inferences for mixed-effects gamma process models are discussed in Section 5.5, with emphasis on a score test for random effects. Section 5.6 revisits the diametral expansion data in Section 3.4 using a gamma process model. Section 5.7 concludes the chapter.

5.2 Estimating Parameters of Gamma Process Models

Recall a gamma process has stationary and independent increments. When no covariate presents in the deterioration data, the increments from the n records of sample paths of the gamma process (x_{ij}, t_{ij}) can be pooled without change of information together as if they are from one sample path with total time length $\Sigma_{i=1}^{n} t_{i,m_i}$. For ease of presentation, we assume for this section that the data has the form of (x_i, t_i), $i = 0, 1, \ldots, n$ with $x_0 = t_0 = 0$. We want to estimate the shape parameter α and the scale parameter β from the given data. Method of moments and maximum likelihood method can be used.

Since nonstationary gamma process can be thought of as a time transformation from a stationary gamma process, the techniques discussed in this section can also be used for the nonstationary cases once the shape function is well parameterized.

5.2.1 Methods of Moments

The basic idea behind the method of moments is to match the moments of a certain random variable with its corresponding statistics. For example, given n independent observations $u_1, \ldots, u_n$ of a Gaussian random variable U with mean μ and variance σ^2,

the sample mean and sample variance are

$$\bar{U} = \frac{1}{n}\sum_{i=1}^{n} u_i \text{ and } S_U^2 = \frac{1}{n-1}\sum_{i=1}^{n}\left(u_i - \bar{U}\right)^2 \tag{5.1}$$

Since $\mathrm{E}\left[\bar{U}\right] = \mu$ and $\mathrm{E}\left[S_U^2\right] = \sigma^2$, the estimates for μ and σ^2 are $\bar{U}$ and S_U^2, respectively.

As far as the gamma process is concerned, let $\Delta x_i = x_i - x_{i-1}$, $\Delta t_i = t_i - t_{i-1}$. The deterioration rate R_i, defined by $\Delta X_i/\Delta t_i$, are independent and gamma distributed. Therefore, similar to the Gaussian case in the above, we can calculate the sample mean and sample variance of the rate as

$$\bar{R} = \frac{1}{n}\sum_{i=1}^{n}\frac{\Delta x_i}{\Delta t_i} \text{ and } S_R^2 = \frac{1}{n-1}\sum_{i=1}^{n}\left(\frac{\Delta x_i}{\Delta t_i} - \bar{R}\right)^2. \tag{5.2}$$

It is clear that $\mathrm{E}\left[\bar{R}\right] = \alpha\beta$ and $\mathrm{Var}\left[\bar{R}\right] = \frac{1}{n^2}\alpha\beta^2\sum_{i=1}^{n}\left(1/\Delta t_i\right)$. Hence

$$\begin{aligned}
\mathrm{E}\left[S_R^2\right] &= \frac{1}{n-1}\sum_{i=1}^{n}\mathrm{E}\left(\frac{\Delta X_i}{\Delta t_i} - \bar{R}\right)^2 \\
&= \frac{1}{n-1}\sum_{i=1}^{n}\mathrm{E}\left[\left(\frac{\Delta X_i}{\Delta t_i} - \alpha\beta\right) - \left(\bar{R} - \alpha\beta\right)\right]^2 \\
&= \frac{1}{n-1}\sum_{i=1}^{n}\left\{\mathrm{Var}\left[\frac{\Delta X_i}{\Delta t_i}\right] - \frac{2}{n}\mathrm{Var}\left[\frac{\Delta X_i}{\Delta t_i}\right] + \mathrm{Var}\left[\bar{R}\right]\right\} \\
&= \frac{1}{n}\alpha\beta^2\sum_{i=1}^{n}\left(\frac{1}{\Delta t_i}\right).
\end{aligned} \tag{5.3}$$

Relating the sample moments to the expected values, we have

$$\alpha\beta = \bar{R}, \tag{5.4a}$$

$$\alpha\beta^2 = \frac{nS_R^2}{\sum_{i=1}^{n}\left(1/\Delta t_i\right)}. \tag{5.4b}$$

Solving them gives the estimates for the parameters.

Çinlar et al. (1977) proposed another scheme of method of moments. Instead of find-

ing the moments of the deterioration rate, they calculated the moments of the increments as

$$\bar{Y} = \frac{\sum_{i=1}^{n} \Delta x_i}{\sum_{i=1}^{n} \Delta t_i} = \frac{x_n}{t_n}, \tag{5.5a}$$

$$S_Y^2 = \sum_{i=1}^{n} \left(\Delta x_i - \bar{Y}\Delta t_i\right)^2. \tag{5.5b}$$

Since

$$\mathrm{E}\left[\bar{Y}\right] = \mathrm{E}\left[\frac{\sum_{i=1}^{n} \Delta x_i}{\sum_{i=1}^{n} \Delta t_i}\right] = \frac{\mathrm{E}\left[X\left(t_n\right)\right]}{t_n} = \alpha\beta \tag{5.6}$$

and

$$\begin{aligned}
\mathrm{E}\left[\sum_{i=1}^{n} \left(\Delta X_i - \bar{Y}\Delta t_i\right)^2\right] &= \mathrm{E}\left[\sum_{i=1}^{n} \left\{\left(\Delta X_i - \alpha\beta\Delta t_i\right) - \left(\bar{Y} - \alpha\beta\right)\Delta t_i\right\}^2\right] \\
&= \sum_{i=1}^{n} \mathrm{Var}\left(\Delta X_i\right) + \sum_{i=1}^{n} \Delta t_i \mathrm{Var}\left(\bar{Y}\right) \\
&= \alpha\beta^2 t_n \left[1 - \sum_{i=1}^{n} \left(\frac{\Delta t_i}{t_n}\right)^2\right],
\end{aligned} \tag{5.7}$$

we match the expected values with the estimations and get

$$\alpha\beta = \bar{Y} = \frac{x_n}{t_n}, \tag{5.8a}$$

$$\alpha\beta^2 = \frac{S_Y^2}{t_n\left[1 - \sum_{i=1}^{n}\left(\Delta t_i/t_n\right)^2\right]}, \tag{5.8b}$$

from which the estimates for parameters α and β are obtained as

$$\hat{\alpha} = \frac{x_n^2\left[1 - \sum_{i=1}^{n}\left(\Delta t_i/t_n\right)^2\right]}{t_n S_Y^2}, \tag{5.9a}$$

$$\hat{\beta} = \frac{S_Y^2}{x_n\left[1 - \sum_{i=1}^{n}\left(\Delta t_i/t_n\right)^2\right]}. \tag{5.9b}$$

We can think of the bracketed terms as a correction factor in the same way as $(n-1)$ for S_U^2 in (5.1) so that the estimates are unbiased. It is clear that when Δt_i $(i = 1, \ldots, n)$ are equal, the estimates from both schemes are the same.

5.2.2 Maximum Likelihood Method

Given the increments $(\Delta x_i, \Delta t_i), i = 1, \ldots, n$, of a gamma process $\{X(t), t \geq 0\}$ with shape α and scale β, the likelihood function for α and β can be easily established. Recall from the definition of the gamma process,

$$\Delta X_i \sim Ga(\alpha \Delta t_i, \beta) = \frac{(\Delta x_i/\beta)^{\alpha \Delta t_i - 1}}{\beta \Gamma(\alpha \Delta t_i)} e^{-\Delta x_i/\beta}. \tag{5.10}$$

The log likelihood function is

$$l(\alpha, \beta) = \sum_{i=1}^{n} (\alpha \Delta t_i - 1) \log \Delta x_i - \alpha t_n \log \beta - \sum_{i=1}^{n} \log \Gamma(\alpha \Delta t_i) - \frac{x_n}{\beta}. \tag{5.11}$$

Differentiating $l(\alpha, \beta)$ with respect to α and β, respectively, we have the following maximum likelihood equations:

$$\frac{\partial l}{\partial \alpha} = \sum_{i=1}^{n} \Delta t_i (\log x_i - \psi(\alpha \Delta t_i) - \ln \beta) = 0, \tag{5.12a}$$

$$\frac{\partial l}{\partial \beta} = \frac{x_n}{\beta^2} - \frac{\alpha t_n}{\beta} = 0, \tag{5.12b}$$

in which $\psi(u)$ denotes the digamma function, the derivative of log gamma function $\log \Gamma(u)$. Solutions of the two simultaneous equations are the maximum likelihood estimates for the parameters. In particular, from the last equation we have

$$\beta = \frac{x_n}{\alpha t_n}, \tag{5.13}$$

which is a natural result from the fact that $\mathrm{E}\left[X\left(t_n\right)\right] = \alpha\beta t_n$. Substituting it back into the first maximum likelihood equation leads to

$$\sum_{i=1}^{n} \Delta t_i \log \Delta x_i - t_n \log \frac{x_n}{\alpha t_n} - \sum_{i=1}^{n} \Delta t_i \psi\left(\alpha \Delta t_i\right) = 0. \tag{5.14}$$

This is a transcendental equation and hence numerical techniques are usually called for.

5.2.3 Effects of Sample Size

Next we discuss the effects of sample size on statistical errors of parameters of gamma processes in terms of asymptotic variances of the maximum likelihood estimates. The asymptotic variances are derived from the observed Fisher's information matrix, I, which is defined as the negative Hessian matrix of log likelihood or the second derivatives of $l\left(\alpha, \beta\right)$. From (5.11), we have

$$I = \begin{bmatrix} \sum_{i=1}^{n} \Delta t_i^2 \psi'\left(\alpha \Delta t_i\right) & t_n/\beta \\ t_n/\beta & \alpha t_n/\beta^2 \end{bmatrix} \tag{5.15}$$

where $\psi'\left(u\right) = d\psi\left(u\right)/du$. The entity I_{22} follows from the fact that $\partial^2 l/\partial\beta^2 = \alpha t_n/\beta^2 - 2x_n/\beta^3$ and $x_n = \alpha\beta t_n$. Taking the inverse of I we obtain the asymptotic covariance matrix for α and β.

Suppose $\Delta t_i = \Delta t = t_n/n$ for $i = 1, 2, \ldots, n$. Then

$$I = \frac{t_n}{\beta} \begin{bmatrix} \beta \Delta t \psi'\left(\alpha \Delta t\right) & 1 \\ 1 & \alpha/\beta \end{bmatrix}. \tag{5.16}$$

Hence, the asymptotic covariance matrix is

$$I^{-1} = \frac{\beta}{t_n\left[\alpha \Delta t \psi'\left(\alpha \Delta t\right) - 1\right]} \begin{bmatrix} \alpha/\beta & -1 \\ -1 & \beta \Delta t \psi'\left(\alpha \Delta t\right) \end{bmatrix}. \tag{5.17}$$

From Bleistein and Handelsman (1975) we have

$$\psi'(u) \sim \frac{1}{u} + \frac{1}{2u^2} + \frac{1}{6u^3} - \cdots, \tag{5.18}$$

and thus

$$u\psi'(u) - 1 \sim \frac{1}{2u} + \frac{1}{6u^2} - \cdots. \tag{5.19}$$

Using the first term of the asymptotic expansion, we have

$$\widehat{\mathrm{Var}}(\hat{\alpha}) = \frac{\alpha}{t_n\left[\alpha\Delta t\psi'(\alpha\Delta t) - 1\right]} \sim \frac{2\alpha^2\Delta t}{t_n} = \frac{2\alpha^2}{n}, \tag{5.20a}$$

$$\widehat{\mathrm{Var}}\left(\hat{\alpha}, \hat{\beta}\right) = -\frac{\beta}{t_n\left[\alpha\Delta t\psi'(\alpha\Delta t) - 1\right]} \sim -\frac{2\alpha\beta}{n}, \text{ and} \tag{5.20b}$$

$$\widehat{\mathrm{Var}}\left(\hat{\beta}\right) = \frac{\beta^2/\alpha}{t_n\left(1 - 1/\left[\alpha\Delta t\psi'(\alpha\Delta t)\right]\right)} \sim \beta^2\left(\frac{2}{n} + \frac{1}{\alpha t_n}\right). \tag{5.20c}$$

The asymptotic variance of α and covariance of α and β are dependent on the size of sample, n: the greater is the sample size, the smaller the standard error will be. However, the asymptotic variance of β, the scale parameter, depends not only the sample size but also on the total time length of the sample path. As the maximum likelihood estimates are asymptotically unbiased, the coefficient of variation (COV) of the estimate for the shape parameter is $\sqrt{2/n}$ and the COV for the scale parameter is $\sqrt{2/n + 1/(\alpha t_n)}$.

To verify the above observations, a Monte Carlo simulation is performed. With fixed shape parameter α and scale parameter β, a sample path of the gamma process is generated with a number n of measurements from the time interval $[0, t_n]$. Using the simulated data, the parameters are estimated and the associated standard errors are computed as well. Figure 5.1 demonstrates the trend of the COV of the estimated shape and scale parameter with increasing n at three different length of sample path t_n. Both plots agree well to the analytical results.

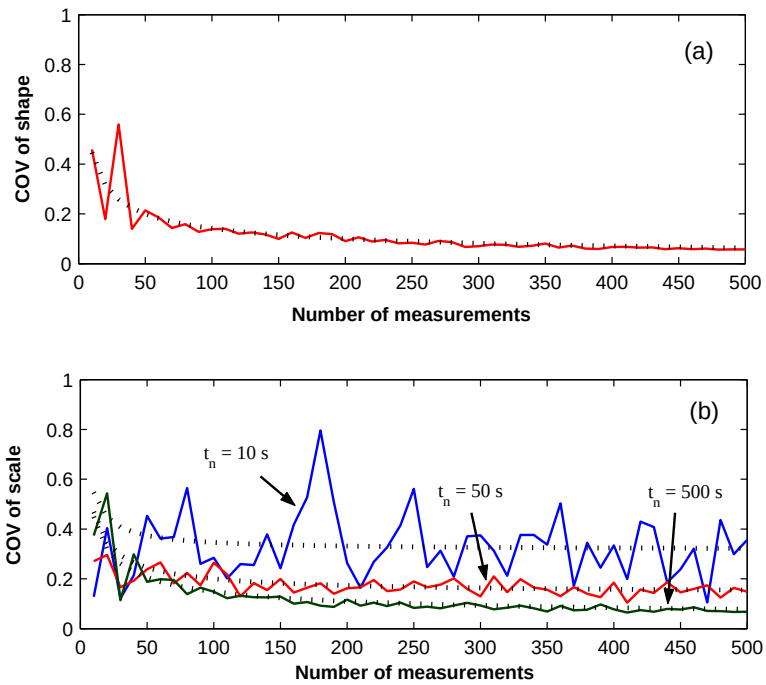

Figure 5.1: Coefficient of variation of the estimated (a) shape and (b) scale parameters from different numbers of measurements. Dotted lines represent the analytical results, and solid lines the simulation results

5.2.4 Comparison of Maximum Likelihood Method and Methods of Moments

A simulation study is undertaken to compare the effectiveness and efficiency of the three methods of parameter estimation. For brevity, we use MLE for maximum likelihood estimates, MoMR for estimates from (5.4) based on the method of moments of rate, and MoMX for estimates from (5.8) based on the method of moments of increments. Table 5.1 lists the mean and standard error of estimated shape and scale parameters for the gamma process with the true shape and scale of 3 and 2, respectively. When the sample size N is greater than 50, three methods all provide reasonable results. But the standard errors of the MLEs are slightly smaller than those from the two methods of moments.

The maximum likelihood method needs a little more computational efforts than the methods of moments does. But the former provides an asymptotic variance of the estimates without much more efforts as discussed above. To get the confidence intervals of the estimates of the methods of moments, however, bootstrap simulation (Efron and Tibshirant 1993), a very computationally intensive tool, is usually called for. Another reason of preferring maximum likelihood method is that this method is adapted to models with more complicated structures, as discussed next.

Table 5.1: Mean and standard errors of estimated parameters from different methods

	MLE		MoMR		MoMX	
N	α	β	α	β	α	β
10	4.2476 (2.5799)	1.8062 (0.8670)	4.0514 (2.5383)	1.9455 (1.0538)	3.9934 (2.5093)	1.9793 (1.0576)
20	3.4936 (1.2253)	1.9018 (0.6157)	3.4600 (1.3230)	1.9735 (0.7651)	3.4063 (1.2819)	1.9899 (0.7194)
50	3.1803 (0.6499)	1.9619 (0.4010)	3.1824 (0.7556)	1.9947 (0.5127)	3.1531 (0.7237)	2.0007 (0.4647)
100	3.0863 (0.4325)	1.9802 (0.2806)	3.0877 (0.5112)	1.9974 (0.3523)	3.0765 (0.4854)	1.9970 (0.3199)
500	3.0148 (0.1882)	1.9973 (0.1282)	3.0174 (0.2317)	1.9999 (0.1616)	3.0140 (0.2132)	2.0000 (0.1452)
1000	3.0093 (0.1317)	1.9979 (0.0911)	3.0087 (0.1633)	2.0007 (0.1144)	3.0075 (0.1498)	2.0002 (0.1028)

5.3 Modeling Fixed-Effects of Covariates in Deterioration

We now consider to estimate the parameters of a gamma process $X(t)$ of which, for general purpose, both the shape and scale parameters are functions of some covariates. Denote the covariates by a vector $\mathbf{z}_i$ for unit i, $i = 1, \ldots, n$. Suppose the shape and scale parameters are linked with the covariates by the following parametric forms

$$\alpha_i = \alpha(\mathbf{z}_i; \delta) \text{ and } \beta_i = \beta(\mathbf{z}_i; \gamma) \tag{5.21}$$

where both δ and γ are parameter vectors to be estimated. Suppose we observed one sample path of length m_i for ith unit . Given deterioration data as (x_{ij}, t_{ij}, z_i), $j = 0, 1, \ldots, m_i$, we cannot pool the data as one sample path as we did in the last section, because each unit here has different shape and scale parameters.

When the sample path record of each unit is long enough, we can use the methods proposed in the last section to estimate the shape and scale parameters separately for each unit at first. The parameters δ and γ can then be estimated using regression techniques based on the parametric relationship of (5.21). This is equivalent to the two-stage method used for growth curve models (Meeker and Escobar 1998). Clearly, the effectiveness and efficiency of this method depends on both large n and large m_i. For practical deterioration data of which m_i is usually very small, this method is not applicable.

Maximum likelihood method is suitable for this case. As a matter of fact, only a small modification of the likelihood function in (5.11) is needed for the method to fit the situation. Instead of pooling all the data into one sample path, we write the log likelihood function of each unit as (5.11) with α and β replaced by α_i and β_i from (5.21). The sum of all the individual log likelihoods gives the log likelihood function for δ and γ. The parameters can then be estimated by maximizing the total log likelihood function. The standard error of the estimates can also be computed from the observed information matrix. Numerical procedures for the maximization have been discussed in Section 3.3.1.

5.3.1 Likelihood Ratio Test

When modeling the effects of covariates, we often want to know the significance of certain covariates. This can be done by a hypothesis test. For example, to check the significance of a covariate, we can check whether the parameter associated with this covariate is zero. Likelihood ratio test is an effective procedure for this purpose.

Denote by θ the parameter vector including both δ and γ. Suppose we want to test the null hypothesis $H_0 : \theta = \theta_0$ against its alternate $H_1 : \theta \neq \theta_0$ for a known θ_0. The likelihood ratio test statistic is defined to be twice the difference between the two maximum log-likelihoods (Lawless 2003),

$$\Lambda(\theta_0) = 2l\left(\hat{\theta}\right) - 2l\left(\theta_0\right) \tag{5.22}$$

where $l\left(\hat{\theta}\right)$ is the maximized log likelihood and $l\left(\theta_0\right)$ is the log likelihood associated with θ_0. If θ is k dimensional, then $\Lambda(\theta_0)$ is asymptotically chi-square distributed with k degrees of freedom, i.e., $\Lambda(\theta_0) \sim \chi^2_{(k)}$. When the observed value of the likelihood ratio statistic is large enough, we have significant evidence against the null hypothesis. As to how large the observed value is enough, it depends on the degrees of freedom and the significance level.

Quite often, we want to test only part of the parameters. This corresponds to a composite hypothetical test. Suppose the parameters are partitioned as $\theta = \left(\theta_1^T, \theta_2^T\right)^T$ and $H_0 : \theta_1 = \theta_{10}$, the likelihood ratio statistic is

$$\Lambda(\theta_{01}) = 2l\left(\hat{\theta}\right) - 2l\left(\tilde{\theta}\right) \tag{5.23}$$

where $l\left(\tilde{\theta}\right)$ is the profile log likelihood with $\theta_1 = \theta_{10}$. In this case, $\Lambda(\theta_{01}) \sim \chi^2_{(p)}$, where p is the dimension of θ_{10}.

5.4 Effects of Measurement Errors

When the measurement error is significant, it cannot be ignored in the data analysis. In this case, inspection data are noise-contaminated sample paths of gamma process. Denote the measured deterioration at time t_{ij} by $y_{ij} = x_{ij} + \varepsilon_{ij}$ where x_{ij} is the actual deterioration and ε_{ij}'s are assumed to be normally and independently distributed random variables with mean zero and variance σ_ε^2. Note $\Delta y_{ij} = \Delta x_{ij} + \varepsilon_{ij} - \varepsilon_{i,j-1}$. So although Δx_{ij} are independent by definition, the observed increments Δy_{ij} are not independent. This complicates the construction of likelihood function. In a matrix form,

$$\begin{pmatrix} \Delta y_{i1} \\ \Delta y_{i2} \\ \vdots \\ \Delta y_{im_i} \end{pmatrix} = \begin{pmatrix} \Delta x_{i1} \\ \Delta x_{i2} \\ \vdots \\ \Delta x_{im_i} \end{pmatrix} + \begin{bmatrix} 1 & & & \\ -1 & 1 & & \\ & \ddots & \ddots & \\ & & -1 & 1 \end{bmatrix} \begin{pmatrix} \varepsilon_{i1} \\ \varepsilon_{i2} \\ \vdots \\ \varepsilon_{im_i} \end{pmatrix} \tag{5.24}$$

or $\mathbf{\Delta y}_i = \mathbf{\Delta x}_i + \mathbf{C}\varepsilon_i = \mathbf{\Delta x}_i + \eta_i$, where $\eta_i \sim N\left(0, \sigma^2\mathbf{\Sigma}\right)$ and

$$\mathbf{\Sigma} = \mathbf{CC}' = \begin{bmatrix} 1 & -1 & & & \\ -1 & 2 & -1 & & \\ & \ddots & \ddots & \ddots & \\ & & -1 & 2 & -1 \\ & & & -1 & 2 \end{bmatrix}. \tag{5.25}$$

Although $\varepsilon_{i1}, \ldots, \varepsilon_{im_i}$ are independent each other, $\eta_{i1}, \ldots, \eta_{im_i}$ are clearly not. The marginal distribution of $\mathbf{\Delta y}_i$ is

$$
\begin{aligned}
& f\left(\Delta y_{i1}, \ldots, \Delta y_{im_i}\right) \\
& = \int \cdots \int_{\{\eta_{ij} \leq \Delta y_{ij}\}} \left[\prod_{j=1}^{m_i} f_{\Delta X_{ij}}\left(\Delta y_{ij} - \eta_{ij}\right)\right] f\left(\eta_{i1}, \cdots, \eta_{im_i}\right) \mathrm{d}\eta_{i1} \cdots \mathrm{d}\eta_{im_i} \\
& = \int \cdots \int_{\{\eta_{ij} \leq \Delta y_{ij}\}} \prod_{i=1}^{m_i} \left[\frac{\left(\Delta y_{ij} - \eta_{ij}\right)^{\alpha_i \Delta t_i - 1}}{\beta_i^{\alpha_i \Delta t_{ij} - 1} \Gamma\left(\alpha_i \Delta t_{ij}\right)} e^{-\left(\Delta y_{ij} - \eta_{ij}\right)/\beta_i}\right] f\left(\eta_i\right) \mathrm{d}\eta_i
\end{aligned}
\tag{5.26}
$$

where $f\left(\eta_i\right) = f\left(\eta_{i1}, \cdots, \eta_{im_i}\right)$ denotes the multivariate normal density function with mean zero and covariance $\sigma^2 \mathbf{\Sigma}$. When the number of repeated measurements m_i is greater than 3, Monte Carlo simulation may be helpful for evaluating the above integration.

The marginal distribution of $\mathbf{\Delta y}_i$ in (5.26) can serve as the likelihood function of the parameters ($\alpha\left(\delta\right)$, $\beta\left(\gamma\right)$ and σ_ε^2) for unit i. Usually, the noise variance σ_ε^2 is known from the characteristic curve of the inspection device. If it is not known, we can also estimate the variance and use likelihood ratio test to check whether the effects of measurement error is statistically significant.

In order to see the significance of measurement error on the parameter estimation, a simulation study is conducted for a stationary gamma process with shape parameter $\alpha = 5$ and scale parameter $\beta = 2$. Two cases are considered. For the first case, 1000 sample paths are generated and each sample path has only one record at time $t = 0.25$. The second case considers 50 sample paths, each having 5 records at time interval $\Delta t = 0.25$. For both cases, each observation of the sample path is contaminated by a measurement error with standard deviation $\sigma_\varepsilon = 0.5$. For both cases, the estimations with and without consideration of the measurement errors are carried out. When the measurement errors are ignored, the parameters are estimated using the method introduced in Section 5.1.2 and the estimates are denoted by α_0 and β_0. The estimates when measurement errors are considered are denoted by α_e, β_e and σ_e for α, β and σ_ε, respectively. To get the

statistics of the estimates, 200 simulations are run for each case.

The histograms of the maximum likelihood estimates with or without consideration of measurement errors are plotted in Figure 5.2 and 5.3. It is clear from the first case that ignoring the measurement errors would lead to biased estimation with misreported standard errors (se) from observed information matrices. For the second case where more repeated measurements are used, however, the differences of results with and without consideration of measurement errors are not so obvious. The reason may be that the measurement error is getting relatively smaller when the deterioration gets larger. Note that less total amount of data are used,in the second case than in the first one. This observation implies that repeated measurement along the time is preferable in the context of compensating the effects of measurement errors.

5.5 Modeling Random Effects in Deterioration

We have discussed how to estimate the parameters of a gamma process model when there are covariates associated the deterioration. But there still are situations where the covariates do not explain all of the differences across the units. The effect due to the unobserved heterogeneity is called a random effect. The random effect in deterioration can be modeled by the mixed-scale gamma process introduced in Section 4.4.

Recall that a mixed-scale gamma process $X(t)$ is a nonstationary gamma process with scale parameter B being an inverted gamma random variable. That is, $W = B^{-1} \sim Ga\left(\delta, \gamma^{-1}\right)$ and given $B = 1/w$, $X(t)$ is a nonstationary gamma process with shape function $\alpha(t)$ and scale parameter $1/w$. When there are covariates attached to the units, the fixed-effects due to the covariates can be incorporated as we did in the Section 5.3. For ease of presentation, we assume the covaiates are integrated in the scale parameter so that the scale parameter B is replaced by $B\xi(z)$, where z denotes the covariates and $\xi(z)$ represents the effect of covariates. Under these assumptions, the joint distribution

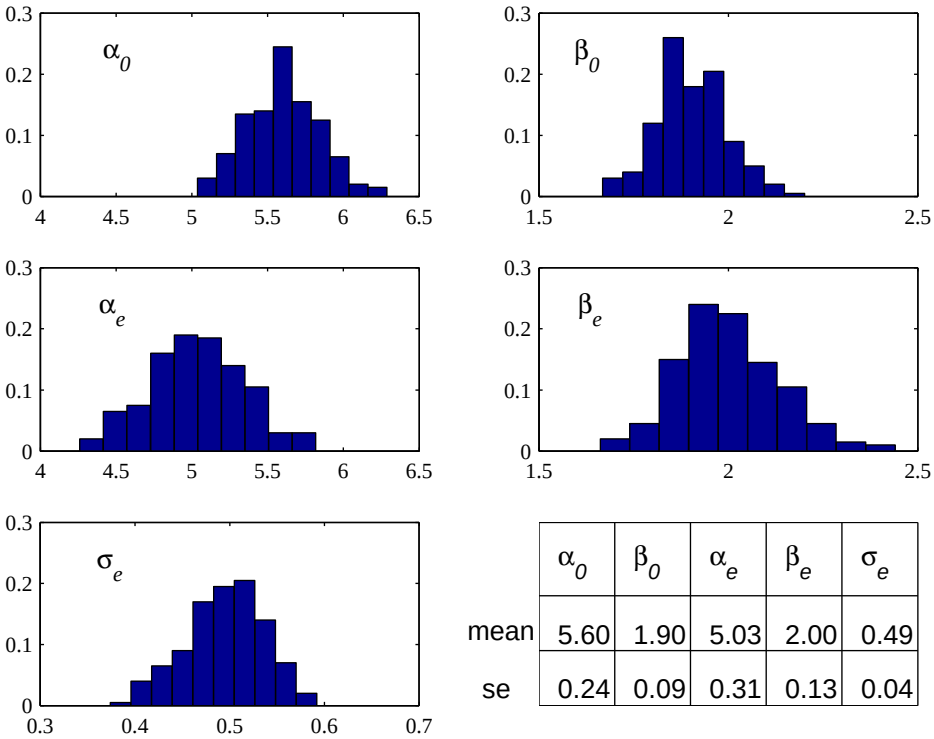

	α_0	β_0	α_e	β_e	σ_e
mean	5.60	1.90	5.03	2.00	0.49
se	0.24	0.09	0.31	0.13	0.04

Figure 5.2: Histograms of maximum likelihood estimates for stationary gamma process with or without consideration of measurement errors. Parameters are estimated based on 1000 sample paths of one record. True values of the parameters are $\alpha = 5$, $\beta = 2$, $\sigma_\varepsilon = 0.5$

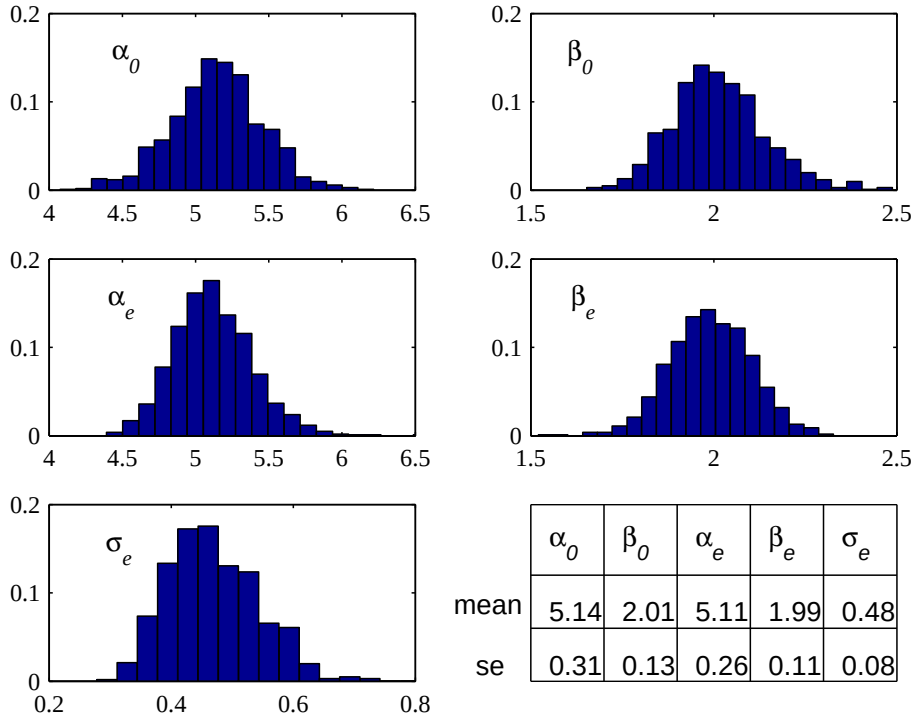

	α_0	β_0	α_e	β_e	σ_e
mean	5.14	2.01	5.11	1.99	0.48
se	0.31	0.13	0.26	0.11	0.08

Figure 5.3: Histograms of maximum likelihood estimates for stationary gamma process with or without consideration of measurement errors. Parameters are estimated based on 50 sample paths of 5 record. True values of the parameters are $\alpha = 5$, $\beta = 2$, $\sigma_\varepsilon = 0.5$

of disjoint increments $\Delta X_1, \ldots, \Delta X_n$, according to (4.29), is expressed as

$$f\left(\Delta x_1, \ldots, \Delta x_n\right) = \frac{\Gamma\left(\delta + \alpha_n\right)}{\Gamma\left(\delta\right) \prod_{i=1}^{n} \Gamma\left(\Delta \alpha_i\right)} \frac{\left(\gamma \xi_z\right)^{\delta} \prod_{i=1}^{n} \left(\Delta x_i\right)^{\Delta \alpha_i - 1}}{\left(\gamma \xi_z + x_n\right)^{\delta + \alpha_n}}, \tag{5.27}$$

where $x_n = \Sigma_{i=1}^{n} \Delta x_i$, $\alpha_n = \Sigma_{i=1}^{n} \Delta \alpha_i$ and $\xi_z = \xi\left(z\right)$ for brevity. Using this joint density as the likelihood function, we can use the maximum likelihood method to estimate parameters δ, γ, and those in $\alpha\left(t\right)$ and ξ_z.

5.5.1 Test of Random Effects

We are certainly interested in testing the significance of the random effects. When $\gamma \to \infty$ and $\delta = \gamma \nu$ with ν fixed and finite, the inverted gamma random variable B will concentrate around $1/\nu$ and the mixed-scale gamma process will tend to the simple gamma process with shape function $\alpha\left(t\right)$ and the common scale parameter ξ_z/ν. Therefor, to test the random effects, we test whether γ is small enough. In this case, the null hypothesis is expressed as $H_0 : \gamma = \infty$.

Lawless and Crowder (2004) proposed a score statistic but made a small mistake on the variance of the statistic. Following them, we want to rederive the score statistic in detail. First note that under the null hypothesis, we have

$$\mathrm{E}_0\left[X_t - \alpha_t\, \xi_z/\nu\right] = 0 \tag{5.28a}$$

$$\mathrm{E}_0\left[\left(X_t - \alpha_t\, \xi_z/\nu\right)^2\right] = \alpha_t\, \xi_z^2/\nu^2 \tag{5.28b}$$

$$\mathrm{E}_0\left[\left(X_t - \alpha_t\, \xi_z/\nu\right)^4\right] = 3\left(1 + 2/\alpha_t\right) \alpha_t^2 \xi_z^4/\nu^4 \tag{5.28c}$$

The subscript "0" is put to emphasize the expectations under the null assumption.

From (5.27), the log likelihood function for a single unit is

$$l = \log\Gamma(\delta+\alpha_n) - \log\Gamma(\delta) - \sum_{i=1}^{n}\log\Gamma(\Delta\alpha_i)$$
$$+\,\delta\log(\gamma\xi_z) + \sum_{i=1}^{n}(\Delta\alpha_i - 1)\log(\Delta x_i) - (\delta+\alpha_n)\log(\gamma\xi_z + x_n)\,. \tag{5.29}$$

Let $\delta = \gamma\nu$. Then

$$\frac{\partial l}{\partial\gamma} = \nu\left\{1 + \log(\gamma\xi_z) + \psi(\gamma\nu+\alpha_n) - \psi(\gamma\nu) - \log(\gamma\xi_z + x_n)\right\}$$
$$-\,\xi_z(\gamma\nu+\alpha_n)(\gamma\xi_z + x_n)^{-1} \tag{5.30}$$

where $\psi(\cdot)$ denotes the first derivative of logarithm gamma function. As $\gamma\to\infty$, $\partial l/\partial\gamma \to 0$, so a more detailed calculation is called for. From Bleistein and Handelsman (1975) we have

$$\psi(u) = \log u - \frac{1}{2u} - \frac{1}{12u^2} + O\left(u^{-3}\right). \tag{5.31}$$

Thus,

$$\frac{\partial l}{\partial\gamma} = \nu\left\{\log\left(1 - \frac{x_n}{\gamma\xi_z + x_n}\right) + \log\left(1 + \frac{\alpha_n}{\gamma\nu}\right) + \frac{\alpha_n}{2\gamma\nu(\gamma\nu+\alpha_n)} + \frac{\alpha_n\xi_z/\nu - x_n}{\gamma\xi_z + x_n} + O\left(\gamma^{-3}\right)\right\} \tag{5.32}$$

Note that for small u, $\log(1+u)$ can be approximated as $u - u^2/2 + u^3/3 - \cdots$. Applying this approximation to the above expression and simplifying those terms, we have $\partial l/\partial\gamma = A\gamma^{-2} + O\left(\gamma^{-3}\right)$ where

$$A = -\frac{1}{2}\nu\xi_z^{-2}\left\{(x_n - \alpha_n\xi_z/\nu)^2 - \alpha_n\xi_z^2/\nu^2\right\}. \tag{5.33}$$

A is the statistic for testing the random effects. Although it is not the raw score statistic as defined by the first derivative of the log likelihood, it is nevertheless the leading term of the derivative. Therefore, it is also called a score statistic.

Note from (5.28) that the quantity inside the bracket of (5.33) represents the difference of sample variance of $X(t_n)$ from its population variance. Therefore, from (5.28) we have

$$\mathrm{E}_0[A] = -\frac{1}{2}\nu\xi_z^{-2}\left\{\mathrm{E}_0\left[(X_n - \alpha_n\xi_z/\nu)^2\right] - \alpha_n\xi_z^2/\nu^2\right\} = 0 \tag{5.34}$$

and

$$\mathrm{Var}_0[A] = \mathrm{E}_0\left[A^2\right] = \frac{1}{4}\nu^2\xi_z^{-4}\left\{\mathrm{E}_0\left[(X_n - \alpha_n\xi_z/\nu)^4 - \alpha_n^2\xi_z^4/\nu^4\right]\right\} = \frac{\alpha_n(\alpha_n+3)}{2\nu^2}. \tag{5.35}$$

According to the large-sample theory (Lehmann 1999), the score statistic defined as

$$U = \frac{A}{\sqrt{\mathrm{Var}_0(A)}} \tag{5.36}$$

follows the standard normal distribution. Therefore, given a dataset, one can estimate the parameters of a gamma process and use the estimates to calculate the score statistic U. If $|U|$ is greater than a normal quantile $z_{\alpha/2}$ where α is the significance level, we have significant evidence against the null hypothesis. If so, we may want to further model the data with a mixed-scale gamma process.

A Monte Carlo simulation study is performed to verify the proposed score statistic. Figure 5.4 and 5.5 show the histograms of the score statistic U for a stationary gamma process with shape parameter $\alpha = 3$ and scale parameter $\beta = 2$. For a relatively small dataset, the distribution of the score statistic is biased and skewed as shown in Figure 5.4. In case of a large dataset with 500 units, each having 30 records, the simulated distribution is very close to the standard normal distribution (Figure 5.5). These verify our derivation of the score statistic.

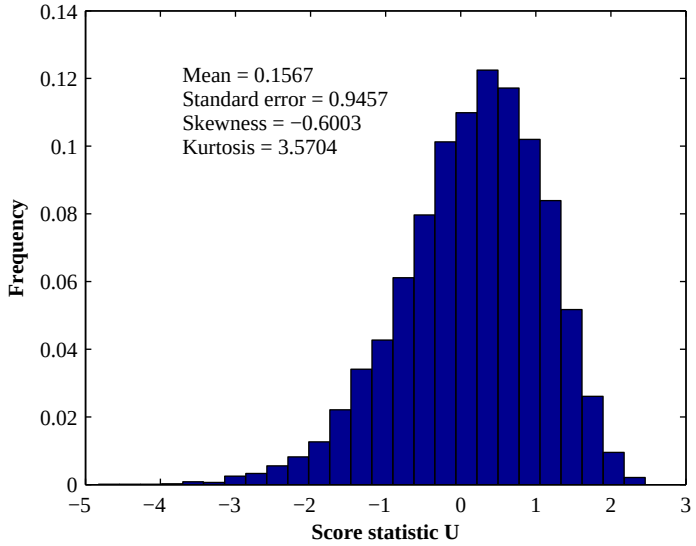

Figure 5.4: Histogram of the score statistic for 20 sample paths of 30 equally sampled records

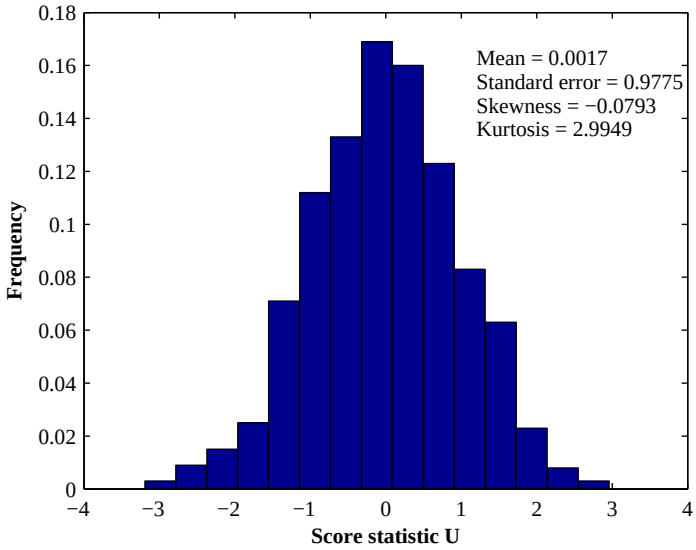

Figure 5.5: Histogram of the score statistic for 500 sample paths of 30 equally sampled records

5.6 Case Study — Creep Deformation

We now re-investigate the dataset of creep deformation of pressure tubes in Chapter 3 where the diametral expansion data was fitted to a linear mixed-effects model. Here we want to explore the possibility of a gamma process model.

Define also the time as the average fluence as did in Chapter 3. Assume the strain increase follows a homogeneous, stationary gamma process with shape parameter α and scale parameter β. The maximum likelihood estimates are

$$\hat{\alpha} = 7.3462\ (1.1420)\,,\ \hat{\beta} = 0.0291\ (0.0045) \tag{5.37}$$

with maximized log likelihood $l\left(\hat{\alpha},\, \hat{\beta}\right) = 9.572$. For the score test for random effects, we get $\hat{A} = -2.78$, $se\left(\hat{A}\right) = 12.41$. Hence $\hat{A}/se\left(\hat{A}\right) = -0.2243$, which indicates no significant evidence of random effects in the data. Considering the measurement errors, the estimates are $\hat{\alpha} = 8.3636\,(1.5230)$, $\hat{\beta} = 0.0256\,(0.0047)$ and $\hat{\sigma}_\varepsilon = 0.0575\,(0.0271)$ with maximized log likelihood $l\left(\hat{\alpha},\, \hat{\beta},\, \hat{\sigma}_\varepsilon\right) = 10.373$. The Likelihood ratio test shows no significant measurement error. Therefore, the random effects and measurement errors are not considered in the subsequent analyses. Figure 5.6 shows the measured versus the fitted creep strain increments with 95% confidence bound.

For an illustration, the lifetime distribution of a typical pressure tube with average flux 2.4×10^{17} n/(m$^2\cdot$s) is shown in Figure 5.7. Comparing to the lifetime from LME model, the lifetime from the GP model has similar mean but smaller standard deviation. The smaller standard deviation seems counter-intuitive as, after all, the GP model includes the temporal uncertainty of the diametral expansion whereas the LME model, as a random variable model in essence, does not. But recall that in the LME model the diametral strain has a quadratic variance function of time, as mentioned in Chapter 3, whereas the GP model implies only a linear variance function. The more scattered deterioration leads to a larger standard deviation of lifetime, of course.

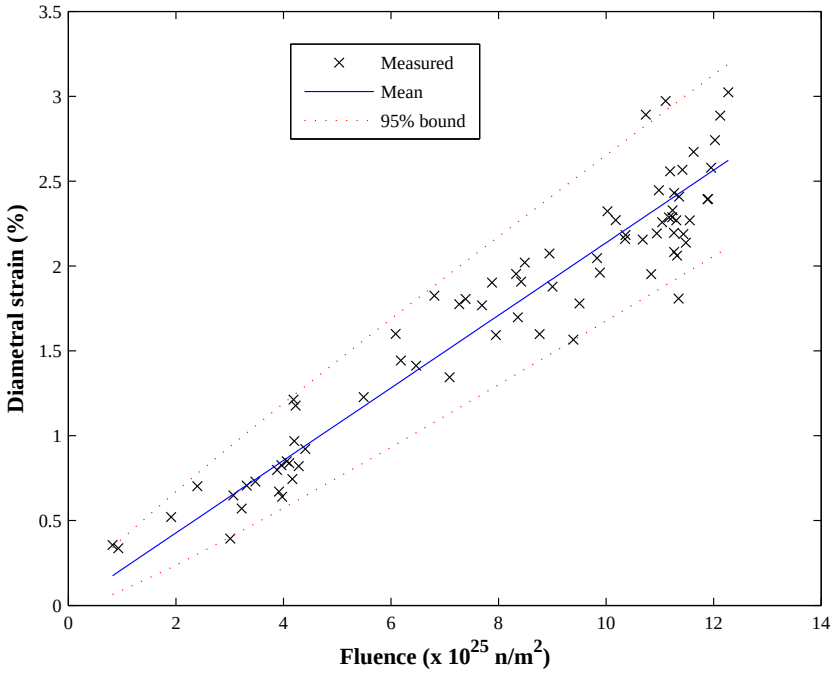

Figure 5.6: Predicted versus observed diametral strain increments from the stationary gamma process model

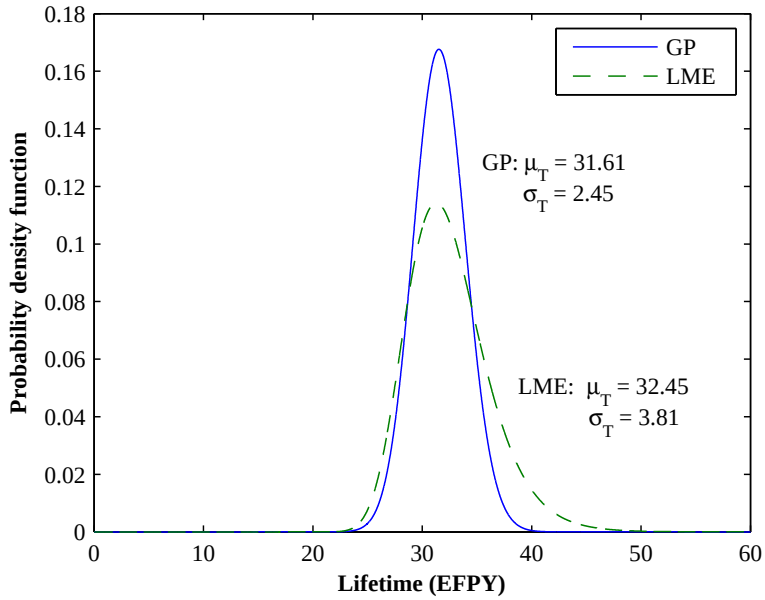

Figure 5.7: Comparison of probability density functions for the lifetime of a typical pressure tube with average flux 2.4×10^{17} n/(m^2·s)

5.7 Summary

A suite of statistical techniques are developed in this chapter for estimating parameters of gamma process models. In particular, both the method of moments and maximum likelihood method are developed for estimating parameters of gamma process models without covariates. An asymptotic covariance matrix of the maximum likelihood estimates for the stationary gamma process is derived and validated by numerical simulation. The maximum likelihood method is further extended for cases with covariates, measurement errors and random effects.

The influence of measurement error on the parameter estimation is studied via a simulation study. The results show that when there are few repeated measurements and the measurement error relative to the deterioration is not small, the inclusion of the measurement error in parameter estimation is important.

In order to test the significance of random effects in a mixed-effects model, a new score statistic is rederived based on the original work of Lawless and Crowder (2004). Monte Carlo simulation results are used to validate the derivation.

The diametral expansion data of pressure tubes discussed in Chapter 3 is re-investigated using a stationary gamma process model. Hypothesis tests show no significant evidence of measurement errors and cross-unit heterogeneity. Although the estimated lifetime from the gamma process has similar mean value to that from the linear mixed-effects model, the former is less dispersed, because the gamma process model assumes the deterioration a linear variance function of time whereas the linear mixed-effects model implies a quadratic function.

Chapter 6

Case Study — Flow Accelerated Corrosion in Feeder Pipes in CANDU Plants

6.1 Background

Feeder pipes are important parts of the primary heat transport system of a CANDU reactor (Figure 1.2). Considerable wall thinning of feeder pipes was observed for the first time at the Point Lepreau reactor in 1995. The degradation mechanism is identified as flow-accelerated corrosion (FAC). Excessive thinning occurs on the inside of the feeder pipes, especially on the outlet elbows close to the exit of the pressure tubes. This prompted generating stations to implement an inspection program to assess the extent of the problem. It is important for a CANDU life extension program to predict the wall thickness and lifetime of feeders based on inspection data.

Flow accelerated corrosion is a process whereby the normally protective oxide layer on carbon steel dissolves into a stream of flowing water or wet steam (Dooley and Chexal

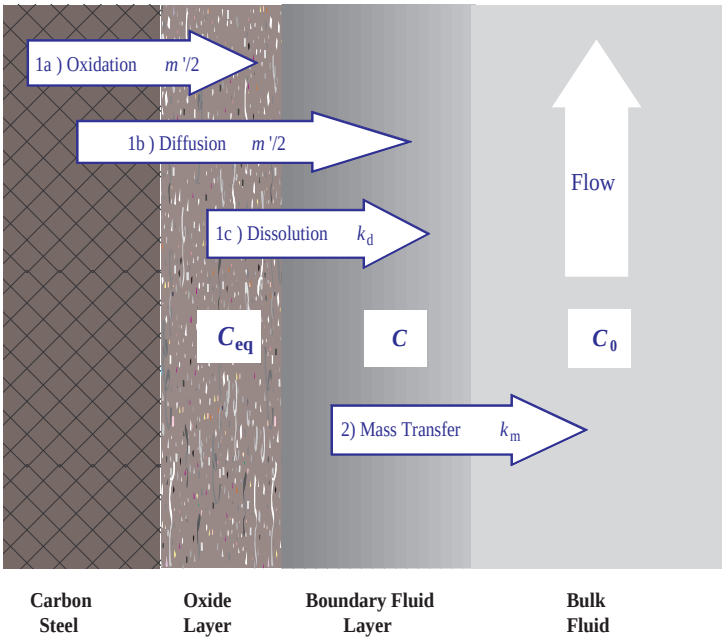

Figure 6.1: Subsequent processes of flow-accelerated corrosion (Burrill and Cheluget 1998)

2000). Although several different physical-chemical mechanisms of the FAC process have been proposed (Berge, Ducreux, and Saint-Paul 1980; Burrill 1995; Burrill and Cheluget 1999; Lang 2000), it is generally agreed that the FAC is an electrochemical corrosion enhanced by mass transfer in flowing water and it can be generally divided into two subsequent processes (Figure 6.1). The first stage is the production of soluble ferrous ions at the oxide-water interface, which involves three simultaneous actions: a) metal oxidation, b) diffusion of ferrous species from the iron surface to the boundary fluid layer through the porous oxide layer, and c) dissolution of magnetite oxide layer. The second stage involves the transfer of the ferrous ions into the bulk water across the diffusion boundary layer.

Feeder pipes connect fuel channels and headers. High-temperature (about 310-312 °C) heavy water flows out of individual fuel channels via the feeder pipes into outlet headers and then goes together to steam generators. After heat exchange in the steam generators,

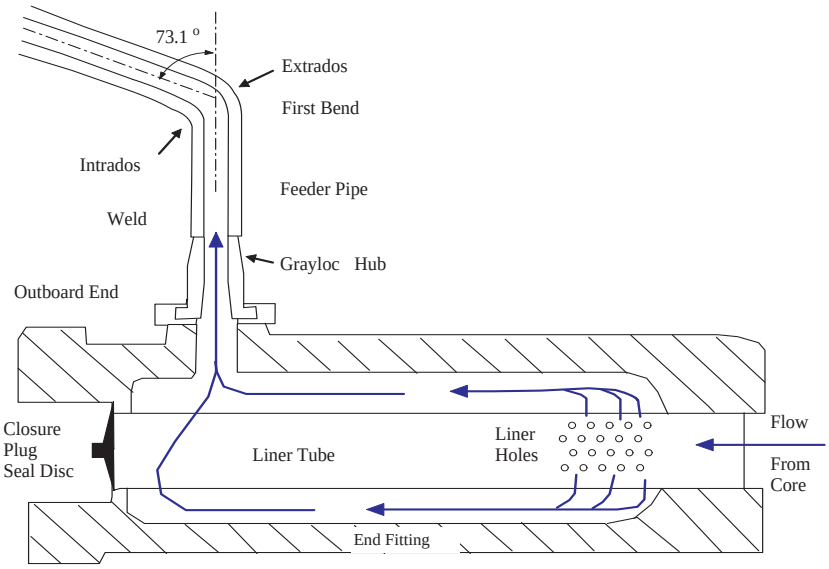

Figure 6.2: Illustration of end-fitting and outlet feeder pipe (Burrill and Cheluget 1999)

the lower-temperature (typically 266°C) heavy water flows back to inlet header and is then distributed to fuel channels through inlet feeders (Burrill and Cheluget 1999). Made of SA 106 Grade B carbon steel, the outlet feeder pipes have typical nominal outer diameter of either 2.0 or 2.5 inches at the reactor face. The flow leaves the end-fitting annulus via a right-angle turn and enters a Grayloc hub (SA 105 carbon steel), resulting in a turbulent flow at the entrance to the outlet feeder pipe, which triggers the flow-accelerated corrosion at the downstream of the hub especially at the first bend (Figure 6.2). The operating flow velocity in individual pipes varies with channel power from 8 to 18 m/s (Burrill and Cheluget 1999). The water is mildly alkaline ($10.2 < pH_a < 10.8$) and contains dissolved deuterium.

The bending process during pipe fabrication causes initial thinning at the extrados and thickening at the intrados (Figure 6.3). Depending upon the bending process and radius of the bend (bending angles), the difference in thickness between intrados and extrados can be up to 25% (Kumar 2004). Therefore, it is presumed that the extrados is

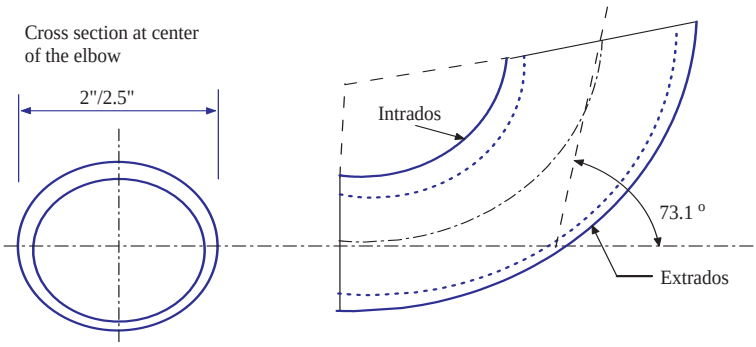

Figure 6.3: Ovality of the feeder cross section and initial wall thinning during fabrication (Kumar 2004)

most vulnerable to FAC because of the lower wall thinning allowance.

Factors affecting the rate of FAC include the fluid flow velocity, pipe geometry (e.g. bend configuration and bend angle), water temperature, water chemistry (e.g. pH value) and metallurgical variables such as chromium content in the steel ((Slade and Gendron 2005)). As far as the FAC in feeder pipes is concerned, however, the effective factors reduce to the flow velocity and geometry configuration of bends, as the other variables are simply constant across the feeders of the reactor. Since there are only a few different geometries used in the pipes, we will discuss in detail the effects of geometry configuration in the data analysis.

For the influence of flow velocity on the FAC rate, Berge, Ducreux, and Saint-Paul (1980) expressed the FAC rate or mass loss of metal per unit time, R, as

$$R = \frac{1}{\frac{1}{2k_d} + \frac{1}{k_m}} \left(C_{eq} - C_0\right) \tag{6.1}$$

where k_d is the magnetite dissolution coefficient, k_m the mass transfer coefficient, C_{eq} and C_0 the concentration of ferrous ions in the metal surface and bulk water, respectively. When mass transfer controls the FAC, which is common for CANDU systems, the

following linear relationship was proposed by Ducreaux (1983):

$$R \approx k_m \left(C_{eq} - C_0\right). \tag{6.2}$$

Since the mass transfer coefficient k_m is usually expressed as a power function of the flow velocity (Berger and Hau 1977), the FAC rate is a power function of the flow velocity, i.e., $R \propto V^{\delta}$ where V stands for the flow velocity and $\delta > 0$.

However, a sophisticated mechanistic FAC model for predicting the wall thinning and end of life has not yet been available, largely because of the complexity of the problem and of the varying working environment. The observed FAC rate varies considerably both across the feeders and over the service life. A probabilistic model that models both the across-feeder uncertainty and the within-feeder uncertainty in the FAC process is essential, as an effective and efficient life-cycle management of the feeders requires an adequate consideration of these uncertainties.

This case study aims to develop a stochastic process model for the feeder thinning and attempts to answer the following questions:

(i) What is the mean lifetime of a feeder, with lifetime defined as the time when the remaining wall thickness falls below a specific substandard threshold w_{th}?

(ii) Given the observed data, what is the remaining lifetime of an inspected feeder?

(iii) How many substandard feeders will there be before the next outage period? and

(iv) When will the first substandard feeder appear?

6.2 Wall Thickness Data and Exploratory Analysis

In this case study a set of wall thickness data from feeder pipes in a CANDU 6 NPP is analyzed. The data consists of 637 measurements of minimum wall thickness near the

Table 6.1: Ratio of repeated measurements of Feeder wall thickness data

Number of Repeated Measurements	**Number of Pipes**	**Percentage (%)**
1	232	61.1
2	94	24.7
3	24	6.3
4	16	4.2
5	6	1.6
6	5	1.3
7	3	0.8
Total	**380**	**100.0**

bend extrados of the first outlet bend taken from all of the 380 feeders at 8 inspection outages. As shown in Table 6.1, about 61% of the inspected bends were measured only once, and only about 15% were measured three or more times. For each feeder, the flow velocity and bend geometry configuration, characterized by its bend type (BT), nominal outer diameter (OD) and bend angle (BA), were recorded. Upon thermohydraulic considerations, two sizes of OD were used in the feeders; 320 feeders (BT1 to BT6) are 2.5" and the other 60 feeders (BT7 to BT12) are 2". Table 6.2 presents the geometry parameters of the first bend of outlet feeders in detail. The flow velocity at the first bend of the outlet feeder was obtained from thermohydraulic analysis and the time-averaged flow velocity from both one- and two-phase flow is used. Different for each feeder, the flow velocity of 2" feeders ranges from 7.72 to 12.63 m/s while that of 2.5" feeders from 6.49 to 14.54 m/s.

The initial wall thickness of the feeders is not known. However, measurements of the wall thickness from two groups of spare bends (16 of 2.5" and 12 of 2") that had not been installed provide the baseline information. The coefficients of variation of the initial wall thickness of the two groups are 1.4% and 1.9%, respectively, both very small. Therefore the mean values, 6.223 mm for 2.5" bends and 4.913 mm for 2" bends, are used as the initial thickness in the subsequent analysis.

Table 6.2: Geometry parameters of the 1st bends of outlet feeders in a CANDU 6 Plant

BT	n	**OD**	**BA**	d	**D**	**Group**
1	2	2.5	32.7	3.90	Out	I
2	8	2.5	42.8	5.14	In	II
3	12	2.5	42.8	5.14	In	II
4A	20	2.5	73.1	3.85	In	III
4B	18	2.5	73.1	3.85	Out	IV
4C	16	2.5	73.1	3.85	Out	IV
5A	12	2.5	73.1	3.85	In	III
5B	16	2.5	73.1	3.85	Out	IV
5C	22	2.5	73.1	3.85	Out	IV
6	194	2.5	73.1	3.85	Out	IV
7	20	2	32.7	4.13	Out	V
8	8	2	42.8	5.44	In	VI
9	6	2	42.8	5.44	In	VI
10A	4	2	73.1	4.40	In	VII
10B	4	2	73.1	4.40	Out	VII
10C	2	2	73.1	4.40	Out	VII
11A	4	2	73.1	4.40	In	VII
11B	2	2	73.1	4.40	Out	VII
11C	2	2	73.1	4.40	Out	VII
12	8	2	73.1	4.40	Out	VII

BT — Bend type
n — Number of feeders per reactor
OD — Outer diameter of bends (inches)
BA — Bend angle (degrees)
d — Distance between end fitting joint and the first bend (inches)
D — Direction that extrados of the first bend faces

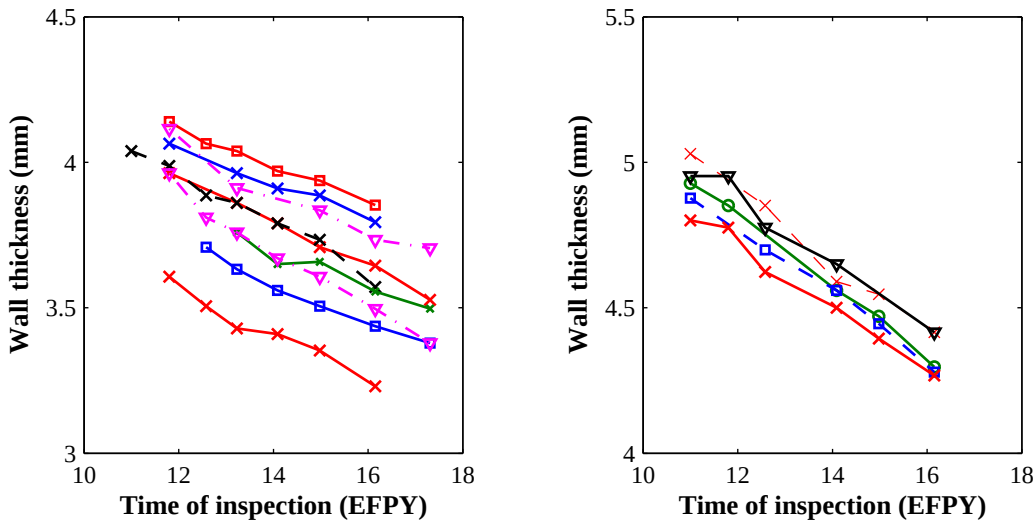

Figure 6.4: Typical wall thinning paths. Left: 2" feeders; right: 2.5" feeders

Figure 6.4 shows typical wall thinning paths with five or more repeated measurements. The loss of wall thickness of the bends appear a nearly linear trend over time. This observation justifies the stationarity of the gamma process that is used in the subsequent analyses.

As discussed in the last subsection, the flow velocity has the most significant impact on the wall thinning rate in comparison to other factors such as bend geometry, coolant temperature and pH values. To illustrate the effect of flow velocity on FAC, the wall thinning rate is calculated as $(w_i - w_0)/t_i$, where w_i is the minimum wall thickness measured at the ith inspection time t_i, and w_0 is the initial wall thickness. The inspection time is measured in effective full power year (EFPY). Figure 6.5 demonstrates great variability in thinning rate and positive correlation between the thinning rate and the flow velocity.

The bend geometry parameters including bend angle, bend direction and distance between end fitting joint and the first bend may be important explanatory variables as

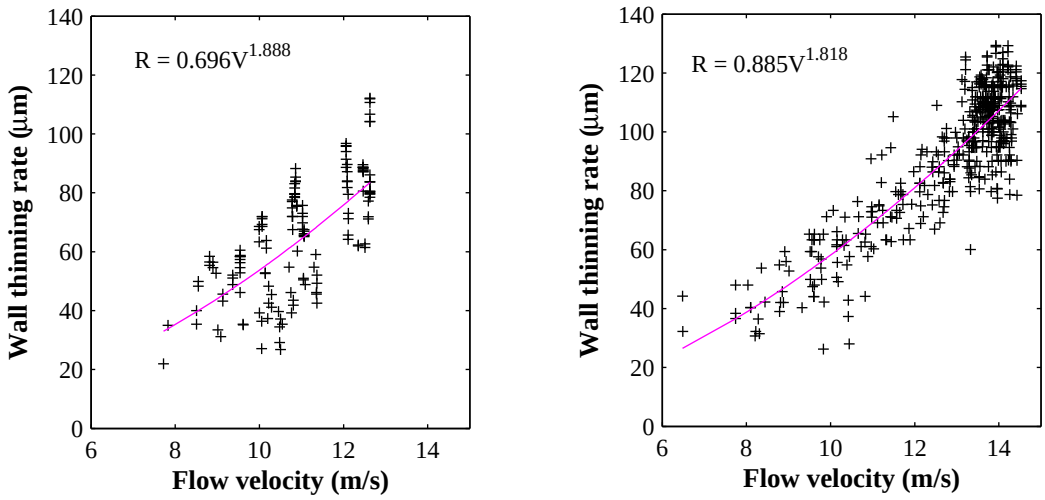

Figure 6.5: Dependence of wall thinning rate on flow velocity. Left: 2" feeders; right: 2.5" feeders

they affect the turbulence structure of the flow at the neighboring area of the bends and thus change the wall thinning rate. According to Table 6.2, we can divide the 2.5" feeders into four groups:

Group I including 2 Type 1 feeders,

Group II including 20 Type 2 and 3 feeders,

Group III including 32 Type 4A and 5A feeders, and

Group IV including 266 Type 4B, 4C, 5B, 5C and 6 feeders.

Similarly, the 2" feeders can be divided into three groups:

Group V including 20 Type 7 feeders,

Group VI including 14 Type 8 and 9 feeders, and

Group VII including 26 Type 10 (A, B, C), 11 (A, B, C) and 12 feeders.

Each group has the same geometry characteristics, except that in Group VII Type 10A and 11A bend into the reactor face whereas the other in the group bend outward. Preliminary study indicated that the bend direction has no significant effect for the 2" feeders, although it does for the 2.5" feeders.

Other FAC factors such as coolant temperature, pH value, metallurgical characteristics are not considered because they are deemed to be the same for all feeders.

6.3 Gamma Process Model and Statistical Inference

6.3.1 Model Structures

The loss of feeder wall thickness due to FAC is a slow, incremental process of mass loss by electrochemical and diffusion reactions, which can be modeled by a gamma process. Since the mean thinning paths appear linear as shown in Figure 6.4, we propose a stationary gamma process with shape parameter α and scale parameter β. To account for the dependence of FAC rate on the flow velocity, the scale parameter is further modeled as a power function as suggested from empirical studies mentioned in Section 6.1:

$$\beta = \eta V^{\delta}. \tag{6.3}$$

Furthermore, both corrosion theory and field experiences of plant engineers indicate that there is an incubation period before any wall thinning can be observed. In other words, the wall thinning due to FAC starts a few years after the system was put in service. Thus it is reasonable to assume that the wall thickness keeps the initial value until some time t_0, the corrosion incubation period. Denote the wall thickness at time t by $W(t)$, the thickness loss by $X(t)$, and its initial value by w_0. Then the wall thickness is expressed as

$$W(t) = \begin{cases} w_0, & 0 \leq t \leq t_0 \\ w_0 - X(t; \alpha, \beta), & t > t, \end{cases} \tag{6.4}$$

in which $X(t)$ is assumed as a stationary gamma process. In summary, the model consists of four parameters: α (shape), η, δ (related to scale) and t_0 (incubation time).

6.3.2 Parameter Estimation

Recall that increments of a stationary gamma process are independent and the gamma distributed with probability density function as

$$g(\Delta x; \alpha, \beta) = \frac{x^{\alpha \Delta t - 1}}{\beta^{\alpha \Delta t} \Gamma(\alpha \Delta t)} e^{-x/\beta}. \tag{6.5}$$

Given the inspection data we can estimate the process parameters by using the method of maximum likelihood. Suppose we inspect a number n of components, each being inspected at m_i different points of time. Then we have the deterioration data in the form of (w_{ij}, t_{ij}, V_i) $(i = 1, \ldots, n,\ \ j = 1, \ldots, m_i)$, in which w_{ij} stands for the wall thickness at time t_{ij} and V_i for the flow velocity associated with the ith pipe. From (6.5) and the independent-increments assumption of gamma process, the likelihood function for the ith feeder with flow velocity V_i is expressed as

$$L_i(\alpha, \eta, \delta, t_0) = \prod_{j=1}^{n_i} \frac{(\Delta w_{ij})^{\alpha \Delta t_{ij} - 1}}{\beta_i^{\alpha \Delta t_{ij}} \Gamma(\alpha \Delta t_{ij})} e^{-\Delta w_{ij}/\beta_i}, \tag{6.6}$$

in which $\Delta w_j = w_i(t_{i,j-1}) - w_i(t_{ij})$, $\Delta t_{ij} = t_{ij} - t_{i,j-1}$, $\beta_i = \eta V_i^{\delta}$, $w_i(t_{i0}) = w_0$ and $t_{i0} = t_0$. Then the complete log likelihood for is expressed as the following:

$$\begin{aligned} l(\alpha, \eta, \delta, t_0) = \sum_{i=1}^{n} \sum_{j=1}^{m_i} [&(\alpha \Delta t_{ij} - 1) \ln \Delta w_{ij} - \ln \Gamma(\alpha \Delta t_{ij}) \\ &- \alpha \Delta t_{ij} (\ln \eta + \delta \ln V_i) - \Delta w_{ij} V_i^{-\delta} / \eta. \end{aligned} \tag{6.7}$$

The parameters are estimated by maximizing the log likelihood function in (6.7). The results from the maximum likelihood estimation are summarized in Table 6.3, in which the

Table 6.3: Maximum likelihood estimates and the score statistics for different groups

Group	η	δ	α	t_0	l	U
II	0.0177 (0.0052)	1.6295 (0.3052)	4.7589 (1.4952)	6.0525 (1.0361)	18.75	0.05
III	0.0158 (0.0038)	1.8334 (0.2224)	4.5921 (1.3484)	3.6872 (1.7469)	22.43	0.47
IV	0.0106 (0.007)	1.5227 (0.0460)	6.6894 (0.4555)	1.3425 (0.2512)	365.17	1.70
V	0.0125 (0.0033)	2.8550 (0.8817)	4.2826 (1.1297)	4.2974 (0.7840)	35.03	0.64
VI	0.0152 (0.0043)	2.1462 (0.2397)	2.9809 (0.8321)	0.0000 (0.0031)	27.31	-0.52
VII	0.0132 (0.0019)	1.6909 (0.1810)	4.9092 (0.6794)	0.5885 (0.5767)	159.82	0.94

Note: Since Group I has only 2 feeders, no meaningful statistical analysis can be done separately. It is pooled into Group V as they have the most similar geometry except OD.

m.l.e., standard errors, and the corresponding maximized log likelihoods are presented. It is interesting to note that the estimated exponent of the flow velocity is about 1.75 whereas previous FAC studies on secondary side pipes suggested an exponent less than 1 (Burrill and Cheluget, 1999)

6.3.3 Model Checks

To check the fitness of the proposed gamma process model for the wall thickness data, the scatter plots with predicted values and 95% confidence bounds are shown in Figure 6.6 to 6.11 for different groups. The gamma process model appears to fit the data fairly well for all the groups.

Besides the qualitative model check, there are three hypotheses to be tested. First, as we mentioned in Chapter 5, the heterogeneity in each group should be checked. Second, we want to test whether a corrosion dormant period does exist, i.e., $t_0 = 0$. Third, we have modeled the effects for each group separately, that is, we used different sets of parameters (α, β, η, t_0) for different groups of feeders. In order to check the effects of the size of OD and of the geometry configuration, we want to test whether two different groups have the same.set of parameters. If they do, it means no significant effects on the wall thinning. For the first hypothesis we use the score test whereas likelihood ratio tests are used for the last two hypotheses.

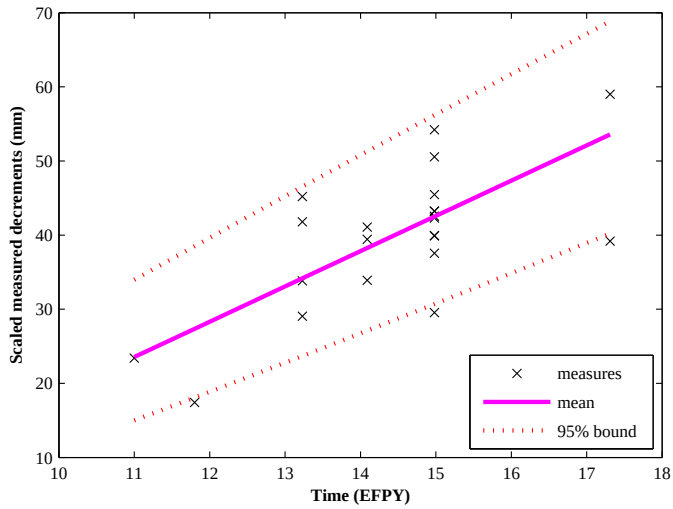

Figure 6.6: Measured versus fitted values with 95% bounds: Group II

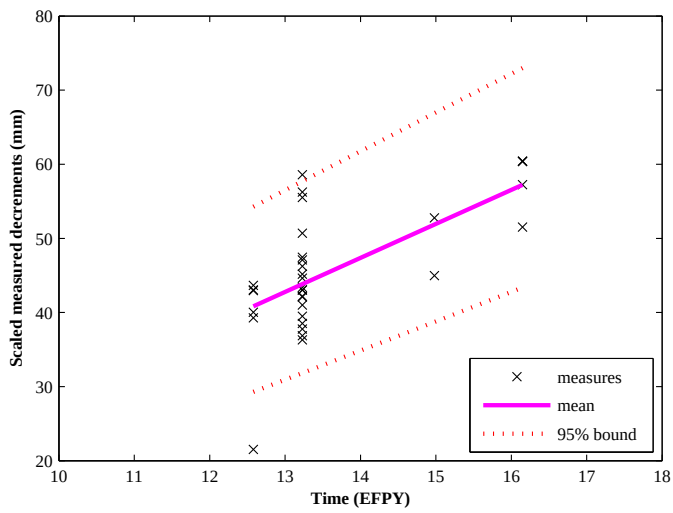

Figure 6.7: Measured versus fitted values with 95% bounds: Group III

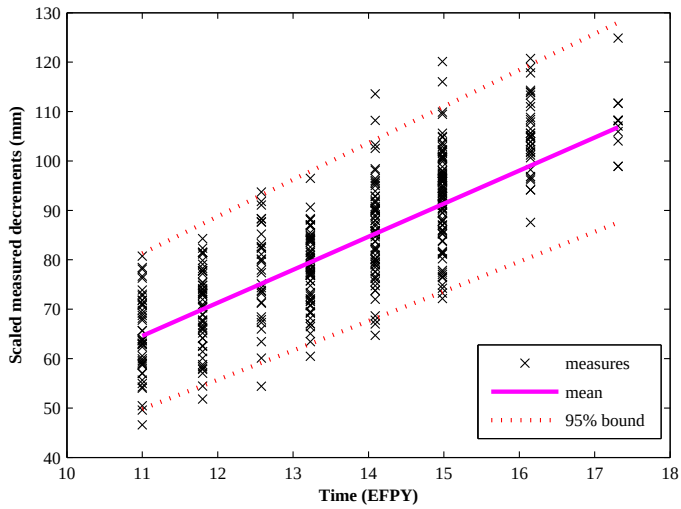

Figure 6.8: Measured versus fitted values with 95% bounds: Group IV

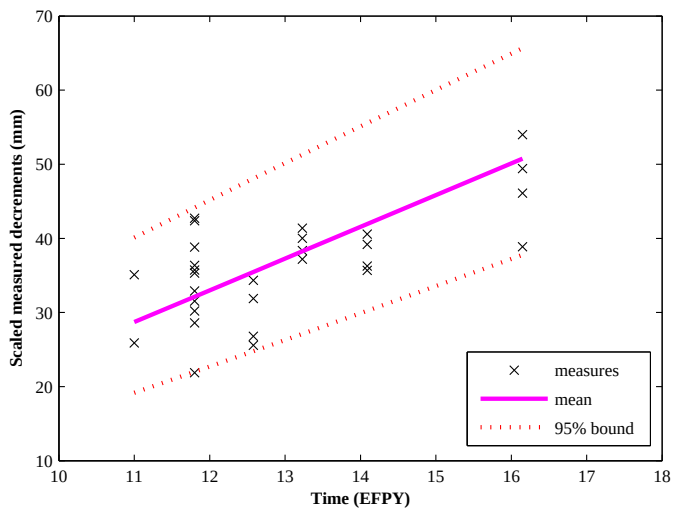

Figure 6.9: Measured versus fitted values with 95% bounds: Group V

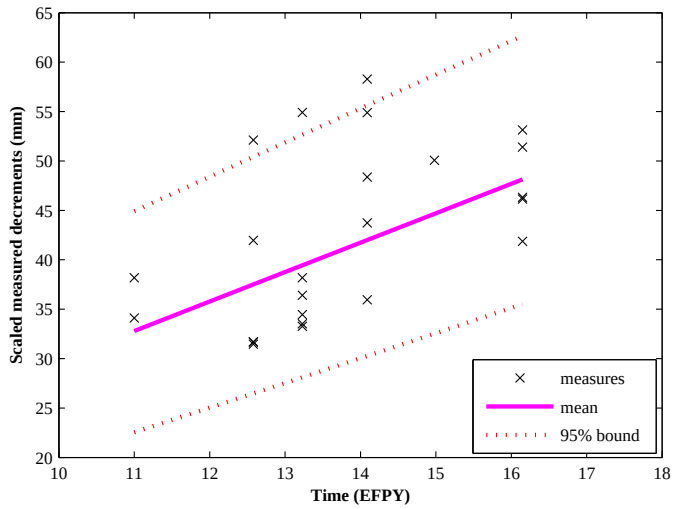

Figure 6.10: Measured versus fitted values with 95% bounds: Group VI

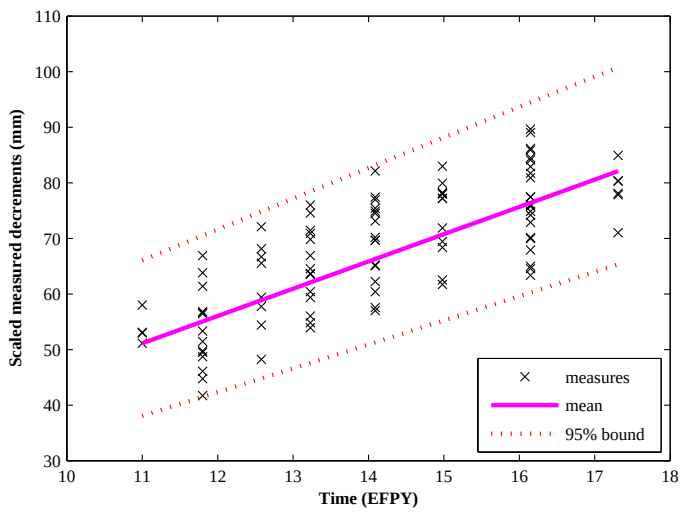

Figure 6.11: Measured versus fitted values with 95% bounds: Group VII

Table 6.4: Likelihood ratio tests for the corrosion incubation period t_0

Group	t_0	l	η_0	δ_0	α_0	l_0	Λ	p
II	6.0525	18.75	0.0269	1.6844	1.8256	13.52	10.5	0.0012
III	3.6872	22.43	0.0169	1.8609	3.1305	21.20	2.46	0.1168
IV	1.3425	365.2	0.0109	1.5345	5.8854	353.1	24.2	0
V	4.2974	35.03	0.0181	2.6262	2.0547	28.32	13.4	0.0003
VI	0.0000	27.31	0.0152	2.1462	2.9809	27.31	0	1
VII	0.5885	159.8	0.0130	1.7035	4.8000	159.3	1.0	0.3173

Let us first look at the test of heterogeneity. For each group, we calculate the score statistics U and they are listed in the last column of Table 6.3. It is clear no group shows strong evidence against the null hypothesis which assumes homogeneity across the feeders in the same group, except for Group IV for which $U = 1.7$, only a mild suggestion of possible heterogeneity. Hence we keep the gamma process model and do not fit a mixed-scale gamma process.

Table 6.4 lists the new maximum likelihood estimates for each group with $t_0 = 0$. The likelihood ratios $\Lambda = 2\,(l - l_0)$ and the corresponding p-values are shown also in the last two columns. Group II, IV and V have shown significant evidence against the null hypothesis while the other three groups have not. Note that no significant evidence against the null hypothesis is not equivalent to accepting the null hypothesis. We may or may not accept the null hypothesis. We choose not to accept the null hypothesis here just for model consistency purpose.

To check the effects of OD and of the geometry configuration, we notice that Group III (Type 4A and 5A) and IV (Type 4B, 4C, 5B, 5C and 6) differ only by the direction that extrados of the first bend faces (see Table 6.2). Both groups have 2.5" OD, the same bend angle of 73.1° and the same distance between the end fitting joint and the first bend. But Group III feeders bend into the reactor face and Group IV feeders bend outward. If we treat the two groups as one and fit them with a gamma process model, we get results shown in Table 6.5 with maximized log likelihood $l = 360.3$. The corresponding likelihood ratio statistic $\Lambda = 2 \times (22.43 + 365.17 - 360.3) = 54.6$. The degree of freedom

Table 6.5: Likelihood ratio test of effects of bend direction

Group	η	δ	α	t_0	l	Λ	p
III	0.0158	1.8334	4.5921	3.6872	22.43		
IV	0.0106	1.5227	6.6894	1.3425	365.17		
III+IV	0.0121	1.6347	5.7211	1.5006	360.3	54.6	≈ 0
VII-1	0.0129	1.7601	4.8551	0.1098	54.11		
VII-2	0.0132	1.6726	4.9612	0.7998	105.89		
VII	0.0132	1.6909	4.9092	0.5885	159.8	0.4	0.98

is $(4+4)-4=4$. Therefore the p-value is $4 \times 10^{-11} \approx 0$, a very significance level.

Similarly, Group VII includes Type 10A and 11A feeders that bend inward, and other feeders that bend outward. We label Type 10A and 11A as Group VII-1 and the other feeders in the group as Group VII-2. In this case, no significant improvement of maximized log likelihood has been found. Hence we can treat them altogether.

Similar exercise can be done for Group II and Group VI, as the two groups differs only by their outer diameters. The results are not shown here to save the space, but the conclusion is that the OD has significant effects on the thinning behavior, at least in terms of parameter estimation.

In summary, the model checks do not show obvious conflict against the assumptions we made in Section 6.3.1 and therefore we use the results in Table 6.3 in the subsequent analyses.

6.4 Prediction of the Lifetime and Remaining Lifetime

When the wall thickness of a feeder reduces to a certain threshold, the feeder is no longer conformed to the standard requirements and becomes a substandard pipe even though it may not break immediately. The time when the feeder reaches the threshold is then called the lifetime of the feeder. Current industrial practice for thinning feeders defines the substandard criteria based on the thinning region and extent and the remaining

wall thickness (Gerber et al. 1992; Deardorff et al. 1999; Hasegawa et al. 2004). For illustration purpose, we consider only the remaining wall thickness as the criterion and the substandard threshold, w_{th}, is chosen as 60% of the nominal thickness, w_0.

Due to the monotone nature of the sample path of the gamma process, the lifetime of the feeder has a cumulative distribution function as

$$\begin{aligned} F_T(t) &= \Pr\{W(t) < w_{th}\} = \Pr\{X(t) > w_0 - w_{th}\} \\ &= \begin{cases} 0, & t \leq \hat{t}_0 \\ 1 - GA(0.4w_0; \hat{\eta}(t - \hat{t}_0), \hat{\delta}), & t > \hat{t}_0 \end{cases} \end{aligned} \tag{6.8}$$

in which $w_{th} = 0.6w_0$, $\hat{\delta} = \hat{\alpha}V^{\hat{\beta}}$, and $\hat{\alpha}$, $\hat{\beta}$, $\hat{\eta}$, $\hat{t}_0$ are the m.l.e. of the parameters, as shown in Table 6.3.

Different feeders have different lifetime distributions, as their flow velocity and geometry configuration differ. The probability density functions of lifetime of the feeders are plotted in Figure 6.12. Each subpanel of the figures shows two density functions associated with maximum and minimum flow velocities of the group. For other feeders in the group, depending on their flow velocity, the lifetime distribution should locate somewhere between the two densities. Table 6.6 lists the maximum and minimum mean lifetimes of each group and their corresponding standard deviations. Figure 6.13 demonstrates the trend of the mean lifetime along the flow velocity. At the same flow velocity, feeders in Group VII (or Type 10, 11 and 12) deteriorate faster than those in the other groups and feeders in Group VI (Type 8 and 9) appear to deteriorate slowliest. At the same flow velocity, the 2.5" feeders (Group II, III and IV) have very close values of lifetime. In contrast, the lifetime of 2" feeders at the same flow velocity has large range across different configurations of bend geometry.

The remaining lifetime, given that the remaining wall thickness of the feeder is known,

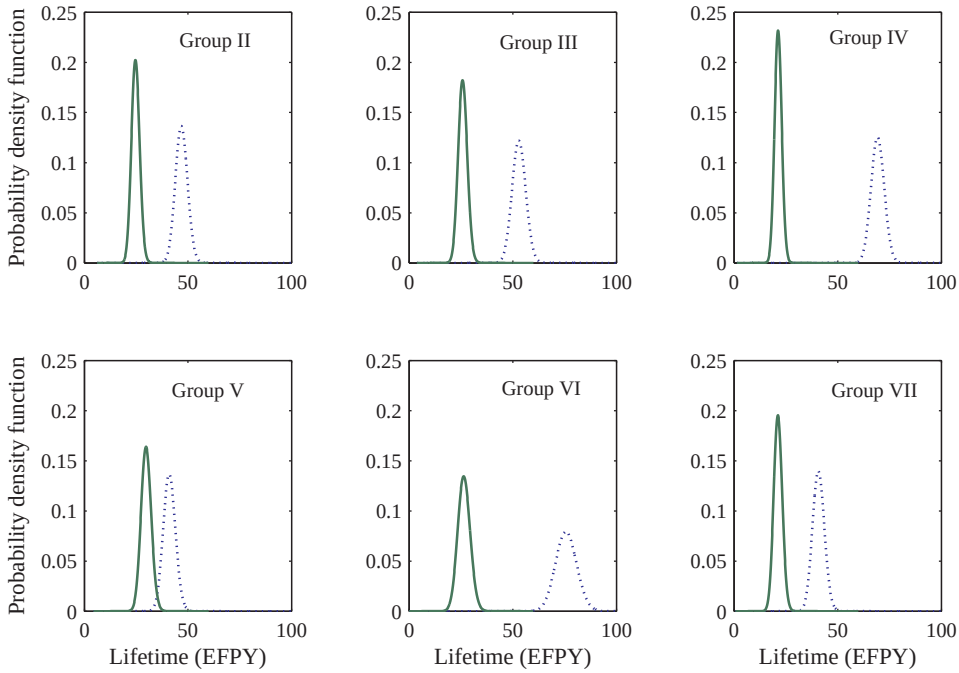

Figure 6.12: Probability density functions of feeder lifetime due to FAC

Table 6.6: Maximum and minimum mean lifetimes and associated standard deviations for different groups

Group	Minimum mean (st. dev.)	Maximum mean (st. dev.)
II	24.64 (2.40)	46.80 (3.55)
III	25.80 (2.65)	52.91 (3.95)
IV	21.23 (2.23)	69.20 (4.11)
V	29.76 (2.91)	40.96 (3.49)
VI	26.41 (3.38)	75.68 (5.74)
VII	21.14 (2.50)	40.65 (3.49)

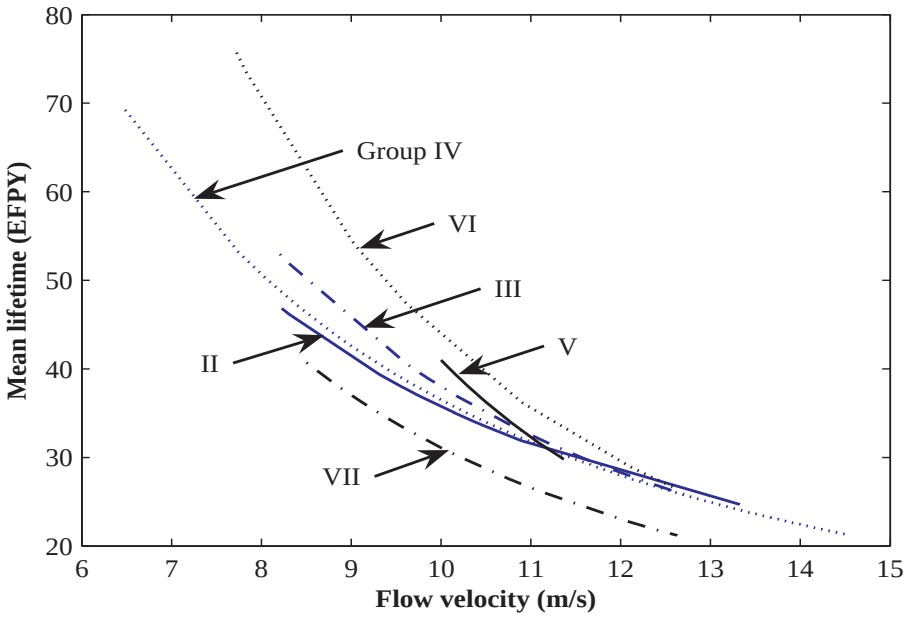

Figure 6.13: Mean lifetime of feeders against flow velocity

say $W(s) = w_s$, is expressed as

$$\begin{aligned} F_T(t|w_s) &= \Pr\{W(t) < w_{th}|W(s) = w_s\} \\ &= \Pr\{X(t) > w_0 - w_{th}|X(s) = w_0 - w_s\} \\ &= \Pr\{X(t) - X(s) > w_s - w_{th}\} \\ &= 1 - GA(w_s - w_{th}; \hat{\eta}(t-s), \hat{\delta}) \end{aligned} \tag{6.9}$$

for $t > s \geq \hat{t}_0$. The second equation holds because of the independent increments.

Figure 6.14 shows the remaining wall thickness measured at the latest inspection times. The substandard threshold is also drawn to shown how close the feeders are to the threshold. The latest measured wall thickness can be used to update the estimation of the lifetime of feeders. For illustration purpose, for each group, one feeder with the least remaining wall thickness is chosen and its remaining lifetime distribution is compared

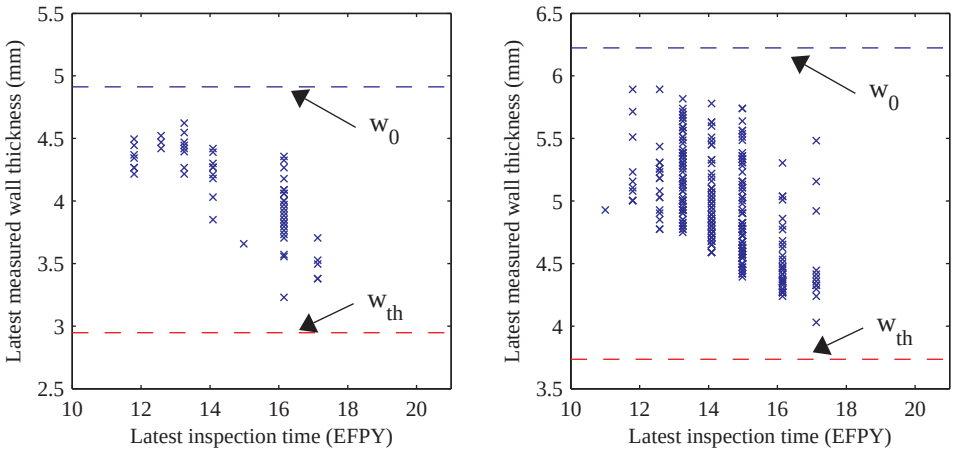

Figure 6.14: The latest measured wall thickness. Left: 2” feeders; right: 2.5” feeders

with the original lifetime distribution, as shown in Figure 6.15 The updated lifetime distributions have less standard deviation than the original ones. This is also true for other feeders that are not displayed here, because the remaining thickness introduces new useful information for the lifetime prediction. But the mean lifetime from the updated distributions should not always be less than the original mean lifetime as shown in the figure, because shown here are only those feeders with the least remaining thickness. For the comparison of the mean lifetime of other feeders, see Figure 6.16. The updated values are evenly scattered around the mean values predicted from the original distribution, as witnessed by the variation of the latest measurements in Figure 6.14. The difference of the predicted mean lifetimes based on the original and updated distribution can be as large as 3 EFPYs.

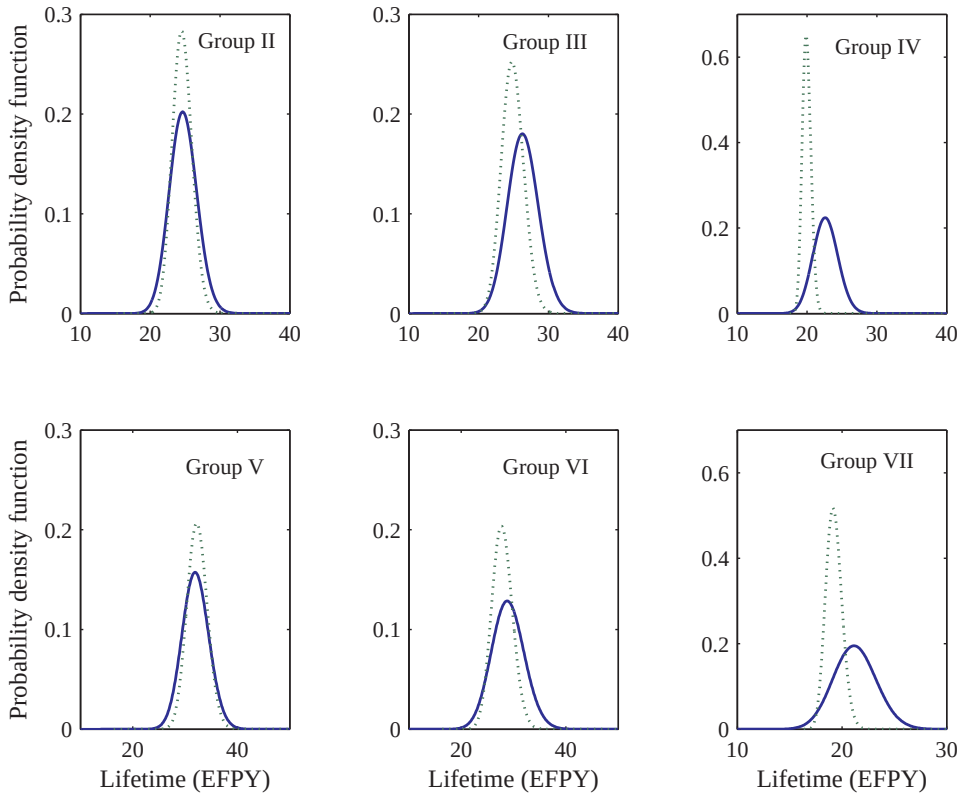

Figure 6.15: Comparision of original (solid lines) and updated (dotted lines) lifetime distributions of the feeders with the least remaining thickness

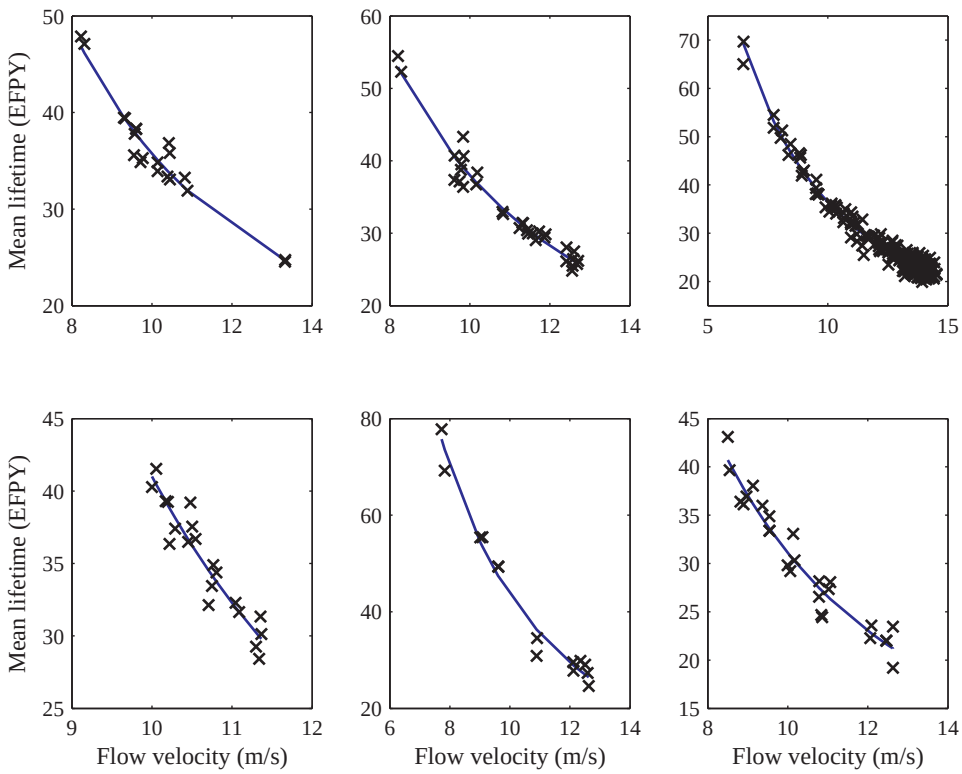

Figure 6.16: Comparison of original (solid line) and updated (crosses) mean lifetimes of feeders

6.5 Probability Distribution of the Number of Substandard Feeders

The lifetime distribution and its associated moments give information of a specific feeder pipe. In order to help decision-making regarding to in-service inspection and outage scheduling, it is also desirable to know the system behavior of the whole core, that is, we want to know the probability distribution of the number of substandard feeders in the next inspection period, or alternatively, the probability distribution of the time when the first substandard feeder appears.

We use combinatorial analysis to find the probability of the number of feeders whose minimum wall thickness would fall below the substandard threshold during the next inspection interval. To do that, we need first to compute the probability of failure for each feeders at time t, denoted by $p_i(t)$ $(i = 1, \cdots, n = 380)$, using (6.9) based on the latest measured wall thickness. Then the probability of the number of failed feeders is evaluated by the following equations:

$$P(0;t) = \Pr\{N(t) = 0\} = \prod_{i=1}^{380} [1 - p_i(t)], \tag{6.10a}$$

$$P(1;t) = \Pr\{N(t) = 1\} = P(0;t) \sum_{i=1}^{380} \frac{p_i(t)}{1 - p_i(t)}, \tag{6.10b}$$

$$P(2;t) = \Pr\{N(t) = 2\} = P(0;t) \sum_{1=i<j}^{380} \left(\frac{p_i(t)}{1 - p_i(t)}\right)\left(\frac{p_j(t)}{1 - p_j(t)}\right), \tag{6.10c}$$

$$P(3;t) = \Pr\{N(t) = 3\} = P(0;t) \sum_{1=i<j<k}^{380} \left(\frac{p_i(t)}{1 - p_i(t)}\right)\left(\frac{p_j(t)}{1 - p_j(t)}\right)\left(\frac{p_k(t)}{1 - p_k(t)}\right), \tag{6.10d}$$

$$\vdots$$

Since the computation increases geometrically with the total number, n, of feeders, a

Monte Carlo simulation algorithm is developed to carry out the combinatorial analysis. For each time t, we first compute $p_i(t)$ for each feeder. Then generate n 0-1 random variates, $U_1, U_2, \ldots, U_n$, where the U_i follows the following distribution: $\Pr(U_i = 0) = p_i(t) = 1 - \Pr(U_i = 1)$. The number of substandard feeders is just the number of zeros in the generated variates. To get the probability distribution of $N(t) = j$, $(j = 1, \ldots, n)$, we count the number of times when the number of substandard feeders equals j and divide this number by the total number of simulations.

Instead of displaying individual probabilities, we plot histograms of the individual failure probability at three different times in Figure 6.17 for sake of conciseness and clarity. Figure 6.17 also compares the histograms from the original lifetime distributions and from the updated distributions using the latest inspection information. At the time of 18 and 19 EFPY, the updated lifetime distributions predict no feeders of which the substandard probability is greater than 0.02 while the original distributions predict several such feeders. At 20 EFPY, however, the updated distributions can tell two feeders of which the substandard probability has already reach over 0.5 whereas the original distributions predict none of such feeders.

This trend is reflected in the plots of probability of the number of substandard feeders in the whole reactor core, as shown in Figure 6.18: The original lifetime distributions predict the probability of no substandard feeder at 18 EFPY is about 0.4 and drops below 0.1 one EFPY later. But the updated lifetime distributions predict the probability of no substandard feeder is above 0.9 at 18 EFPY and just around 0.4 at 19 EFPY. As a result of this difference, the system behavior differs significantly, as demonstrated in Figure 6.19. The original lifetime distributions predict the mean time to the first appearance of a substandard feeder being 17.75 EFPY with standard deviation 0.61 EFPY and the updated distributions predict the mean time of 18.85 EFPY and associated standard deviation of 0.43 EFPY, again smaller than the previous standard deviation.

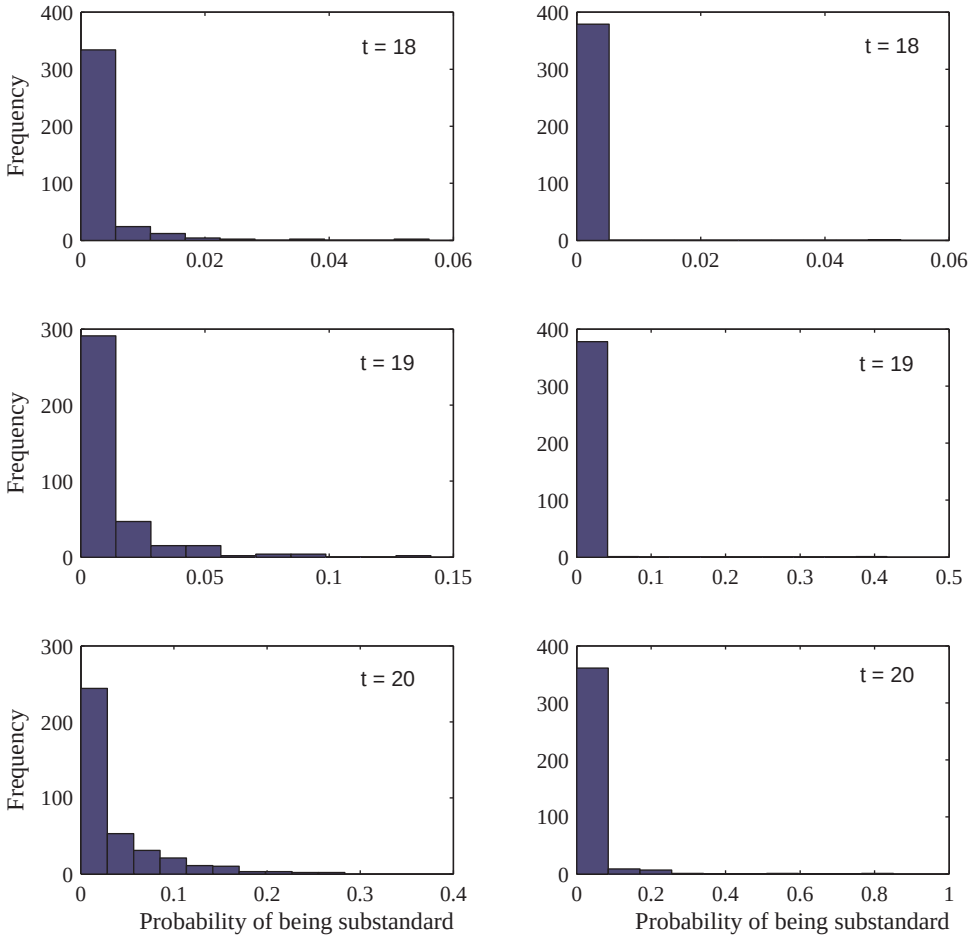

Figure 6.17: Histograms of probability of feeders reaching substandard state based on original (left panels) and on updated (right panels) lifetime distributions

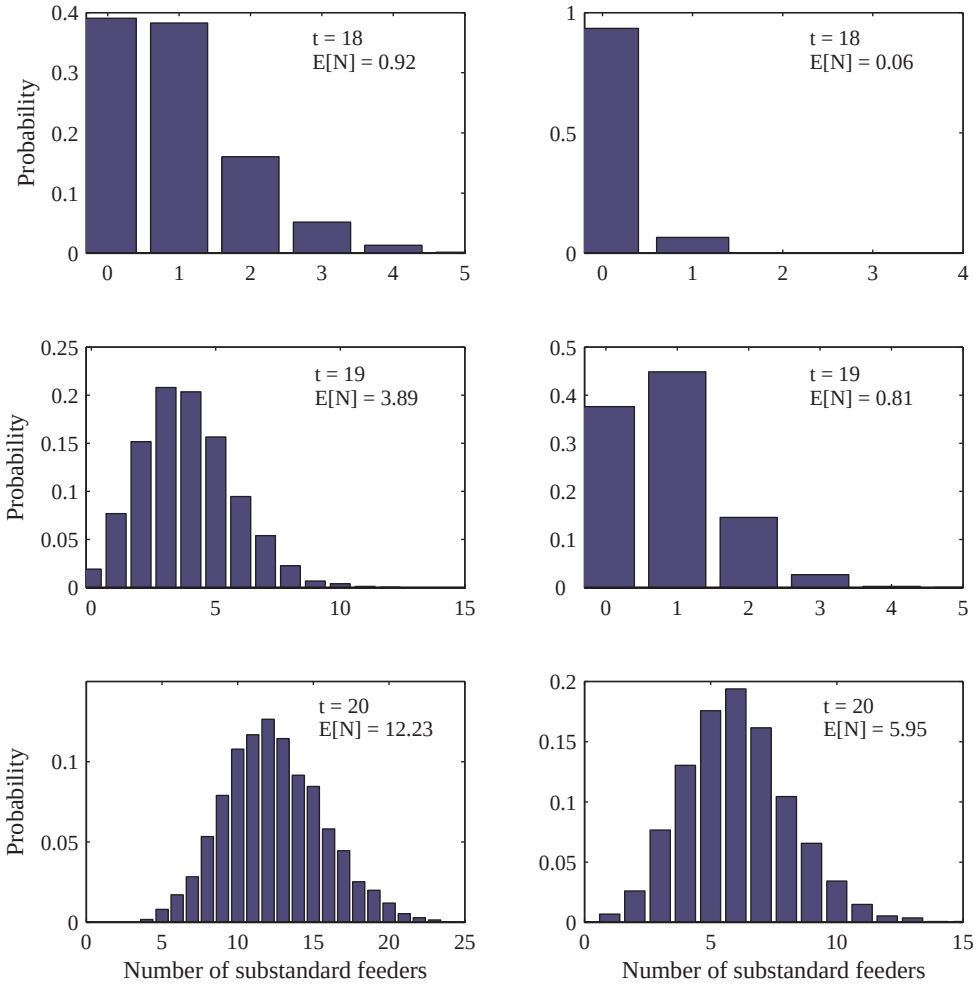

Figure 6.18: Probability distribution of the number of substandard feeders based on original (left panels) and on updated (right panels) lifetime distributions

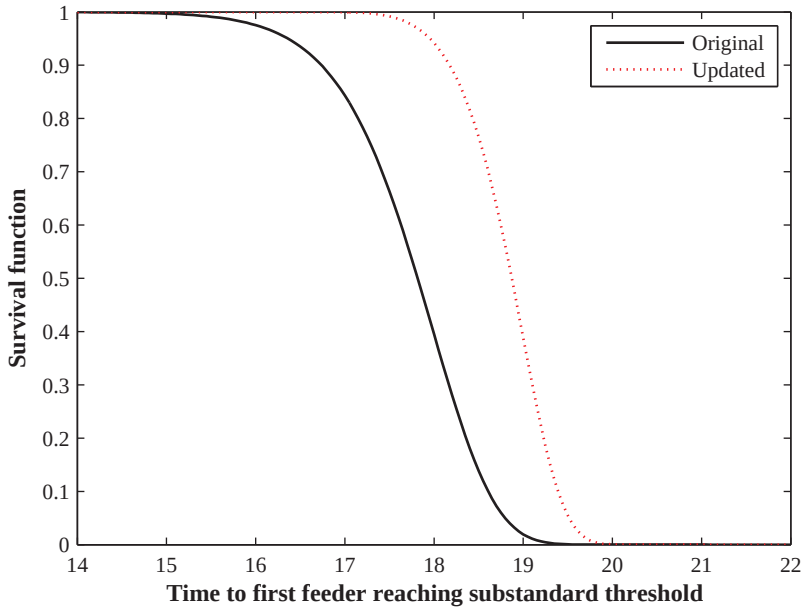

Figure 6.19: Survival functions of the time to the first appearance of a substandard feeder

6.6 Summary

Wall thinning due to the flow accelerated corrosion is a pervasive degradation in the outlet feeder pipes of the CANDU nuclear power plants. This chapter undertakes a comprehensive analysis of the wall thickness data from the outage inspections and fits them with the gamma process model proposed in Chapter 4 and 5. Taking into account the empirical knowledge of FAC, the model integrates both temporal variation and fixed effects of flow velocity and of geometry configuration of the bends. The parameters are estimated by using the maximum likelihood method and the model is carefully checked using both qualitative and quantitative techniques.

Based on the stochastic thinning process, the lifetime of every feeder pipe is estimated. The reliability of the feeder piping system is then computed by a combinatorial analysis, which can be easily implemented by a simple Monte Carlo simulation. An advantage of the gamma process model is that when new inspection data is available, the remaining

lifetime can be updated in a simple way. The value of inspection is seen from the change of mean number of substandard feeders and the system survival curve.

Chapter 7

Effects of Temporal Uncertainty in Planning Maintenance

7.1 Introduction

Maintenance decisions regarding the time and frequency of inspection, repair and replacement are complicated by temporal uncertainty associated with the deterioration of systems. Although many stochastic models of deterioration with applications have been reported (see Chapter 2), the impact of temporal uncertainty on maintenance optimization problem has been lacking in the engineering literature. To address this issue, this chapter chooses a random variable (RV) model as the benchmark and evaluates the effects of temporal uncertainty in planning maintenance through comparisons of optimized maintenance strategies of a gamma process (GP) model and the RV model.

The chapter is organized as follows. First of all, the RV model is reviewed and basic results about it are given for easy reference. Then the maintenance optimization problems including both age-based replacement (ABR) and condition-based maintenance (CBM) are formulated. For each policy, we use as a case study the diametral expansion data

of pressure tubes discussed in the earlier chapters to compare the two models. To get a better insight into the effects of temporal uncertainty, a sensitivity analysis is carried out, in which the deteriorate rate is assumed as a gamma random variable for the RV model and the two models are calibrated in terms of the first two moments of lifetime. The two versions of the deterioration models are then compared in terms of the life-cycle cost of both ABR and CBM policies. The last section concludes the chapter with summaries.

7.2 Random Variable Model

The random variable model characterizes the randomness of deterioration by a finite-dimension vector of random variables Θ as $X(t;\Theta)$. Consider here a simple random deterioration rate model as

$$X(t) = At \tag{7.1}$$

where A is the random deterioration rate that reflects the uncertain nature of deterioration in a population of similar components. Given the probability distribution of the random rate, $F_A(a)$, the probability distribution of the amount of the deterioration, $X(t)$, is derived as $F_{X(t)}(x) = F_A(x/t)$. The mean, variance and coefficient of variation (COV) of $X(t)$ are expressed, respectively, as

$$\mu_{X(t)} = \mu_A t,\ \sigma^2_{X(t)} = \sigma^2_A t^2 \text{ and } \nu_{X(t)} = \frac{\sigma_{X(t)}}{\mu_{X(t)}} = \nu_A. \tag{7.2}$$

The lifetime, defined as the first passage time over a threshold ζ and denoted by T, has the probability distribution function as

$$F_T(t) = \Pr(T \leq t) = \Pr(At \geq \zeta) = 1 - F_A(\zeta/t). \tag{7.3}$$

Depending on the distribution of A, the lifetime distribution can be derived analytically or computed numerically.

7.3 Age-Based Replacement

Age-based replacement (ABR) is the simplest policy for the renewal of deteriorating fleets of components. Under this policy, a component is replaced when it reaches a specific age regardless of its condition. The specific age is called replacement age and denoted by t_a. The component is of course also replaced if failure occurs before the replacement age.

Denote by C_F the total cost associated with all the consequences of a failure, and by C_P the cost of a preventive replacement. According to the renewal theory, the average cost per unit time in long term, also known as the mean cost rate K_a, can be computed as the ratio of mean cycle cost to mean cycle length. A renewal cycle refers to the period from the instant when the unit is put in service to the instant when the unit is replaced upon failure or upon the replacement age. Therefore the renewal cycle length, denoted by L, has the probability distribution as

$$F_L(s) = \Pr\{L \leq s\} = \begin{cases} F_T(s), & \text{for } s < t_a, \text{ or a premature failure} \\ 1, & \text{for } s \geq t_a, \text{ or a preventive replacement,} \end{cases} \tag{7.4}$$

Since for a positive random variable with survival function G, its mean value equals $\int_0^\infty G(s)\,ds$, the mean cycle length is evaluated by $\mathrm{E}[L(t_a)] = \int_0^{t_a} [1 - F_T(s)]\,ds$. The cycle cost is the cost incurs during a renewal cycle. This includes a possible failure cost C_F with $F_T(t_a)$ as the probability of failure before t_a and a possible preventive maintenance cost C_P with $1 - F_T(t_a)$ as the probability of no failure by t_a. Therefore the mean cycle cost is $\mathrm{E}[C(t_a)] = F_T(t_a)\,C_F + [1 - F_T(t_a)]\,C_P$. Hence the mean cost rate is expressed as (Barlow and Proschan 1965):

$$K_a(t_a) = \frac{F_T(t_a)\,C_F + [1 - F_T(t_a)]\,C_P}{\int_0^{t_a} [1 - F_T(s)]\,ds}. \tag{7.5}$$

It is easy to check that $K_a \to C_F/\mu_T$ as $t_a \to \infty$, where μ_T is the mean lifetime. Using (7.5), an optimal age of preventive replacement (t_a) can be found that would minimize

the mean cost rate.

Since the calculation of the mean cost rate is sensitive to the lifetime distribution $F_T(t)$, it would be of interest to examine the impact of RV and GP models on the replacement policy. For an illustration, the ABR of pressure tubes due to irradiation creep is discussed in the next.

7.3.1 Example: Age-Based Replacement of Pressure Tubes for Creep Deformation

Section 3.4 and 5.6 fitted a linear mixed-effects (LME) model and a GP model, respectively. In Section 3.4, the diametral strain due to creep expansion, is modeled by an LME model: $Y(t) = \beta_0 + \beta_1 t + \Theta t + \varepsilon$, where $\beta_0 = 0.0637$ and $\beta_1 = 0.2077$ are regression constants and Θ is a normal random variable $N\left(0, \sigma_\Theta^2\right)$ with $\sigma_\Theta = 0.0232$ to account for the random effects. Note here t stands for the total fluence experienced on the pressure tubes, which is the product of average flux and working time. Since ε represents measurement error, the true deterioration $X(t)$ is the remaining value of $Y(t)$ without ε. That is, $X(t) = \beta_0 + Bt$ where $B \sim N\left(\beta_1, \sigma_\Theta^2\right)$. β_0 is a fixed number and can be absorbed into the failure threshold ζ. So the LME model is in effect a RV model discussed in Section 7.2. The growth of the diametral strain is also modeled in Section 5.6 by a gamma process with shape parameter 7.3462 and scale parameter 0.0291.

Let again the substandard threshold $\zeta = 5.1$. The lifetime distributions in Figure 5.7 are used for finding the optimal ABR policy. Recall that these two lifetime distributions correspond to a typical pressure tube with average flux 2.4×10^{17} n/(m^2·s). The coefficient of variation of the lifetime is around 0.1 in the RV model whereas it is 0.08 in the GP model.

Suppose $C_P = 10$ and $C_F = 50$. The mean cost rates for the RV and GP model are plotted against the replacement age in Figure 7.1. Interestingly, although the limited mean cost rate in the GP model is less than that in the RV model, the minimal mean

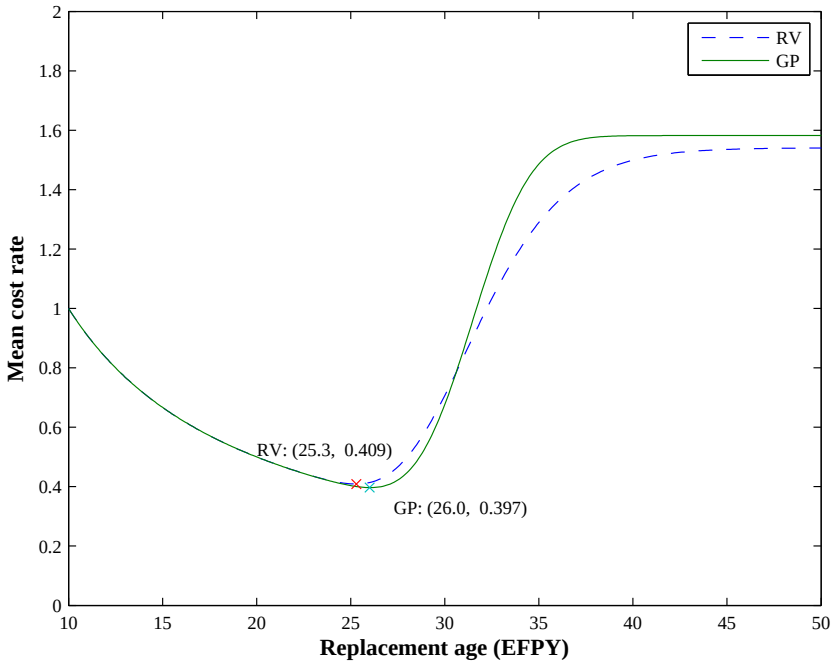

Figure 7.1: Optimal age-based replacement policies for a pressure tube due to diametral expansion

cost in the GP model is higher than the minimal value in the RV model. Nevertheless, the difference of the ABR policies from the two models is slight.

7.4 Condition-Based Maintenance

The deterioration along a specific sample path is deterministic in the RV model, whereas it varies probabilistically in the GP model. In the linear RV model, one inspection determines the deterioration rate and it fixes the future deterioration path. An inspection in GP model, however, reveals only the current state of deterioration from which we can infer only the probability distribution of future deterioration. This distinction has profound implications to the optimization of condition-based maintenance strategies.

7.4.1 The Strategies

The condition-based maintenance (CBM) strategy involves the periodic inspection of a deteriorating component at a fixed time interval t_I and cost C_I. We assume that the inspection is accurate such that the deterioration $X(t)$ can be measured with negligible error. The threshold for the preventive maintenance (PM), $\zeta_P = c\zeta$ $(0 < c < 1)$ is a fraction of the failure threshold. c is called PM ratio. The PM results in a complete renewal (as good as new) of the component. If $X(t_I) < c\zeta$, no action is taken until the next inspection. A component is renewed with PM cost C_P when $c\zeta \leq X(t_I) < \zeta$. If the structure fails between two successive inspections, i.e., $X(t) \geq \zeta$, failure is detected immediately and a corrective maintenance (CM) would renew the structure immediately, incurring a total failure cost, C_F. Typically PM cost is much lower than the failure cost, i.e., $C_P < C_F$.

The optimization of the condition-based maintenance means finding the inspection interval (t_I) and the PM ratio (c) that would minimize the long-run mean cost rate. This in principle involves a two-dimensional optimization problem. When, however, the PM threshold $c\zeta$ is known from experience or prescribed by industry standards or regulations, the inspection interval is the only optimization variable.

7.4.2 Formulation for Random Variable Model

For the RV model, the three possibilities that arise at the time of first inspection (t_I) are: do nothing, PM or CM followed by a failure, as shown in the decision tree in Figure 7.2.

When $X(t_I) < c\zeta$, no action is taken, but the time of preventive maintenance in future can be predicted as $t_{PM} = c\zeta t_I / X(t_I)$, since one inspection is sufficient to determine the linear sample path. The other two situations are straightforward. The PM is immediately conducted when $c\zeta < X(t_I) < \zeta$, and it is correctively replaced when $X(t_I) > \zeta$.

The most important point is that under the assumption of the linear RV deterioration

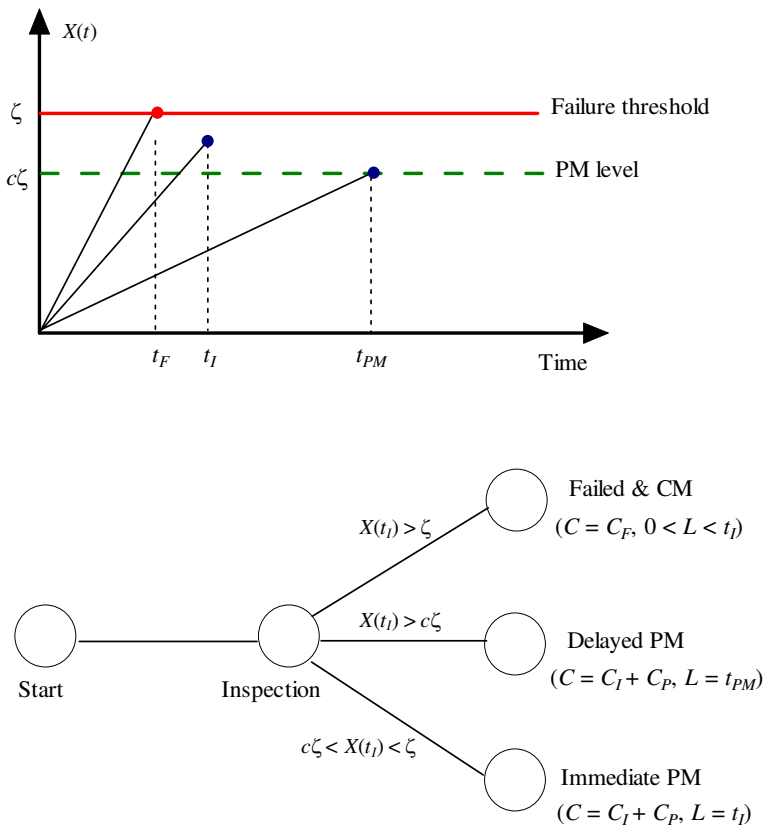

Figure 7.2: CBM decision tree for the RV model

model, only one inspection is required for the implementation of CBM strategy. In a general RV model with n random variables, only n inspections are required for the implementation of CBM.

From the decision tree and associated costs shown in Figure 7.2, the mean value of renewal cycle cost (C) is simply evaluated as

$$\begin{aligned} \mathrm{E}\left[C\left(t_I, c\right)\right] &= \left(C_I + C_P\right) \Pr\left\{X\left(t_I\right) \leq \zeta\right\} + C_F \Pr\left\{X\left(t_I\right) > \zeta\right\} \\ &= \left(C_I + C_P - C_F\right) F_A\left(\zeta / t_I\right) + C_F. \end{aligned} \tag{7.6}$$

Similarly, we have the mean cycle length is evaluated as

$$\begin{aligned} \mathrm{E}\left[L\left(t_I, c\right)\right] &= \int_0^{t_I} \Pr\left\{X\left(t\right) < \zeta\right\} dt + \int_{t_I}^{\infty} \Pr\left\{X\left(t\right) < c\zeta\right\} dt \\ &= \int_0^{t_I} F_A\left(\zeta / t\right) dt + \int_{t_I}^{\infty} F_A\left(c\zeta / t\right) dt. \end{aligned} \tag{7.7}$$

Equations (7.6) and (7.7) can be easily evaluated given the parameter of the distribution of the deterioration rate. According to renewal theory, the mean cost rate is given as

$$K_i\left(t_I, c\right) = \frac{\mathrm{E}\left[C\left(t_I, c\right)\right]}{\mathrm{E}\left[L\left(t_I, c\right)\right]}. \tag{7.8}$$

As $t_I \to 0$, the mean cycle cost approach to $C_I + C_P$ and the mean cycle length approaches the mean time to the PM threshold that equals to $\int_0^{\infty} F\left(c\zeta / t\right) dt$. As $t_I \to \infty$, the mean cycle cost approaches to C_F and the CBM policy becomes equivalent to the corrective replacement policy. When $c = 1$, the mean cycle length equals the mean lifetime irrespective of the inspection interval.

The cumulative probability of failure up to time is simple to obtain as

$$P_f\left(t\right) = \Pr\left\{X\left(t\right) > \zeta\right\} = \begin{cases} 1 - F_A\left(\zeta; t\right), & 0 \leq t < t_I \\ 0, & t \geq t_I \end{cases} \tag{7.9}$$

Note that $P_f(t)$ becomes zero for $t > t_I$, because one inspection reveals the actual sample value of the deterioration rate and removes the uncertainty about the time of failure after the first inspection.

7.4.3 Formulation for Gamma Process Model

The inspection and replacement scenarios in the GP model are more involved due to temporal uncertainty. The three possible situations arise at every inspection, namely, safe state and do nothing, PM, or failure and subsequent corrective maintenance, as shown in Figure 7.3.

According to the decision tree, a PM renewal happens at $L = nt_I$ when $X_{n-1} < c\zeta$ and $c\zeta < X_n < \zeta$, where $X_n = X(nt_I)$ with PM cost $nC_I + C_P$. When $X_{n-1} < c\zeta$ but $X_n > \zeta$, a CM renewal is called for with cost $(n-1)C_I + C_F$ for $n \geq 2$ and C_F for $n = 1$. In this case, the renewal is done at a point of time interval from $(n-1)t_I$ to nt_I. Accordingly, the mean cost associated with a renewal cycle is derived as

$$\mathrm{E}\left[C\left(t_I, c\right)\right] = \sum_{n=1}^{\infty}\left[\left(nC_I + C_P\right)P_m\left(n\right) + \left(\left(n-1\right)C_I + C_F\right)P_f\left(n\right)\right] \tag{7.10}$$

where

$$P_m\left(n\right) = \Pr\left\{\text{PM at } nt_I\right\} = \Pr\left\{X_{n-1} < c\zeta,\ c\zeta < X_n < \zeta\right\} \tag{7.11}$$

and

$$P_f\left(n\right) = \Pr\left\{\text{Failed in } \left(\left(n-1\right)t_I, nt_I\right]\right\} = \Pr\left\{X_{n-1} < c\zeta,\ X_n > \zeta\right\}. \tag{7.12}$$

From the property of independent increments of gamma process, we have, for $n \geq 2$,

$$\begin{aligned} P_m\left(n\right) &= \Pr\left\{X_{n-1} < c\zeta,\ c\zeta - X_{n-1} < X_n - X_{n-1} < \zeta - X_{n-1}\right\} \\ &= \int_0^{c\zeta} ga_{n-1}\left(x\right)\left[GA_1\left(\zeta - x\right) - GA_1\left(c\zeta - x\right)\right]dx, \end{aligned} \tag{7.13}$$

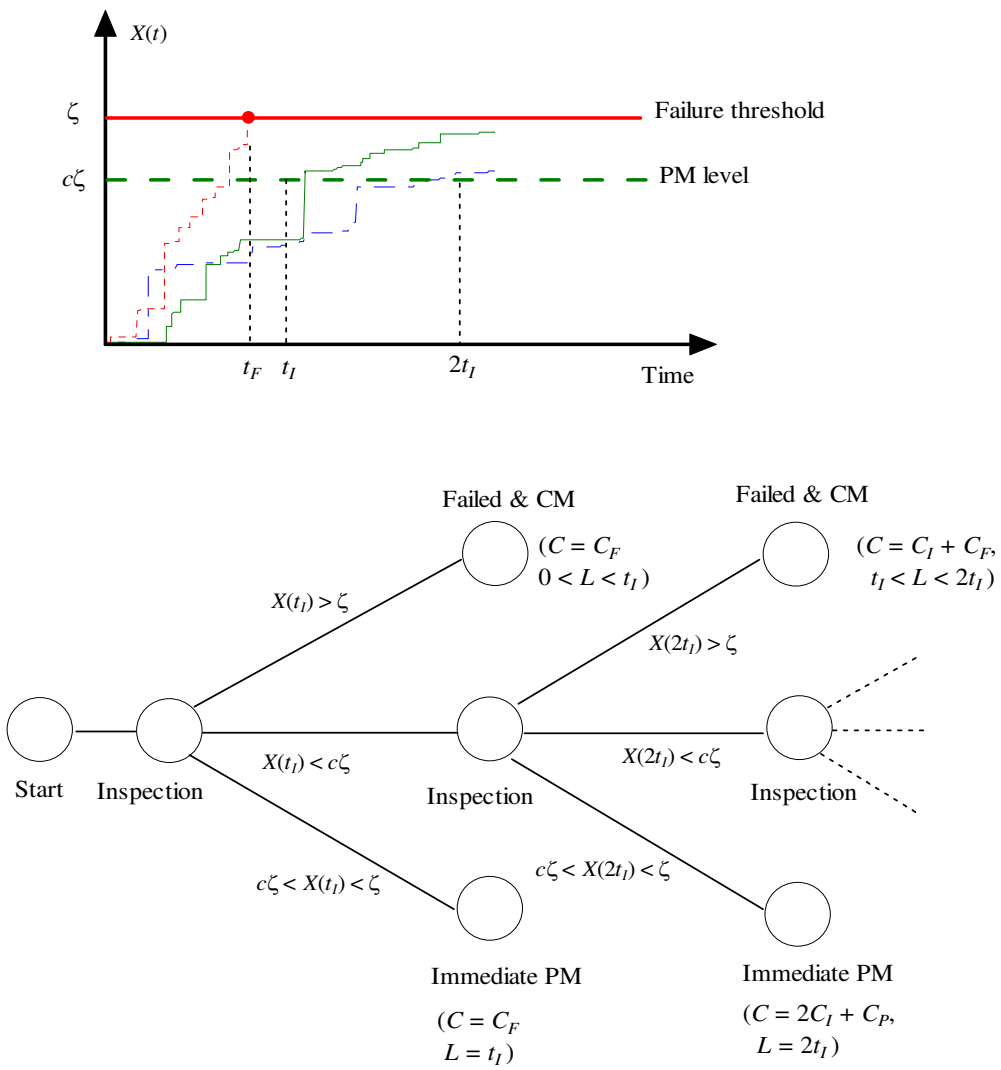

Figure 7.3: CBM decision tree for the GP model

in which $ga_n(\cdot)$ and $GA_n(\cdot)$ denotes the pdf and CDF of a gamma distribution $Ga(n\alpha t_I, \beta)$, respectively. It is clear that $P_m(1) = GA_1(\zeta) - GA_1(c\zeta)$. Similarly,

$$\begin{aligned} P_f(n) &= \Pr\{X_{n-1} < c\zeta,\ X_n - X_{n-1} > \zeta - X_{n-1}\} \\ &= \int_0^{c\zeta} ga_{n-1}(x)\,[1 - GA_1(\zeta - x)]\,dx \end{aligned} \tag{7.14}$$

for $n = 2, 3, \ldots$, and $P_f(1) = 1 - GA_1(\zeta)$. Substituting these probabilities into (7.10) and simplifying them, we have

$$\begin{aligned} \mathrm{E}[C(t_I, c)] &= C_P + (C_F - C_I)\,[1 + S(c\zeta)] \\ &\quad - (C_F - C_I - C_P)\left[GA_1(\zeta) + \int_0^{c\zeta} s(x)\,GA_1(\zeta - x)\,dx\right] \end{aligned} \tag{7.15}$$

where $S(x) = \sum_{n=1}^{\infty} GA_n(x)$ and $s(x) = \sum_{n=1}^{\infty} ga_n(x)$.

The mean cycle length can be obtained as

$$\mathrm{E}[L(t_I, c)] = \sum_{n=1}^{\infty} [nt_I P_m(n) + \mathrm{E}_n(T_F)] \tag{7.16}$$

where $\mathrm{E}_n(T_F)$ represents the mean failure time between $(n-1)\,t_I$ and nt_I and is expressed as

$$\mathrm{E}_n(T_F) = \int_0^{c\zeta} ga_{n-1}(x) \int_0^{t_I} [(n-1)\,t_I + s]\,f_T(s; \zeta - x)\,dsdx, \tag{7.17}$$

in which $f_T(s; \zeta - x)$ is the pdf of the first passage time of the gamma process with a threshold $\zeta - x$. Using integration by parts and rearranging all the terms, we obtain

$$\mathrm{E}[L(t_I, c)] = \int_0^{t_I} GA(\zeta; \alpha t, \beta)\,dt + \int_0^{c\zeta} \int_0^{t_I} s(x)\,GA(\zeta - x; \alpha t, \beta)\,dtdx \tag{7.18}$$

where $GA(x; a, b)$ denotes the CDF of the gamma distribution with shape a and scale b.

Equations (7.15) and (7.18) are derived by Park (1988a, 1988b). An alternative

way to compute the mean cycle cost and the mean cycle length is by using the Poisson approximation for the lifetime distribution of the gamma process, as suggested by van Noortwijk et al. (1995). When the inspection interval is n times of the reciprocal of the shape parameter α, the Poisson approximation gives an exact solution to the mean cycle cost. But this approach gives only an approximation to the mean cycle length and therefore it is not used in the subsequent computations.

There are two limiting cases of the CBM policy. As the inspection interval t_I becomes large, the mean cost rate tends to C_F/μ_T where μ_T is the mean lifetime. As the PM ratio $c \to 1$, t_I converges to the optimal replacement interval obtained from the age-based replacement policy.

The probability of failure over time within any inspection interval is given by the following expression:

$$P_f(t) = \Pr\{X(t) \geq \zeta,\ X((n-1)t_I) < c\zeta\}, \text{ for } (n-1)t_I \leq t < nt_I. \tag{7.19}$$

In particular, for $n = 1$, i.e., the first inspection interval,

$$P_f(t) = 1 - GA(\zeta; \alpha t, \beta) \tag{7.20}$$

and for $n \geq 2$,

$$P_f(t) = \int_0^{c\zeta} ga_{n-1}(x)\{1 - GA(\zeta - x; \alpha[t-(n-1)t_I], \beta)\}\,dx. \tag{7.21}$$

Note that the probability of failure at the time of inspection reduces to zero, since the inspection is perfect in the sense that it reveals the actual situation without any uncertainty.

For a GP model dealing with imperfect inspection, we refer to Kallen and van Noortwijk (2005). More recently, Crowder and Lawless (2007) discussed a simplified CBM policy for a mixed-scale gamma process model.

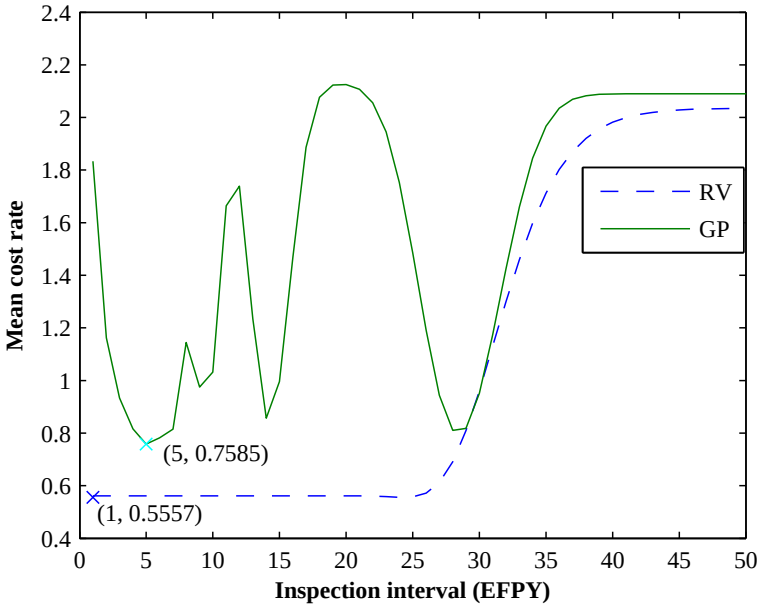

Figure 7.4: Comparison of condition-based maintenance policy based on different deterioration models for a pressure tube due to diametral expansion

7.4.4 Example: Condition-Based Maintenance of Pressure Tubes for Creep Deformation

The diametral expansion data are used again for illustration purpose. Suppose $C_I = 1$, $C_P = 10$ and $C_F = 50$. Figure 7.4 shows the mean cost rate versus the inspection interval for the RV and GP model. The minimal mean cost rate for the GP model is greater than that for the RV model, as the GP model takes into consideration the temporal uncertainty even though it predicts the same mean value and smaller variance of lifetime. Figure 7.5 and 7.6 show the cost decomposition for the RV and GP model, respectively.

At the optimal inspection interval of 5 EFPY, the probability of the pressure tube reaching substandard performance (i.e. the diametral strain exceeding 5.1%) has been controlled within 0.08, as illustrated in Figure 7.7. This shows the indirect benefit of the inspection and preventive maintenance.

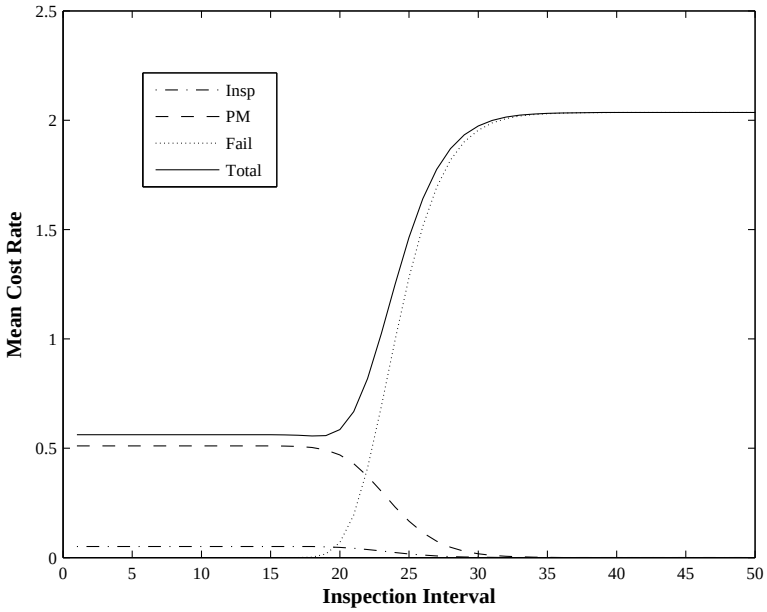

Figure 7.5: Decomposition of mean cost rate for the RV model

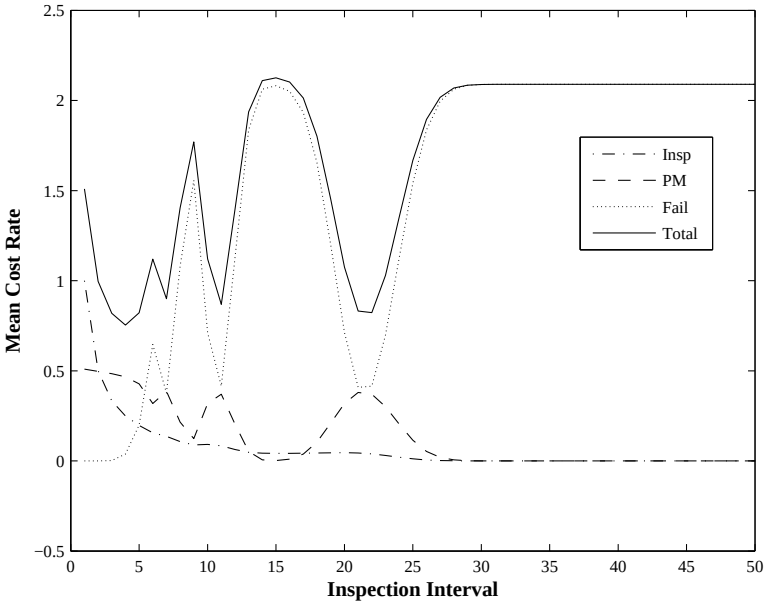

Figure 7.6: Decomposition of mean cost rate for the GP model

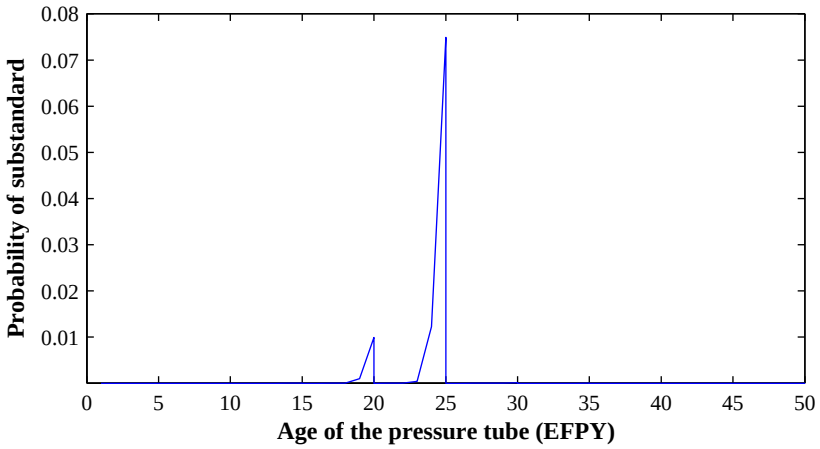

Figure 7.7: Probability of the pressure tube being substandard over time under the optimal CBM policy based on the GP model

7.5 Sensitivity Analysis

The case studies of pressure tubes in the previous examples give interesting but nevertheless very limited comparisons of the RV and GP models in maintenance optimization. To get a better insight, we proceed next with a comprehensive sensitivity analysis for the two deterioration models, considering different degree of variation of deterioration. In this analysis, the variation of deterioration is described by the coefficient of variation (COV) of the lifetime. By fixing the mean lifetime and varying the lifetime COV, we compares the impacts of temporal uncertainty in both ABR and CBM policies.

In order to have a consistent comparison between the RV and GP models, a careful scheme is required for the calibration of the model parameters. In this study, we assume the mean and COV of the lifetime are given. Calibration of the models is based on the two moments of the lifetime.

7.5.1 Calibration of the Models

Suppose the deterioration rate A in the RV model is a gamma distributed random variable with shape parameter η and scale parameter δ, i.e., $A \sim Ga\left(\eta,\, \delta\right)$. Then the deterioration at any time t also follows a gamma distribution $Ga\left(\eta, \delta t\right)$. The lifetime T, defined as $T = \zeta/A$, however follows an inverted gamma distribution. Its pdf is expressed

$$f_T\left(t\right) = \frac{\left(\delta/\zeta\right)}{\Gamma\left(\eta\right)}\left(\frac{\zeta}{\delta t}\right)^{\eta+1}\exp\left(-\frac{\zeta}{\delta t}\right) \tag{7.22}$$

and the CDF as

$$F_T\left(t\right) = 1 - GA\left(\zeta/t; \eta, \delta\right) = 1 - GA\left(\zeta; \eta,\, \delta t\right) \tag{7.23}$$

The moments of the lifetime distribution can be derived as

$$\mu_T = \frac{\zeta}{\delta\left(\eta - 1\right)},\;\; \sigma_T^2 = \frac{\zeta^2}{\delta^2\left(\eta-1\right)^2\left(\eta-2\right)} \text{ and } \nu_T = \frac{1}{\sqrt{\eta - 2}} \tag{7.24}$$

for $\eta > 2$. Therefore, given the values of μ_T and ν_T, the parameters of deterioration rate A can be easily calculated by the following expressions:

$$\eta = 2 + 1/\nu_T^2 \;\text{ and }\; \delta = \frac{\zeta\nu_T^2}{\mu_T\left(1+\nu_T^2\right)}. \tag{7.25}$$

Recall that the CDF of the lifetime in a GP model with shape parameter α and scale parameter β is expressed as the following:

$$F_T\left(t\right) = 1 - GA\left(\zeta;\, \alpha t,\, \beta\right) \tag{7.26}$$

Although (7.26) differs from (7.23) only at whether the time t is associated with the shape parameter or scale parameter in the gamma distribution, the lifetime in the GP model has no explicit expression for its moments. Therefore in the case of GP model, given μ_T and ν_T, the shape and scale parameters can be only obtained by numerically solving the

Table 7.1: Parameters used in the model calibration

Mean lifetime μ_T	COV of lifetime ν_T	Failure threshold ζ
50 units of time (fixed)	Varied from 0.1 to 0.9	100 units of deterioration (fixed)

Table 7.2: Example parameters in the RV and GP models

Parameters		$\nu_T = 0.3$	$\nu_T = 0.6$	$\nu_T = 0.9$
RV model	Shape (η)	13.1111	4.7778	3.2346
	Scale (δ)	0.1651	0.5294	0.8950
GP model	Shape (α)	0.2099	0.0408	0.0078
	Scale (β)	10.01	64.63	1453.6

following equations of the first and second moments (c.f. (4.14)):

$$\mu_T = \int_0^\infty GA\left(\zeta;\, \alpha t, \beta\right) dt \tag{7.27a}$$

$$\mu_{T^2} = \mu_T^2\left(1 + \nu_T^2\right) = 2\int_0^\infty t\, GA\left(\zeta;\, \alpha t, \beta\right) dt \tag{7.27b}$$

The parameters of the two models are given in Tables 7.1 and 7.2. The two models are equivalent in the sense that they have identical mean and variance of the lifetime.

7.5.2 Age-Based Replacement

Although the RV and GP models are calibrated so that they have the same mean and variance of the lifetime, the lifetime distributions in the two models are nevertheless different. As an example, Figure 7.8 compares the probability density functions and survival functions for $\nu_T = 0.3$. The survival function shows that the tails of the lifetime distribution in the RV and GP models can be remarkably different and the RV model overestimates the reliability of the component.

A comprehensive comparison of ABR results about the minimum cost rate and optimal replacement age for different coefficients of variation of lifetime, ν_T, in the RV and GP models are shown in Figure 7.9. $C_P = 10$ and $C_F = 50$ are assumed in the analysis. The results of optimal replacement age obtained from the two models are qualitatively

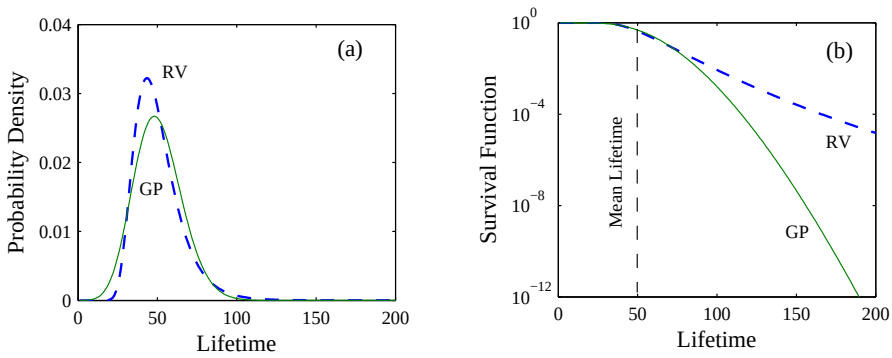

Figure 7.8: Comparison of lifetime distributions of the equivalent RV and GP models for $\nu_T = 0.3$: (a) probability density function, and (b) survival function

different. In the RV model, the optimal replacement age decreases continuously as the lifetime COV ν_T increases. This observation is somewhat intuitive in the sense that when faced with increased uncertainty about lifetime, it is prudent to reduce the replacement age. The results of GP model exhibit two distinct trends. Initially, with increase in lifetime COV the replacement age decreases. However, as ν_T increases beyond 0.5, the trend reverses and the replacement age begins to increase. It suggests that in case of highly uncertain lifetime, the life-cycle cost could not be optimized by manipulating the replacement age. Note that a similar reasoning can be applied for an exponentially distributed lifetime – having a constant failure rate and a COV of 1 – for which it is optimal to never schedule a preventive replacement (Barlow and Proschan 1965).

Figure 7.9(b) shows that mean cost rate obtained from GP model is always higher than that of the RV model as a result of additional temporal uncertainty associated with it. The difference between the optimum cost rates increases with increase in lifetime uncertainty. This explains the very small difference of the ABR in Figure 7.1 because relatively small variation exhibits in the growth of diametral strain.

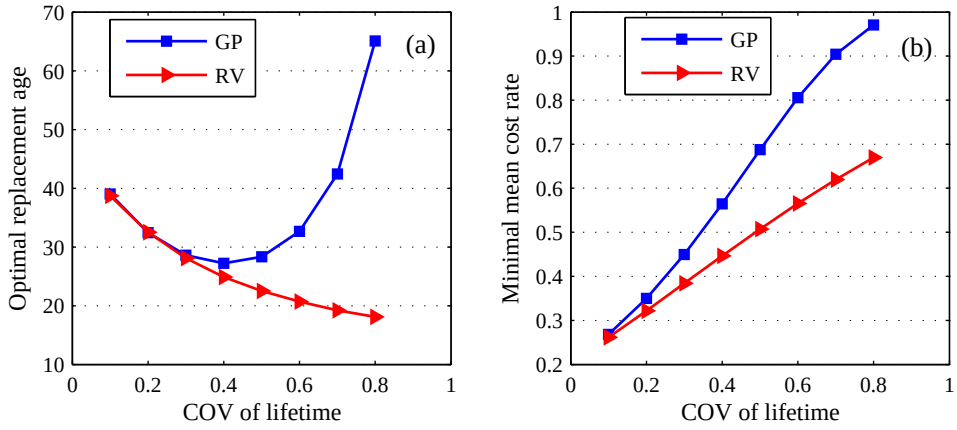

Figure 7.9: Comparison of age-based replacement policies in equivalent RV and GP mdoels: (a) optimal replacement age, and (b) minimal mean cost rate

7.5.3 Condition-Based Maintenance

Assume $C_I = 1$, $C_P = 10$ and $C_F = 50$. The optimization results of CBM for RV and GP models for different values of the lifetime COV are compared in Figure 7.10. It is remarkable that in the RV model both the optimum cost rate and inspection interval are insensitive to the variability of the lifetime distribution, which is due to the lack of consideration of temporal uncertainty. In contrast, the minimum cost rate in the GP model increases with lifetime uncertainty. The cost rate increases from 0.38 to 0.97 as the COV of lifetime is increased from 0.1 to 0.8. In general, the GP cost rate is higher than that for the RV model due to the effect of temporal uncertainty.

7.5.4 Comparison of Age-Based and Condition-Based Policies

Although the CBM policy is generally considered as a more advanced approach to the life-cycle management, an age-based strategy is easier to implement than the condition-based one after all. In light of this, we would like to compare the cost rates of ABR and CBM policies. In this Section, the results are presented for the GP model only because

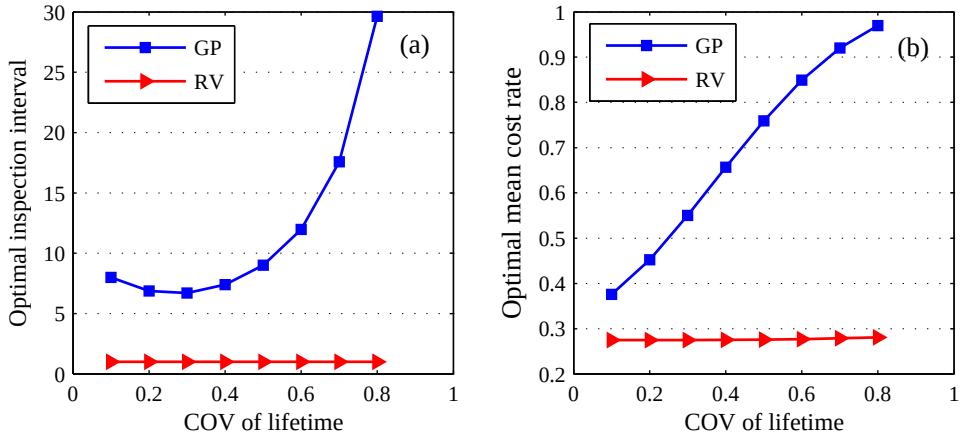

Figure 7.10: Comparison of CBM results for equivalent RV and GP models: (a) optimal inspection interval, and (b) minimal mean cost rate

we have concluded that the RV model is too unrealistic for a CBM policy.

The results for minimum mean cost rate shown in Figures 7.9(b) and 7.10(b) are plotted together in Figure 7.11. It is remarkable that the cost rate of CBM is higher than age-based replacement policy, especially when the lifetime COV is relatively small ($\nu_T < 0.5$).

Although the above comparison is dependent on the specific cost structure ($C_I = 1$, $C_P = 10$ and $C_F = 50$), it is clear that CBM is not universally superior to the age-based policy. In fact, an optimum domain of application of CBM policy in terms of the lifetime COV and costs can be explicitly derived to develop the life-cycle management strategies. We next illustrate this point in details.

Two-Dimensional CBM Optimization

It has been argued that the one-dimensional optimization of inspection interval leads to suboptimal results (Grall et al. 2002; Jia and Christer 2002; Dieulle et al. 2003). The mean cost rate can be further optimized by allowing the PM ratio, c, be another

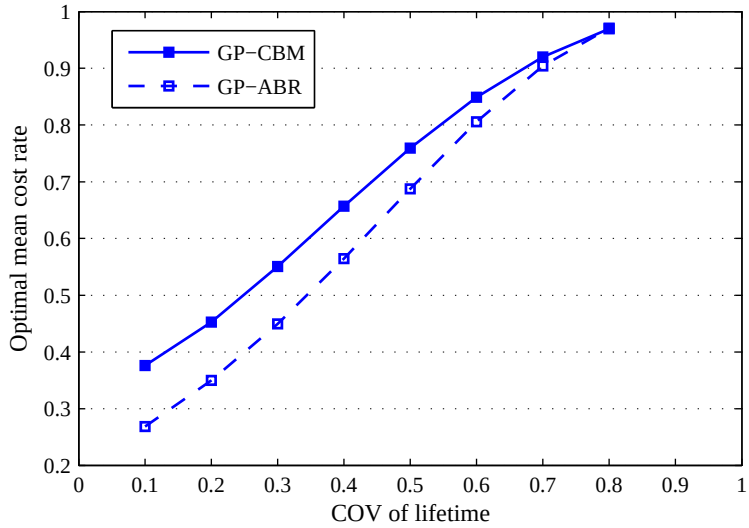

Figure 7.11: Comparison of the CBM policies with the ABR in the GP model

optimization variable. This leads to a two-dimension (2D) CBM optimization.

Taking $\nu_T = 0.3$ for an example, the surface of minimum cost rate for various combinations of inspection interval (t_I) and PM ratio is plotted in Figure 7.12. On this surface, the optimal point corresponds to $t_I = 13$, $c = 0.54$ and the associated minimum mean cost rate is 0.44. This cost rate is much less than that obtained from either the corresponding one-dimensional CBM optimization (0.54 at $t_I = 7$ and $c = 0.8$) or the ABR policy (0.45 at $t_I = 29$ and $c = 1$).

Now, a more fair comparison of ABR and CBM can be taken. Figure 7.13 compares the minimal mean cost rate from the 2D CBM optimization with that of the ABR policy. It shows that an age-based policy is better than CBM when $\nu_T < 0.25$. In other words, the benefit of a condition-based policy gained from the value of deterioration information through inspection outweighs the cost of inspection only when the uncertainty associated with deterioration is large ($\nu_T > 0.25$). Given a fixed ν_T, the CBM policy is preferable only if the inspection cost is below a certain value. This motivates us to find out the

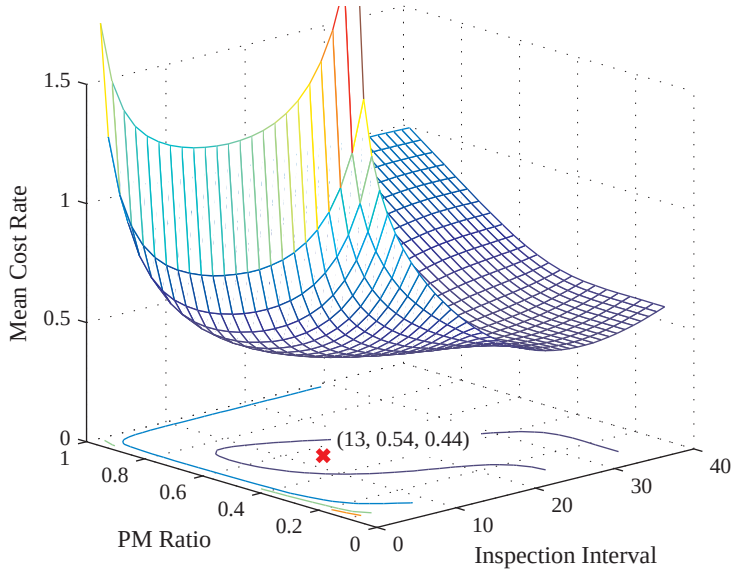

Figure 7.12: A two-dimensional CBM optimization for the GP model ($\nu_T = 0.3$)

maximum allowable inspection cost to justify the CBM policy. This threshold value of inspection cost provides an answer to a question such as, how much money can be justifiably spent for inspections given the probabilistic characteristics of a deterioration process. For example, Figure 7.13 shows that maximum allowable inspection cost is 1 (20% of the PM cost) when $\nu_T = 0.25$ and $C_P/C_F = 5/50 = 10\%$. Next we investigate the maximum allowable inspection cost for more general cases.

Maximum Allowable Inspection Cost to Justify the CBM Policy

By definition, the maximum allowable inspection cost can be calculated from the following equality:

$$K_a\left(t_{a,opt};\, \nu_T,\, C_P,\, C_F\right) = K_i\left(t_{a,opt},\, c_{opt};\, \nu_T,\, C_I,\, C_P,\, C_F\right) \tag{7.28}$$

where K_a and K_i are the optimal cost rates for the ABR policy and two-dimensional CBM polices that are calculated from (7.5) and from (7.15) and (7.18), respectively. The

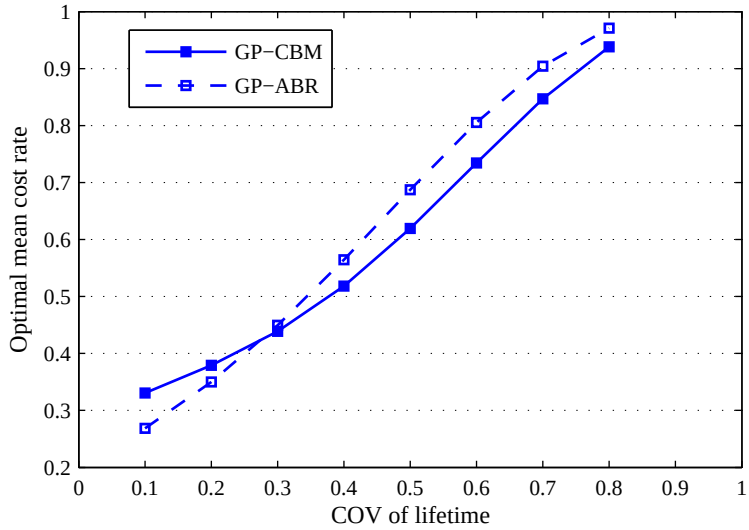

Figure 7.13: Comparison of two-dimensional CBM policies with ABR policies

maximum allowable inspection cost is obtained by solving (7.28) with fixed and while $t_{a,opt}$, $t_{I,opt}$ and c_{opt} are the optimization results depending on C_I.

In Figure 7.14, the optimal inspection cost is expressed as a percentage of the PM cost. The increasing trend shows that the higher inspection cost is justified with increase in uncertainty associated with the lifetime distribution and the deterioration process. On the other hand, inspection cost proportionately decreases with increasing PM cost, though the cost still increases in an absolute sense. The optimal inspection cost curves provide guidance about the optimal cost structure of a maintenance program.

7.6 Summary

The chapter emphasizes an important fact that the random variable rate (RV) model cannot capture temporal variability associated with evolution of deterioration. As a consequence, the deterioration along a specific sample path is deterministic in the RV model,

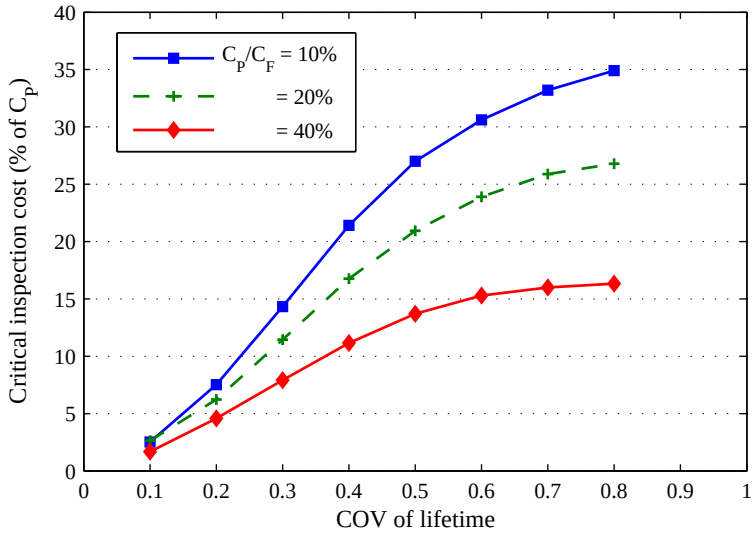

Figure 7.14: Maximum allowable inspection cost with COV of lifetime and PM to CM cost ratio

whereas it varies probabilistically in the GP model. This distinction has profound implications to the maintenance optimization of both age-based and condition-based strategies.

The results presented in the chapter show that the optimum cost and inspection interval obtained from the GP model are qualitatively different than those obtained from the RV model. The RV model tends to underestimate the life-cycle cost due to lack of consideration of temporal uncertainty.

The age-based replacement policy is easier to implement than the condition-based maintenance. The chapter determines a domain of inspection, preventive maintenance and corrective costs in which the condition-based policy is always superior to the age-based policy. A general observation is that condition-based maintenance strategy is justified when the uncertainty associated with deterioration is large. In other words, under a given cost structure the tradeoff between the cost of inspection and value of information gained is beneficial only when the uncertainty of deterioration exceeds a critical limit.

Chapter 8

Conclusions and Recommendations

8.1 Conclusions

The thesis presents a versatile stochastic gamma process model for modeling deterioration in engineering systems, structures and components. Questions relevant to stochastic modeling of deterioration, such as why and which stochastic process model should be used and how to calibrate and validate the model using practical data, have been addressed. Detailed practical applications of the proposed models to feeder pipe systems and fuel channels in CANDU reactors are presented. The thesis also formulated the maintenance optimization problems for both age-based replacement and condition-based maintenance strategies.

Traditional regression models consist of a parameterized mean function and an error term that quantifies the deviation of the observations from the mean function. The errors are usually assumed independent of each other. Under this assumption data analysis and modeling of deterioration becomes a straightforward task, though it confounds the

estimation of the lifetime distribution. The thesis proposes a linear mixed-effects model to resolve the inconsistency of interpretation associated with ordinary regression model. By introducing the random effects into the model, the varying variance of deterioration and correlation with time are characterized, which leads to a logical method for lifetime estimation.

A gamma process is a continuous-time stochastic process with stationary and independent, gamma-distributed increments. Comparing to other deterioration models, the gamma process is a versatile stochastic process model for a wide variety of degradation phenomena. As a pure jump process, it includes both tiny and big jumps, making the model flexible for deterioration that develops either gradually or abruptly. The gamma process has nonnegative, monotonically increasing sample paths, which is suitable to model an irreversible degradation process.

The gamma process model is statistically tractable. Using its property of independent and gamma-distributed increments, the likelihood function can be easily constructed for parameter estimation purposes. Two algorithms based on the method of moments are also developed in the thesis and they are as effective as maximum likelihood method when a reasonable long record of deterioration is available. Asymptotic analysis of maximum likelihood estimates showed that the asymptotic variance of the shape parameter is inversely proportional with the sample size, whereas the asymptotic variance of the scale parameter depends not only on the sample size but also on the total time length of the recorded sample paths.

The gamma process model is also flexible for modeling both fixed and random effects. Fixed effects of observed covariates can be modeled by the scale parameter with a parametric form that depends on the mechanistic knowledge about degradation process. The underlying heterogeneity that is not explained by the observed covariates is termed random effect and it can be modeled by a random scale parameter in the gamma process. Estimating the parameters in the mixed-scale gamma process model is similar to

the gamma process, but testing the existence of random effects is challenging. The thesis proposed a score test for this purpose and verified its effectiveness by simulations.

Another common way to model deterioration in civil engineering is to treat the rate of deterioration as a random variable. In the context of condition-based maintenance, the thesis shows that the random variable rate model (RV) is inadequate to incorporate temporal variability, because the deterioration along a specific sample path becomes deterministic. In the gamma process model however, the deterioration along a sample path varies probabilistically. This distinction has profound implications to the maintenance optimization of both age-based and condition-based strategies. The results presented in the thesis show that the optimal cost and inspection interval obtained from the gamma process model are qualitatively different than those obtained from the RV model. The RV model tends to underestimate the life-cycle cost due to lack of consideration of temporal uncertainty. Although the linear mixed-effects model is found to be effective in fitting given data, it is essentially a random variable model in nature.

The age-based replacement policy is easier to implement than the condition-based maintenance. The thesis determined a domain of inspection, preventive maintenance and corrective costs in which the condition-based policy is always superior to the age-based policy. A general observation is that condition-based maintenance is justified when the uncertainty associated with deterioration is large. In other words, under a given cost structure the tradeoff between the cost of inspection and value of information gained is beneficial only when the uncertainty of deterioration exceeds a critical limit.

In summary, a careful consideration of the nature of uncertainties associated with deterioration is important for a credible model of deterioration and its effective application to the life-cycle management of engineering systems. If the deterioration process is affected by temporal uncertainty, it is important to model it as a stochastic process.

8.2 Recommendations for Future Research

Likelihood ratio test and score test have been proposed to check the significance of fixed effects and random effects. But the assumption of independent increments is still an important assumption in the gamma process model left unchecked. More research work should be done to address this issue.

Another promising work is about the Hougaard process mentioned in Chapter 4. As pointed out there, when the index parameter goes to zero, the Hougaard process reduces to a gamma process. Following the model expansion approach, estimation of the index parameters can validate whether or not the choice of gamma process model is legitimate. The parameter estimation is not easy, because the Hougaard process has no explicit expression for the probability density function. This needs further studies.

This thesis focuses on deterioration modeling from the temporal uncertainty perspective. However, the spatial uncertainty can be an important aspect of the deterioration. For example, the wall thickness data of feeders were actually the minimum thickness found at the inspection time along a finite inspection area. The reported thickness of the same feeder at different times may not come from the same position. A more sophisticated stochastic field model of deterioration may be an area of future investigation.

Appendix A

Abbreviations And Notations

ABR	Age-based replacement
CBM	Condition-based maintenance
CD	Cumulative damage model
CDF	Cumulative distribution function
COV	Coefficient of variation
CPP	Compound Poisson process
EFPH	Effective full-power hour
EFPY	Effective full-power year
GLM	Generalized linear model
GP	Gamma process
i.i.d.	Independent and identically distributed
IWLS	Iteratively weighted least squares
LME	Linear mixed-effects model
LR	Linear regression
LS	Least squares
MAP	Markov additive process
MCMC	Markov chain Monte Carlo simulation method

NLME	Nonlinear mixed-effects model
NPP	Nuclear power plants
OLS	Ordinary least squares
pdf	Probability density function for continuous random variable
pmf	Probability mass function for discrete random variable
SF	Survival function
SMC	Semi-Markov chain
SSI	Strength-Stress Interference
r.v.	random variable(s)
RV	Random variable model
WLS	Weighted least squares

$\mathrm{E}(X)$	Expectation of a random variable
cov	Covariance function
$f_X(x)$	pdf of a random variable X
$F_X(x)$	CDF of a random variable X
$ga(x; a, b)$	pdf of a gamma random variable with shape parameter a and scale parameter b
$Ga(a, b)$	Gamma distribution with shape parameter a and scale parameter b
$GA(x; a, b)$	CDF of a gamma random variable with shape parameter a and scale parameter b
$N(\mu, \sigma^2)$	Normal (Gaussian) distribution with mean μ and variance σ^2
$\mathrm{Var}(X)$	Variance of a random variable
$\Phi(z)$	CDF of standard normal distribution
$\Gamma(z)$	Gamma function defined by $\Gamma(z) = \int_0^\infty u^{z-1}e^{-u}du$
$\Gamma(w, z)$	Incomplete gamma function, defined by $\Gamma(w, z) = \int_w^\infty u^{z-1}e^{-u}du$
$\psi(z)$	digamma function, the derivative of log gamma function, i.e., $d\log\Gamma(z)/dz$
ζ	Threshold for a first passage failure

References

Abdel-Hameed, M. (1984a). "Deterioration processes." *Semi-Markov Models: Theory and Applications*, J. Janssen, ed., New York. Plenum Publishing Corporation, 231–252.

Abdel-Hameed, M. (1984b). "Life distribution properties of devices subject to a Lévy wear process." *Mathematics of Operations Research*, 9, 606–614.

Abdel-Hameed, M. (1984c). "Life distribution properties of devices subject to a pure jump damage process." *Journal of Applied Probability*, 21, 816–825.

Abdel-Hameed, M. (1987). "Inspection and maintenance policies of devices subject to deterioration." *Advances in Applied Probability*, 19, 107–114.

Abdel-Hameed, M. (1995). "Inspection, maintenance and replacement models." *Computers & Operations Research*, 22, 435–441.

Abdel-Hameed, M. S. and Proschan, F. (1973). "Nonstationary shock models." *Stochastic Processes and their Applications*, 1, 383–404.

Abdel-Hameed, M. S. and Proschan, F. (1975). "Shock models with underlying birth process." *Journal of Applied Probability*, 12, 18–28.

Ang, A. H.-S. and Tang, W. H. (1975). *Probability Concepts in Engineering Planning and Design, Vol. II, Decision, Risk and Reliability.* John Wiley & Sons.

Ang, A.-S. and De Leon, D. (2005). "Modeling and analysis of uncertainties for risk-informed decisions in infrastructures engineering." *Structure and Infrastructure Engineering*, 1(1), 19 – 31.

Atomic Energy of Canada Limited (2007). "20 years of active and planned life extension projects". AECL web page: http://www.aecl.ca/Assets/Publications/Fact+Sheets/Current-Projects.pdf.

Aven, T. (2003). *Foundations of Risk Analysis.* John Wiley & Sons, New York.

Barlow, R. E. and Proschan, F. (1965). *Mathematical Theory of Reliability.* John Wiley & Sons, New Yorks.

Barlow, R. E. and Proschan, F. (1981). *Statistical Theory of Reliability and Life Testing: Probablity Models.* To Begin With, Silver Spring.

Bedford, T. and Cooke, R. M. (2001). *Probabilistic Risk Analysis: Foundations and Methods.* Cambirdge University Press, Cambridge.

Berge, P., Ducreux, J., and Saint-Paul, P. (1980). *Effects of chemistry on corrosion-erosion of steels in water and wet steam*, Vol. 1 of *Proc. 2nd BNES Int. Conf. Water Chemistry of Nuclear Reactor Systems*, 19–23. British Nuclear Energy Society, Bournemouth, U.K.

Berger, F. P. and Hau, K.-F. F.-L. (1977). "Mass transfer in turbulent pipe flow measured by the electrochemical method." *International Journal of Heat and Mass Transfer*, 20, 1185–1194.

Birnbaum, Z. W. and Saunders, S. C. (1958). "A statistical model for life-length of materials." *Journal of the American Statistical Association*, 53(281), 151–160.

Birnbaum, Z. W. and Saunders, S. C. (1969). "A new family of life distributions." *Journal of Applied Probability*, 6, 319–327.

Bleistein, N. and Handelsman, R. A. (1975). *Asymptotic Expansions of Integrals.* Holt, Rinehart and Winston, New York.

Bogdanoff, J. L. and Kozin, F. (1985). *Probabilitistic Models of Cumulative Damage.* John Wiley & Sons, New York.

Box, G. P. (1976). "Science and statistics." *Journal of the American Statistical Association*, 71(356), 791–799.

Burrill, K. (1995). "Modeling flow-accelerated corrosion in candu." *Report No. AECL-11397, COG-95-384*, Atomic Energy of Canada Limited, AECL, Reactor Chemistry Branch, Chalk River Laboratories, Chalk River, Ontario.

Burrill, K. and Cheluget, E. L. (1999). "Corrosion of candu outlet feeder pipes." *Report No. AECL-11965, COG-98-292-1*, Atomic Energy of Canada Limited, AECL, Reactor Chemistry Branch, Chalk River Laboratories, Chalk River, Ontario.

Caregy, M. B. and Koenig, R. H. (1991). "Reliability assessment based on accelerated degradation: a case study." *IEEE Transactions on Reliability*, 40(5), 499–506.

Carlin, B. P. and Louis, T. A. (2000). *Bayes and Empirical Bayes Methods for Data Aanlysis.* Chapman & Hall, second edition.

Çinlar, E. (1972). "Markov additive processes. I & II." *Z. Wahrscheinlichkeitstheorie verw. Geb.*, 24, 85–121.

Çinlar, E. (1977). "Shock and wear models and Markov additive process." *The Theory and Applicatio of Reliability*, I. N. Shimi and C. P. Tsokos, eds., New York. Academic, 193–214.

Çinlar, E. (1980). "On a generalization of Gamma processes." *Journal of Applied Probability*, 17, 467–480.

Çinlar, E., Bazănt, Z. P., and Osman, E. (1977). "Stochastic process for extrapolating concrete creep." *Journal of the Enginnering Mechanics Division, ASCE*, 103(EM6), 1069–1088.

Chiao, C.-H. and Hamada, M. (2001). "Analyzing experiments with degradation data for improving reliability and for achieving robust reliability." *Quality and Reliability Engineering International*, 17, 333–344.

Choate, P. and Walter, S. (1983). *America in Ruins: the Decaying Infrastructure.* Duke Press Paperbacks. Originally published by Coucil of State Planning Agencies in 1981.

Ciampoli, M. (1998). "Time dependent reliability of structural systems subject to deterioration." *Computers and Structures*, 67(1-3), 29 – 35.

Ciampoli, M. (1999). "A probabilistic methodology to assess the reliability of deteriorating structural elements." *Computer Methods in Applied Mechanics and Engineering*, 168, 207–220.

Cont, R. and Tankov, P. (2005). *Financial Modelling with Jump Processes.* Chapman & Hall/CRC.

Crk, V. (2000). "Reliability assessment from degradation data." *Proceedings Annual Reliability and Maintainability Symposium, IEEE.*

Crowder, M. and Lawless, J. (2007). "On a scheme for predictive maintenance." *European Journal of Operational Research*, 176, 1713–1722.

Crowder, M. J. and Hand, D. J. (1990). *Analysis of Repeated Measures.* Chapman and Hall, London.

Crowder, M. J., Kimber, A. C., Smith, R. L., and Sweeting, T. J. (1991). *Statistical Analysis of Reliability Data.* Chapman & Hall.

Daley, D. J. and Vere-Jones, D. (1988). *An Introduction to the Theory of Point Processes.* Springer-Verlag.

Daniels, H. E. (1954). "Saddlepoint approximations in statistics." *The Annals of Mathematical Statistics*, 25, 631–650.

Dasgupta, A. and Pecht, M. (1991). "Material failure mechanism and damage models." *IEEE Transactions on Reliability*, 40, 531–536.

Deardorff, A., Goyette, L., Krishnaswamy, P., and Kupinski, M. (1999). "ASME section XI evaluation methods and acceptance criteria for analytical evaluation of wall thinning due to flow accelerated corrosion (FAC)." *Service Experience in Fossil and Nuclear Power Plants*, J. Pan, ed., PVP-Vol. 392, 1999 ASME/JSME Pressure Vessels and Piping Conference, Boston, MA, USA. 187 – 206.

Demidenko, E. (2004). *Mixed Models: Theory and Applications.* John Wiley & Sons.

DeStefano, P. D. and Grivas, D. A. (1998). "Method for estimating transition probability in bridge deterioration models." *Journal of Infrastructure Systems*, 4(2), 56–62.

Dieulle, L., Bérenguer, C., Grall, A., and Roussignol, M. (2003). "Sequential condition-based maintenance scheduling for a deteriorating system." *European Journal of Operational Research*, 150, 451–461.

Ditlevsen, O. and Madsen, H. O. (1996). *Structural Reliability Methods.* John Wiley & Sons.

Dobson, A. J. (2002). *An Introduction to Generalized Linear Models.* Chapman & Hall.

Doksum, K. A. and Hoyland, A. (1992). "Models for variable-stress accelerated life testing experiments based on Wiener processes and the inverse Gaussian distribution." *Technometrics*, 34(1), 74–82.

Dooley, R. B. and Chexal, V. K. (2000). "Flow-accelerated corrosion of pressure vessels in fossil plants." *The International Journal of Pressure Vessels and Piping*, 77(2-3), 85–90.

Draper, D. (1995). "Assessment and propagation of model uncertainty, with discussions." *Jouranl of Royal Statistical Society, Series B*, 57(1), 45–97.

Drosen, J. W. (1986). "Pure jump shock models in reliability." *Advances in Applied Probability*, 18, 423–440.

Ducreaux, J. (1983). "The influence of flow velocity on the erosion-corrosion of carbon steel in pressurized water." *Water Chemistry of Nuclear Reactor Systems 3*, Institution of Chemical Engineers, Royal Society of Chemistry, 227–233.

Dufresne, F., Gerber, H. U., and Shiu, E. S. W. (1991). "Risk theory with the gamma process." *ASTIN Bulletin*, 21(2), 177–192.

Dykstra, R. L. and Laud, P. (1981). "A Bayesian nonparametric approach to reliability." *The Annals of Statistics*, 9, 356–367.

Efron, B. and Tibshirant, R. (1993). *An Introduction to the Bootstrap.* Chapman & Hall.

Ellingwood, B. R. and Mori, Y. (1993). "Probabilistic methods for condition assessment and life prediction of concrete structures in nuclear power plants." *Nuclear Engineering and Design*, 142, 155–166.

Enright, M. P. and Frangopol, D. M. (1998). "Failure time prediction of deteriorating fail-safe structures." *Journal of Structural Engineering*, 124(12), 1448–1457.

Esary, J. D., Marshall, A. W., and Proschan, F. (1973). "Shock models and wear processes." *The Annals of Probability*, 1, 627–649.

Feldman, R. M. (1976). "Optimal replacement with semi-Markov shock processes." *Journal of Applied Probability*, 13, 108–117.

Feldman, R. M. (1977). "Optimal replacement for systems governed by Markov additive shock processes." *The Annals of Probability*, 5(3), 413–429.

Ferguson, T. S. and Klass, M. J. (1972). "A representation of independent increment processes without Gaussina component." *The Annals of Mathematical Statistics*, 43(5), 1634–1643.

Ferson, S., Joslyn, C. A., Helton, J. C., Oberkampf, W. L., and Sentz, K. (2004). "Summary from the epistemic uncertainty workshop: Consensus amid diversity." *Reliability Engineering and System Safety*, 85(1-3), 355 – 369.

Fook Chong, S. M. C. (1992). "A study of Hougaard distributions, Hougaard processes and their applications," Master's thesis, McGill University.

Frangopol, D. M., Kallen, M.-J., and van Noortwijk, J. M. (2004). "Probabilistic models for life-cycle performance of deteriorating structures: review and future directions." *Progress in Structural Engineering and Materials*, 6, 197–212.

Freudenthal, A. M. (1947). "The safety of strucutres." *Transactions, ASCE*, 112, 125–180.

Ganesan, R. (2000a). "A data-driven stochastic approach to model and analyze test data on figue response." *Computers and Structures*, 76, 517–531.

Ganesan, R. (2000b). "A stochastic modelling and analysis methodology for quantification of fatigue damage." *Computer Methods in Applied Mechanics and Engineering*, 190, 1005–1019.

Gerber, T. L., Deardorff, A. F., Norris, D. M., and Lucas, W. F. (1992). "Acceptance criteria for structural evaluation of erosion-corrosion thinning in carbon steel piping." *Nuclear Engineering and Design*, 133(1), 31–36.

Gertsbakh, I. (2000). *Reliaibility Theory with Application to Preventive Maintenance.* Springer-Verlag, Berlin.

Gertsbakh, I. B. (1989). *Statistical Reliability Theory.* Marcel Dekker, New York.

Gertsbakh, I. B. and Kordonskiy, K. B. (1969). *Models of Failures.* Springer-Verlag.

Ghanem, R. G. and Spanos, P. D. (2003). *Stochastic Finite Elements: A Spectral Approach.* Dover Publications, revised edition edition.

Gottlieb, G. (1982). "Optimal replacement for shock models with general failure rate." *Operations Research*, 30(1), 82–92.

Goutis, C. and Casella, G. (1999). "Explaining the saddlepoint approximation." *The American Statistician*, 53(3), 216–224.

Grall, A., Dieulle, L., Bérenguer, C., and Roussignol, M. (2002). "Continuous-time predictive-maintenance scheduling for a deteriorating system." *IEEE Transactions on Reliability*, 51(2), 141–150.

Grigoriu, M. (1984). "Crossing of non-Gaussian translation processes." *Journal of Engineering Mechanics, ASCE*, 110(4), 610–620.

Grigoriu, M. (2002). *Stochastic Calculus: Applications in Scientific and Engineering.* Birkhäuser, Botston.

Gut, A. and Hüsler, H. (1999). "Extreme shock models." *Extremes*, 2(3), 295–307.

Hamada, M. (2005). "Using degradation data to assess reliability." *Quality Engineering*, 17, 615–620.

Hasegawa, K., Goyette, L. F., Wilkowski, G. M., and Scarth, D. A. (2004). "Development of analytical evaluation procedures and acceptance criteria for pipe wall thinning in asme code section xi." *Fracture Methodologies and Manufacturing Processes*, P. L. Lam, ed., PVP-Vol. 474, 2004 ASME/JSME Pressure Vessels and Piping Conference, San Diego, CA, United States. 83 – 89.

Hashemi, R., Jacqmin-Gadda, H., and Commenges, D. (2003). "A latent process model for joint modeling of events and marker." *Lifetime Data Analysis*, 9, 331–343.

Hora, S. C. (1996). "Aleatory and epistemic uncertainty in probability elicitation with an example from hazardous waste management." *Reliability Engineering and System Safety*, 54(2-3), 217 – 223.

Hougaard, P. (1986). "Survival models for heterogeneous populations derived from stable distributions." *Biometrika*, 73(2), 387–396.

Hougaard, P. (2000). *Analysis of Multivariate Survival Data*. Springer.

Huang, W. and Askin, R. G. (2004). "A generalized SSI reliability model considering stochastic loading and strength aging degradation." *IEEE Transactions on Reliability*, 53(1), 77–82.

International Atomic Energy Agency (1997). "Assessment and management of ageing of major nuclear power plant components important to safety: Steam generators." *IAEA-TECDOC-981*, Vienna, Austria.

International Atomic Energy Agency (1998). "Assessment and management of ageing of major nuclear power plant components important to safety: CANDU pressure tubes." *IAEA-TECDOC-1037*, Vienna, Austria.

International Atomic Energy Agency (2001). "Assessment and management of ageing of major nuclear power plant components important to safety: CANDU reactor assemblies." *IAEA-TECDOC-1197*, Vienna, Austria.

International Atomic Energy Agency (2007). "Nuclear power plants information: Operational reactors by age". Web page: http://www.iaea.org/programmes/a2/index.html.

Ishwaran, H. and James, L. F. (2004). "Computational methods for multiplicative intensity models using weighted gamma processes: proportaional hazards, marked point processes, and panel count data." *Journal of the American Statistical Association*, 99(465), 175–190.

J. Janssen, ed. (1984). *Semi-Markov Models: Theory and Applications*, New York. Plenum Press.

Jia, X. and Christer, A. H. (2002). "A prototype cost model of functional check decisions in reliability-centred maintenance." *Journal of the Operational Research Society*, 53, 1380–1384.

Johnson, N. L., Kotz, S., and Balakrishnan, N. (1994). *Continuous Univariate Distributions*, Vol. 1. John Wiley & Sons, 2nd edition.

Kalbfleisch, J. D. and Prentice, R. L. (2002). *The Statistical Analysis of Failure Time Data*. John Wiley & Sons, second edition.

Kallen, M. J. and van Noortwijk, J. M. (2005). "Optimal maintenance decisions under imperfect inspection." *Reliability Engineering and System Safety*, 90, 177–185.

Kameda, H. and Koike, T. (1975). "Reliability theory of deteriorating structures." *Journal of the Structural Division, ASCE*, 101(1), 295 – 310.

Karlin, S. and Taylor, H. M. (1981). *A Second Course in Stochastic Processes*. Academic Press, New York.

Kotz, S., Lumelskii, Y., and Pensky, M. (2003). *The Stress-Strength Model and Its Generalizations: Theory and Applications.* World Scientific, New Jersey.

Kumar, R. (2004). "Assessment of remaining life for class 1 piping components experiencing wall thinning." *Aging Management and License Renewal*, M. H. Sanwarwalla, ed., PVP-Vol. 487, 2004 ASME/JSME Pressure Vessels and Piping Conference, San Diego, CA, United States. 15 – 21.

Lang, L. C. (2000). "Modelling the corrosion of carbon steel feeder pipes in candu reactors," Master thesis, University of New Brunswick.

Laskey, K. B. (1996). "Model uncertainty: theory and practical implications." *IEEE Transactions on Systems, Man and Cybernetics—Part A: Systems and Humans*, 26(3), 340–348.

Lawless, J. F. (2003). *Statistical Models and Methods for Lifetime Data.* John Wiley & Sons, second edition.

Lawless, J. F. and Crowder, M. (2004). "Covariates and random effects in a gamma process model with application to degradation and failure." *Lifetime Data Analysis*, 10, 213–227.

Lee, M.-L. T., DeGruttola, V., and Schoenfeld, D. (2000). "A model for markers and latent health status." *Journal of Royal Statistical Society, Series B*, 62, 747–762.

Lehmann, E. L. (1999). *Elements of Large-Sample Theory.* Springer.

Lemoine, A. J. and Wenocur, M. L. (1985). "On failure modeling." *Naval Research Logistics Quarterly*, 32, 497–508.

Lewis, E. and Chen, H.-C. (1994). "Load-capacity interference and the bathtub curve." *IEEE Transactions on Reliability*, 43(3), 470 – 475.

Li, C. Q. (1995). "Computation of the failure probability of deteriorating structural systems." *Computers & Structures*, 56(6), 1073–1079.

Li, C. Q. and Melchers, R. E. (2005a). "Time-dependent reliability analysis of corrosion-induced concrete cracking." *ACI Structural Journal*, 102(4), 543–549.

Li, C. Q. and Melchers, R. E. (2005b). "Time-dependent risk assessment of structural deterioration caused by reinforcement corrosion." *ACI Structural Journal*, 102(5), 754–762.

Limnios, N. and Oprişan, G. (2001). *Semi-Markov Processes and Reliability.* Birkhäuser, Boston.

Lin, Y. K. and Cai, G. Q. (1995). *Probabilistic Structural Dynamics: Advanced Theory and Applications.* McGraw-Hill, Inc., New York.

Lindsey, J. K. (1997). *Applying Generalized Linear Models.* Springer.

Liski, E. P. and Nummi, T. (1996). "Prediction in repeated-measures models with engineering applications." *Technometrics*, 38(1), 25–36.

Lu, C. J. and Meeker, W. Q. (1993). "Using degradation measure to estimate a time-to-failure distribution." *Technometrics*, 35(2), 161–174.

Lu, J. (1995). "Degradation processes and related reliability models," Phd thesis, McGill University, Faculty of Management.

Madanat, S. and Ibrahim, W. H. W. (1995a). "Estimation of infrastructure transition probabilities from condition rating data." *Journal of Infrastructural Systems, ASCE*, 1, 120–125.

Madanat, S. and Ibrahim, W. H. W. (1995b). "Poisson regression models of infrastructure transition probabilities." *Journal of Transportation Engineering*, 121(3), 267–272.

Madsen, H. O., Krenk, S., and Lind, N. C. (1986). *Methods of Structural Safety.* Prentice-Hall.

McAllister, T. and Ellingwood, B. (2001). "Reliability-based condition assessment of welded miter gate structures." *Journal of Infrastructure Systems*, 7(3), 95 – 106.

McCullagh, P. and Nelder, J. A. (1983). *Generalized Linear Models.* Chapman & Hall.

Meeker, W. Q. and Escobar, L. A. (1998). *Statistical Methods for Reliability Data.* John Wiley & Sons.

Melchers, R. E. (1999). *Structural Reliability Analysis and Prediction.* John Wiley & Sons, Chichester, second edition.

Mercer, A. and Smith, C. S. (1959). "A random walk in which the steps occur randomly in time." *Biometrika*, 46, 30–35.

Micevski, T., Kuczero, G., and Coombes, P. (2002). "Markov model for storm water pipe deterioration." *Journal of Infrastructure Systems*, 8(2), 49–56.

Miner, M. A. (1945). "Cumulative damage in fatigue." *Journal of Applied Mechanics*, 12, A159–A164.

Moon, F. and Aktan, A. (2006). "Impacts of epistemic (bias) uncertainty on structural identification of constructed (civil) systems." *Shock and Vibration Digest*, 38(5), 399 – 420.

Morey, R. C. (1966). "Some stochastic properties of a compound renewal damage model." *Operations Research*, 14(5), 902–908.

Mori, Y. and Ellingwood, B. R. (1993a). "Reliability-based service-life assessment of aging concrete structures." *Journal of Structural Engineering*, 119(5), 1600 – 1621.

Mori, Y. and Ellingwood, B. R. (1993b). "Time-dependent system reliability analysis by adaptive importance sampling." *Structural Safety*, 12(1), 59 – 73.

Mori, Y. and Ellingwood, B. R. (1994a). "Maintaining reliability of concrete structures. I: role for inspection/repair." *Journal of Structural Engineering*, 120(3), 824 – 845.

Mori, Y. and Ellingwood, B. R. (1994b). "Maintaining reliability of concrete structures. II: optimum inspection/repair." *Journal of Structural Engineering*, 120(3), 846 – 862.

Nelson, W. (1990). *Accelerated Testing: statistical models, test plans, and data analyses.* John Wiley & Sons.

Oberkampf, W. L., Helton, J. C., Joslyn, C. A., Wojtkiewicz, S. F., and Ferson, S. (2004). "Challenge problems: Uncertainty in system response given uncertain parameters." *Reliability Engineering and System Safety*, 85(1-3), 11 – 19.

Osaki, S. (1985). *Stochastic System Reliability Modeling.* World Scientific, Singapore.

Oswald, G. F. and Schueller, G. I. (1984). "Reliability of deteriorating structures.." *Engineering Fracture Mechanics*, 20(3), 479 – 488.

Pachner, J. (2002). "Overview of IAEA project on safety aspects of NPP ageing." IAEA Technical Meeting on Enhancing NPP Safety, Performance and Life Extension through Effictive Ageing Management, Vienna.

Padgett, W. J. and Tomlinson, M. A. (2004). "Inference from accelerated degradation and failure data based on Gaussian process models." *Lifetime Data Analysis*, 10(2), 191–206.

Pandey, M. D., Yuan, X.-X., and van Noortwijk, J. M. (2006). "The influence of temporal uncertainty of deterioration on life-cycle management of structures." *Structure and Infrastructure Engineering.* in print.

Park, C. and Padgett, W. J. (2006). "Stochastic degradation models with several accelerating variables." *IEEE Transactions on Reliability*, 55(2), 379–390.

Park, K. S. (1988a). "Optimal continuous-wear limit replacement under periodic inspections." *IEEE Transactions on Reliability*, 37(1), 97–102.

Park, K. S. (1988b). "Optimal wear-limit replacement with wear-dependent failure." *IEEE Transactions on Reliability*, 37(3), 293–294.

Parry, G. (1996). "The characterization of uncertainty in probabilistic risk assessments of complex systems." *Reliability Engineering and System Safety*, 54(2-3), 119 – 26.

Pinheiro, J. C. and Bates, D. M. (2000). *Mixed-Effects Models in S and S-PLUS*. Springer.

Posner, M. J. M. and Zuckerman, D. (1986). "Semi-Markov shock models with additive damage." *Advances in Applied Probability*, 18, 882–890.

Rao, C. R. (1973). *Linear Statistical Inference and Its Applications*. John Wiley & Sons, second edition.

Rawlings, J. O., Pantula, S. G., and Dickey, D. A. (2001). *Applied Regression Analysis*. Springer, second edition.

Robinson, M. E. and Crowder, M. J. (2000). "Bayesian methods for a growth-curve degradation model with repeated measures." *Lifetime Data Analysis*, 6, 357–374.

Sato, K.-I. (1999). *Lévy Processes and Infinitely Divisible Distributions*. Cambridge University Press.

Sato, K.-I. (2001). "Basic results on Lévy processes." *Lévy Processes: Theory and Applications*, O. E. Barndorff-Nielsen, T. Mikosch, and S. I. Resnick, eds., Boston. Birkhäuser, 3–37.

Saunders, S. C. (1982). "Cumulative damage models." *Encyclopedia of Statistical Sciences*, S. Kotz and N. L. Johnson, eds., Vol. 2. John Wiley & Sons, 230–233.

Sen, A. K. (1990). *Regression Analysis: Theory, Method and Applications*. Springer-Verlag.

Shaked, M. and Shanthikumar, J. G. (1988). "On the first-passage times of pure jump processes." *Journal of Applied Probability*, 25, 501–509.

Singpurwalla, N. (1997). "Gamma processes and their generalizations: an overview." *Engineering Probabilistic Design and Maintenance for Flood Protection*, R. Cooke, M. Mendel, and H. Vrijling, eds. Kluwer Academic Publishers, 67–75.

Singpurwalla, N. D. (1995). "Survival in dynamic environment." *Statistical Science*, 10, 86–103.

Slade, J. P. and Gendron, T. S. (2005). "Flow accelerated corrosion and cracking of carbon steel piping in primary water — operating experience at the point lepreau generating station." *Environmental Degradation of Materials in Nuclear Systems XII*, T. D. Allen, P. J. King, and L. Nelson, eds., Proceedings from the 12th International Conference on Environmental Degradation of Materials in Nuclear Systems-Water Reactors, Salt Lake City, UT. 773–782.

Sobczyk, K. and Spencer, B. F. J. (1992). *Random Fatigue: From Data to Theory.* Academic Press, Boston.

Soong, T. T. (2004). *Fundamentals of Probability and Statistics for Engineers.* John Wiley & Sons.

Soong, T. T. and Grigoriu, M. (1993). *Random Vibration of Mechanical and Structural Systems.* Prentice Hall, Englewood Cliffs, New Jersey.

Thoft-Christensen, P. and Baker, M. J. (1982). *Structural Reliability and its Applications.* Springer-Verlag.

van Noortwijk, J. and Klatter, H. (1999). "Optimal inspection decisions for the block mats of the Eastern-Scheldt barrier." *Quality and Reliability Engineering International*, 65, 203–211.

van Noortwijk, J. and Klatter, H. (2004). "The use of lifetime distributions in bridge maintenance and replacement modelling." *Computers and Structures*, 82(13-14), 1091 – 1099.

van Noortwijk, J. M., Cooke, R. M., and Kok, M. (1995). "Bayesian failure model based on isotropic deterioration." *European Journal of Operational Research*, 82(2), 270 – 282.

van Noortwijk, J. M. and Frangopol, D. M. (2004). "Two probabilistic life-cycle maintenance models for deteriorating civil infrastructures." *Probabilistic Engineering Mechanics*, 19(4), 345 – 359.

van Noortwijk, J. M. and Peerbolte, E. B. (2000). "Optimal sand nourishment decisions." *Journal of Waterway, Port, Coastal and Ocean Engineering*, 126(1), 30 – 38.

van Noortwijk, J. M. and van Gelder, P. H. A. J. M. (1996). "Optimal maintenance decisions for berm breakwaters." *Structural Safety*, 18(4), 293 – 309.

Verbeke, G. and Molenberghs, G. (2000). *Linear Mixed Models for Longitudinal Data.* Springer.

Weisberg, S. (2005). *Applied Linear Regression.* John Wiley & Sons, third edition.

Wenocur, M. L. (1988). "Diffusion first passage times: approximations and related differential equations." *Stochastic Processes and their Applications*, 27, 159–177.

Whitmore, G. A. (1995). "Estimating degradation by a Wiener diffusion process subject to measurement error." *Lifetime Data Analysis*, 1, 307–319.

Whitmore, G. A., Crowder, M. J., and Lawless, J. F. (1998). "Failure inference from a marker process based on a bivariate Wiener model." *Lifetime Data Analysis*, 4, 229–251.

Whitmore, G. A. and Schenkelberg, F. (1997). "Modelling accelerated degradation data using Wiener diffusion with a time scale transformation." *Lifetime Data Analysis*, 3, 27–45.

Wu, W. F. and Ni, C. C. (2003). "A study of stochastic fatigue crack growth modeling through experimental data." *Probabilistic Engineering Mechanics*, 18, 107–118.

Xue, J. and Yang, K. (1997). "Upper & lower bounds of stress-strength interference reliability with random strength-degradation." *IEEE Transactions on Reliability*, 46(1), 142–145.

Yang, J. and Manning, S. (1996). "A simple second order approximation for stochastic crack growth analysis." *Engineering Fracture Mechanics*, 53(5), 677 – 86.

Yang, K. and Xue, J. (1996). "Continuous state reliability analysis." *Proceedings of Annual Reliability and Maintenance Symposium, IEEE*. 251–257.

Yuan, X.-X., Pandey, M. D., and Bickel, G. A. (2006). "A probabilistic degradation model for the estimation of the remaining life distribution of feeders." *Nuclear Energy: A World of Service to Humanity*, 27th Annual Conference of Canadian Nuclear Society, Toronto, Ontario, Canada, June 11-14.

Zheng, R. and Ellingwood, B. (1998). "Stochastic fatigue crack growth in steel structures subject to random loading." *Structural Safety*, 20(4), 303 – 323.

Zimmermann, H.-J. (2000). "An application-oriented view of modeling uncertainty." *European Journal of Operational Research*, 122, 190–198.

Zuo, M. J., Jiang, R., and Yam, R. C. M. (1999). "Approaches for reliability modeling of continuous-state devices." *IEEE Transactions on Reliability*, 48(1), 9–18.